AD-A057 056 CHARLES STARK DRAPER LAB INC CAMBRIDGE MA F/G 17/7
FUNCTIONAL REQUIREMENTS OF THE INTERFACE BETWEEN THE NAVSTAR GP--ETC(U)
DEC 77 B A KRIEGSMAN, W M STONESTREET F04701-75-C-0212
UNCLASSIFIED R-981-VOL-2 SAMSO-TR-77-120-VOL-2 NL

1 OF 2
AD A057656

AIR FORCE REPORT
SAMSO TR 77-120
VOLUME II

LEVEL II

(2)

B.S.

AD A057656

AD NO. _____
DDC FILE COPY

R-861
FUNCTIONAL REQUIREMENTS OF THE INTERFACE BETWEEN THE NAVSTAR GPS RECEIVER MODEL X AND THE ADVANCED INERTIAL REFERENCE SPHERE

FINAL REPORT FOR
SAMSO CONTRACT F04701-75-C-0212
VOLUME II

by
Bernard A. Kriegsman, William M. Stonestreet, Duncan B. Cox, Jr.

December 1977

The Charles Stark Draper Laboratory, Inc.
Cambridge, Massachusetts 02139

(19)

(18) AIR FORCE REPORT
SAMSO TR-77-120-VOL-2
VOLUME II

(14) R-981-VOL-2

(6) FUNCTIONAL REQUIREMENTS OF THE
INTERFACE BETWEEN THE NAVSTAR GPS RECEIVER MODEL X AND THE
ADVANCED INERTIAL REFERENCE SPHERE. Volume II.

(9) FINAL REPORT, FOR SAMSO CONTRACT F04701-75-C-0212

(15)

VOLUME II

by

(10) Bernard A. Kriegsman
William M. Stonestreet
Duncan B. Cox, Jr.

(11) Dec[redacted]77

(12) 99 p.

Approved:

Joseph F. Luse
Joseph F. Luse
Project Officer
Space and Missile
Systems Organization

Approved:

William G. Denhard
William G. Denhard
Head, Air Force
Programs Department

AD57659

The Charles Stark Draper Laboratory, Inc
[redacted]ambridge, Massachusetts 02139

408 386

78 14 08 027

ACKNOWLEDGEMENT

The authors wish to express their appreciation to Mr. Joseph Luse of SAMSO and Mr. Kevin Mahar of CSDL for their helpful suggestions and discussions during the course of the study.

This report was prepared by The Charles Stark Draper Laboratory, Inc., under Contract F04701-75-C-0212 with the NAVSTAR GPS Joint Program Office (JPO) at the Space and Missile Systems Organization of the Air Force Systems Command. Mr. Joseph Luse (SAMSO/YEO) is the Project Officer on this contract.

This technical report has been reviewed and is approved for publication.

TABLE OF CONTENTS

SECTION 1

ABSTRACT

FUNCTIONAL REQUIREMENTS OF THE INTERFACE BETWEEN THE NAVSTAR GPS RECEIVER MODEL X AND THE ADVANCED INERTIAL REFERENCE SPHERE

The performance requirements for the GPS X-set* impose difficult and conflicting design problems on the receiver. To accurately track the incoming signals in a high-dynamics environment, a wide-bandwidth tracking loop is required with a high-order tracking network. For best performance in the presence of noise, on the other hand, a narrow bandwidth tracking loop is desired.

Techniques for utilizing an Inertial Measurement Unit (IMU), such as the Advanced Inertial Reference Sphere (AIRS), to aid the receiver tracking loops are studied here. The IMU can provide accurate information on translational accelerations and orientation changes experienced by the receiver. By properly using the IMU data, the receiver bandwidth can be reduced without increasing the dynamics-induced tracking error. The end result is an improvement in performance in noisy or jamming situations.

To evaluate the benefits of IMU aiding, a comprehensive digital-computer simulation was developed for the IMU-aided X-set receiver. Included in the simulation of the receiver were detailed models for the error detectors, integrate-and-dump circuits, digital tracking networks, and RM/IPMs (digital VCOs) for both the code and carrier tracking loops. The effects of RM/IPM quantization, cross-coupling between code and carrier tracking loop, dynamic clock errors, and the

*The NAVSTAR GPS X-set is one of several baseline Phase I GPS receivers being developed by Magnavox Advanced Products Division under subcontract to General Dynamics under a contract with the GPS Joint Program Office at SAMSO.

finite sampling rates in each tracking loop were among the effects accounted for. In the IMU model, provisions were made for measuring the orientation and translational acceleration of the support vehicle. Included as IMU error sources were attitude readout errors, IMU misalignment, gyro drift bias, accelerometer bias, and accelerometer scale-factor uncertainty.

The simulation results present code and carrier tracking-loop errors, based on Monte-Carlo runs, for a wide range of conditions. Of particular interest are the thresholds of input noise and vehicle dynamics at which the tracking loops lose lock. Performance-comparison data are presented for the aided and unaided receiver as a function of system variables such as tracking loop bandwidth, RM/IPM noise, IMU errors, clock errors, and sampling rates for receiver and IMU.

SECTION 2
INTRODUCTION

The incoming GPS (Global Positioning System) signal considered here consists of a high-frequency L-band carrier signal (1.575 GHz) modulated by a PRN (Pseudo-Random-Noise) code signal (10.23 MHz).[+] Binary data with satellite ephemeris and other information are modulated on these signals at 50 b.p.s. The function of the receiver is to demodulate the transmitted data, and simultaneously track both the carrier and code signal components. From the code signal information can be derived on the pseudo-range from the receiver to satellite (corrupted by various errors), and from the carrier signal the time rate-of-change of this pseudo-range can be found.

Receiver operation in a high-dynamics environment, such as might be encountered in a missile or tactical aircraft, is considered here. The design-reference input signal to the X-set receiver is assumed to consist of a 10 g/s jerk (rate of change of acceleration) for 0.6 seconds, followed by a constant acceleration of 6 g's. If the receiver can cope with an input of this magnitude without losing lock (or rapidly slipping cycles), then it is felt that it will not have difficulty with the normally-encountered input dynamics.

The extremely severe dynamic inputs mentioned above pose very stringent requirements on the X-set carrier-tracking loop. In order to avoid loss of lock (or cycle slipping), the carrier-loop tracking error (as will be shown later) must be limited to about 0.15 ft. (about 0.25 cycles at 1.575 GHz). To hold the peak transient error to values of this magnitude a wide-bandwidth tracking loop is required. A third-order tracking loop is also necessary to track a constant-acceleration input with zero steady-state error. The requirements of wide bandwidth and high-order tracking network in the presence of sampling and transport lags tend to make stabilization of the carrier tracking loop difficult.

[+]See Reference 2-1 for a description of the complete GPS signal structure.

Input noise to the receiver, on the other hand, leads to receiver-design requirements diametrically opposed to those imposed by input dynamics. Small tracking-loop bandwidths are desired in this case in order to minimize the tracking errors caused by the input noise.

If the carrier-tracking loop maintains lock, it can be used to aid the code loop and essentially isolate it from the incoming high-dynamics input signal. Under these conditions it is relatively easy to limit the code-loop tracking error to 25 ft. (1/4 chip), which is necessary for proper code-loop tracking. If, however, the carrier-tracking loop loses lock and starts slipping cycles at a rapid rate, then it will no longer be able to meaningfully aid the code-tracking loop. Under these conditions the unaided code loop will lose lock in a very short time if any significant input dynamics are present, since the current X-set code-tracking loop has only a first-order tracking-loop capability and a relatively narrow bandwidth.

An inertial measurement unit (IMU) mounted in the missile (or aircraft) is capable of providing information on the motion of the receiver antenna with respect to an inertially-fixed frame. If the IMU is collocated with the receiver antenna, then only gravity-corrected accelerometer data are required. If, on the other hand, the IMU is a significant distance from the receiver antenna, then attitude data are required to compute the rotational velocity of the antenna with respect to the IMU.

By properly using IMU-derived data to aid the X-set tracking loops, the effective input dynamics to which these loops are subjected can be significantly reduced. For the carrier loop* this means a lower-bandwidth loop for a given input-dynamics level. The end result is a less difficult tracking-loop stabilization problem, and a reduction of the input-noise induced tracking error. For the code loop, IMU-derived data is very useful in the loss-of-carrier-lock situation. Under these conditions external input-

*The current design of the X-set does not provide for aiding of the carrier loop. Implementation of the aiding techniques presented herein would require modifications to the receiver design and to the interfaces between the receiver, data processor, and IMU.

dynamics information is necessary to help the low-bandwidth first-order code-tracking loop maintain lock.

This report is concerned with techniques for utilizing IMU-derived information to aid the X-set code and carrier tracking-loop channels. Extremely important factors here are the rate at which new IMU-derived aiding information can be obtained, and the aiding prediction algorithms that are employed. The finite read times for the IMU (the basic measurement is average acceleration) and the required information processing times are both relevant. In addition, several different IMU-related error sources must be considered. The most important of these are attitude readout errors, IMU alignment errors, accelerometer bias, and accelerometer scale-factor uncertainties.

In the immediately-following section, a detailed description is given of the study-model X-set receiver. For simplicity and clarity, only baseband models are considered. The primary emphasis is on those items that significantly affect the stability and accuracy of the tracking loops. A discussion of the IMU-aiding schemes examined is also contained in this section. Included here are the algorithms used to extrapolate IMU-derived information between successive data processing times.

Section 4 presents the results of the detailed simulation. Peak-transient and rms tracking errors are shown as a function of tracking-loop noise bandwidth for several different assumed conditions. Both aided and unaided system data are presented so that meaningful performance tradeoffs can be made. Monte-Carlo simulation results are also included for selected cases to provide data on the minimum C/N_0 (signal/noise power spectral density) at which tracking-loop lock can be maintained with the high-dynamics input present.

Section 5 presents a summary and conclusions of the study.

Section 6 is a list of references used in this report.

SECTION 3

DESCRIPTION OF SIMULATION

To properly evaluate the benefits from IMU-aiding of the GPS receiver, a comprehensive digital-computer simulation has been developed for the X-set receiver. This simulation is based on the functional description of the receiver described in Reference 3-1.*

The receiver simulation is essentially a base-band representation of a single X-set channel, including both code and carrier tracking loops. Detailed models are given in the following sections for the error detectors, the integrate-and-dump circuits, the digital tracking networks, the RM/IPMs (digital VCOs), and the IMU. Included in the receiver model are the effects of RM/IPM quantization levels, cross coupling between code and carrier tracking loops, the binary-data modulation, and the various tracking-loop sampling delays.

The IMU model describes the basic measurements of vehicle translational acceleration and orientation. Included as error sources are the attitude readout errors, IMU alignment, gyro drift bias, accelerometer bias, and accelerometer scale factor uncertainties. Also accounted for are errors introduced by the finite sampling rate of the IMU.

3.1 X-SET RECEIVER MODELING

3.1.1 Overview

Basic functional diagrams for the X-set receiver carrier and code tracking loops are shown in Figures 3-1 and 3-2. These figures are based on information from Ref. 3-1. For simulation convenience the tracking-loop is subdivided into four basic elements (subsystems): 1) signal correlator; 2) signal converter; 3) tracking network; and 4) RM/IPM (digital VCO). Although their basic functions are similar, the characteristics of the carrier and code channel elements are generally different.

The correlator provides the basic measure of the tracking errors between the satellite-transmitted carrier and code information, and the

*Due to changes in the design of the X-set receiver and the desire to reflect these changes in Ref. 3-1, the description of the simulation presented in this section differs slightly from the functional description of the receiver presented in Ref. 3-1. It is felt that these design changes will have little effect on the results of this study.

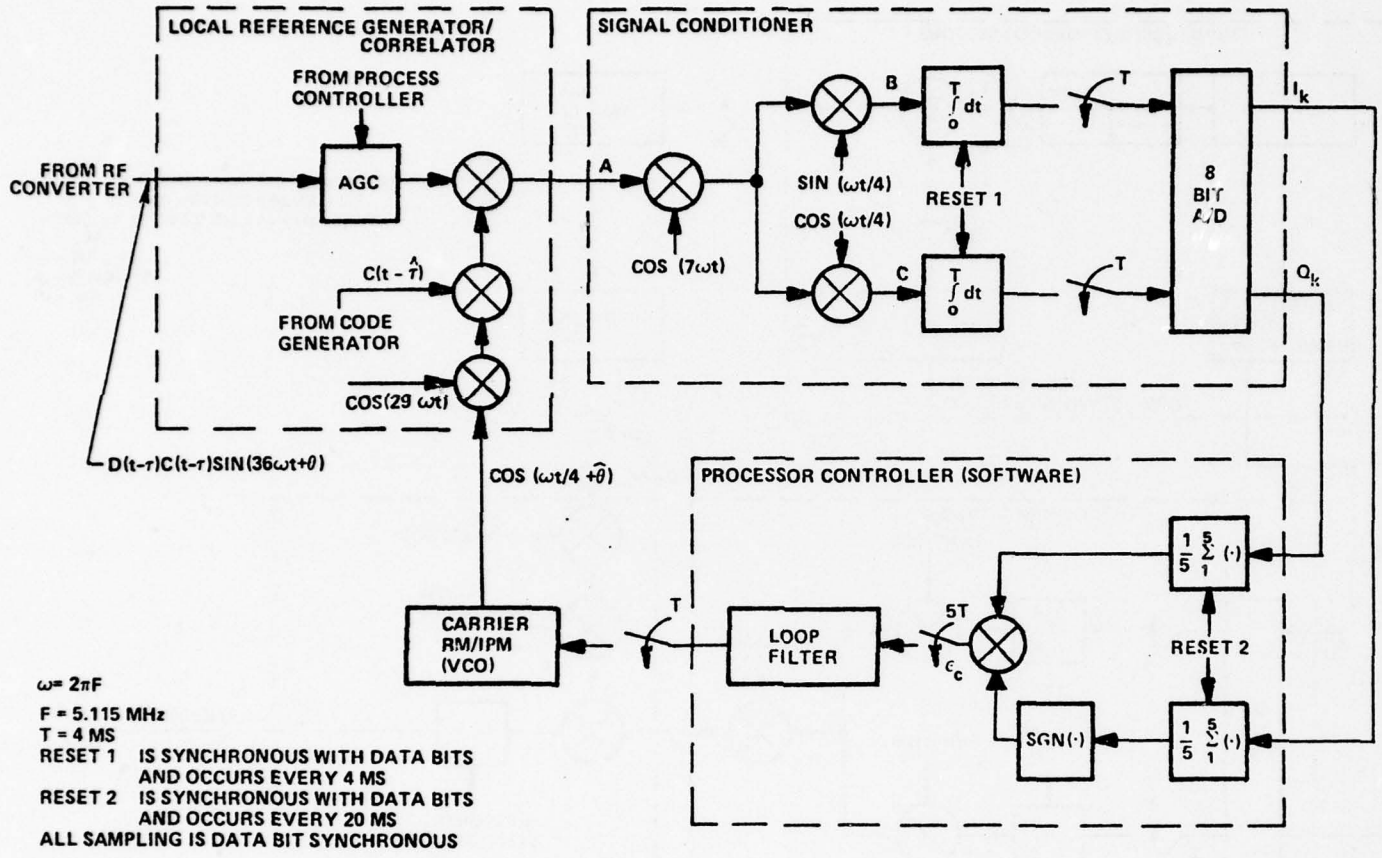

Figure 3-1: Carrier-tracking loop. (Costas)

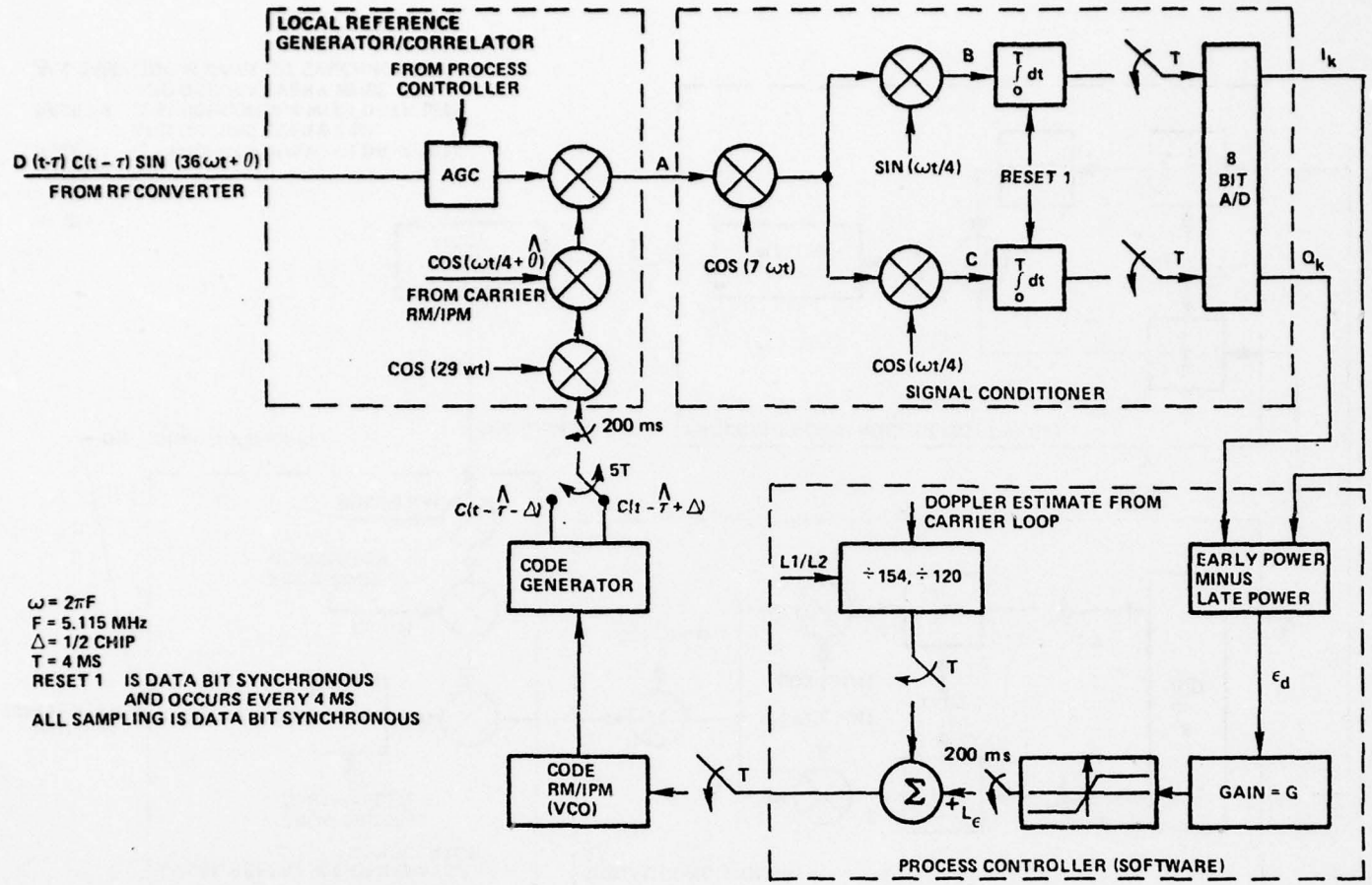

Figure 3-2: Code-tracking loop.

corresponding signals generated in the receiver. The signal converter changes the error signals to the proper format for use in their respective feedback tracking loops. The tracking networks provide the necessary tracking-loop gains and integration paths to obtain acceptable tracking-loop errors in the presence of the expected dynamic inputs to the receiver. Finally, the RM/IPMs provide the physical means whereby the carrier or code phase is advanced or retarded with respect to the incoming signals.

In the following sections the carrier loop will be considered first, and then the code loop. The models to be described, as mentioned earlier, are baseband models.

3.1.2 Carrier Tracking Loop (Costas)

3.1.2.1 Signal Correlator

The incoming signal is correlated with the carrier-loop feedback signal (from the RM/IPM) multiplied by the on-time code. From the correlator output signal, the basic quadrature and inphase error signals for the carrier loop are obtained as described in Ref. 3-1. The simulation models for these signals ($e_{q_{CA}}$ and $e_{i_{CA}}$) are:

$$e_{q_{CA}} = D(t-\tau)C(t-\tau)C(t-\hat{\tau})\sin(e_{CA}) \qquad (3\text{-}1)$$

$$e_{i_{CA}} = D(t-\tau)C(t-\tau)C(t-\hat{\tau})\cos(e_{CA}) \qquad (3\text{-}2)$$

where e_{CA} is the error between the true and estimated carrier phase ($\theta_{TRUE} - \hat{\theta}$). The quantity $D(t-\tau)$ represents the binary data modulation (50 b.p.s.), the satellite transmission time is denoted by t, and the true propagation delay (satellite to receiver) is represented by τ. The receiver's estimate of propagation delay, i.e. code-tracking-loop range, is $\hat{\tau}$. The code-tracking-loop error (e_{CO}) is simply the difference between τ and $\hat{\tau}$. The quantities $C(t-\tau)$ and $C(t-\hat{\tau})$ represent the transmitted and receiver-estimated codes.

An important point to be seen from Eqs. (3-1) and (3-2) is that the quadrature and inphase signals for the carrier loop

($e_{q_{CA}}$ and $e_{i_{CA}}$) are related to the code-loop tracking error through the term $C(t-\tau)C(t-\hat{\tau})$. This term, as indicated in Fig. 3-3, is a triangular function of code-loop tracking error, with a maximum value at zero code-tracking loop error (normalized to unity in Fig. 3-3) and with a zero value for code-loop tracking errors greater than a chip (100 feet).

For small carrier-loop tracking errors (w.r.t. one radian) and small code-loop tracking errors (w.r.t. one chip), it can be seen that $e_{q_{CA}}$ corresponds roughly to the carrier-loop tracking error (e_{CA}) multiplied by the sign of the binary data bit (+1 or -1). Likewise, $e_{i_{CA}}$ corresponds to the sign of the data bit.

3.1.2.2 Signal Converter

The signal converter first takes the correlator output signals $e_{q_{CA}}$ and $e_{i_{CA}}$ and averages them over the time-interval T to obtain the average-error samples $Q'_{k_{CA}}$ and $I'_{k_{CA}}$. The mathematical relations for the study model are:

$$Q'_{k_{CA}} = \frac{1}{T} \int_{t_k-T}^{t_k} e_{q_{CA}} \, dt \tag{3-3}$$

$$I'_{k_{CA}} = \frac{1}{T} \int_{t_k-T}^{t_k} e_{i_{CA}} \, dt \tag{3-4}$$

where the integrate-and-dump interval (T) used here is 4 ms. The outputs of the integrators are, of course, reset to zero after the average-error samples $Q'_{k_{CA}}$ and $I'_{k_{CA}}$ are taken.

The receiver input noise for the carrier channel is incorporated into the simulation at the output of the integrate-and-dump circuits. Independent Gaussian-distributed random sequences (n_q and n_i) with zero mean and variance σ^2_{CA} are added to $Q'_{k_{CA}}$ and $I'_{k_{CA}}$ to obtain

$$Q_{k_{CA}} = Q'_{k_{CA}} + n_{q_{CA}} \tag{3-5}$$

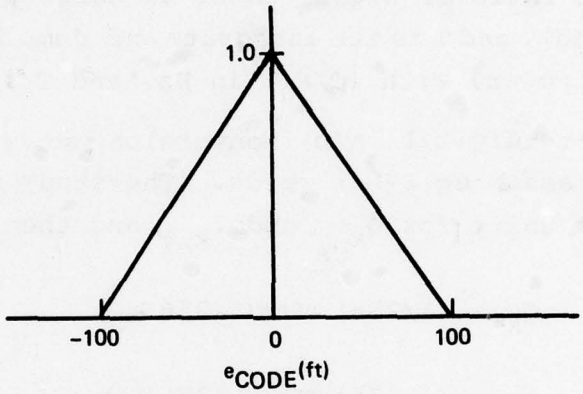

Figure 3-3. On-time code correlator characteristics.

$$I_{k_{CA}} = I'_{k_{CA}} + n_{i_{CA}} \tag{3-6}$$

The variance σ^2_{CA} is given by:

$$\sigma^2_{CA} = \frac{1}{2(C/N_0)T} \tag{3-7}$$

where C/N_0 is the ratio of signal power to noise power spectral density (single-sided), and T is the integrate and dump interval. The dimensions of σ^2_{CA} are power, with (C/N_0) in Hz, and T in seconds.

An analog-to-digital (A/D) conversion is next performed on the Q_k and I_k signals*, assuming 8-bit words. The study model assumes maximum values of unity for $Q_{k_{CA}}$ and $I_{k_{CA}}$, and then uses the relations

$$Q_k = (1/256)\ \text{TRUNC}\ (256\, Q_k) \tag{3-8}$$

$$I_k = (1/256)\ \text{TRUNC}\ (256\, I_k) \tag{3-9}$$

where the operation TRUNC(•) saves only that part of (•) to the left of the decimal point.

The final operations in the signal converter are the computation of data-bit sign and tracking error, using 5-sample averages of I_k and Q_k. The data bit sign ($\hat{S}_{DAT}$) is estimated from the sum

$$\hat{S}_{DAT} = \text{SGN}\left(\frac{1}{5}\sum_{k=1}^{5} I_k\right) \tag{3-10}$$

where the operation SGN (•) means that the algebraic sign of (•) is taken. The notation of a caret ($\hat{\cdot}$) is used to indicate the estimated or computed value (not the true value). Using $\hat{S}_{DAT}$, the computed carrier-loop error signal is given by

$$\hat{e}_{CA} = \hat{S}_{DAT}\ \frac{1}{5}\sum_{k=1}^{5} Q_k \tag{3-11}$$

*The subscript CA is removed here from $Q_{k_{CA}}$ and $I_{k_{CA}}$ to simplify notation. There is no ambiguity since only the carrier loop signals are used here.

It should be noted that the 5-sample averages $\sum I_k$ and $\sum Q_k$ are synchronized with the data bits, i.e. each set of $\sum I_k$ and $\sum Q_k$ is taken over a particular 20-ms data-bit interval.

3.1.2.3 Tracking-Loop Network

The digital tracking-loop network, as described in Ref. 3-1, is modeled by the difference equations

$$\Delta\phi_{CA_n} = C_1 T_{CA} \hat{e}_{CA_n} + v_{n-2} \tag{3-12}$$

$$v_n = C_2 T_{CA}^2 \hat{e}_{CA_n} + v_{n-1} + a_{n-1} \tag{3-13}$$

and

$$a_n = C_3 T_{CA}^3 \hat{e}_{CA_n} + a_{n-1} \tag{3-14}$$

where the digital carrier-loop tracking network operates at a cycling period T_{CA} of 20 ms, which equals $t_n - t_{n-1}$. The quantities C_1, C_2 and C_3 are tracking-loop gains for the proportional, integral, and double-integral paths, and $\hat{e}_{CA}$ is the computed carrier-loop error at time t_n described in the preceding section. The quantities a_n and v_n, as noted in Ref. 3-1, represent the contents of the tracking-loop accumulators (integrators) at time t_n. The desired phase change $\Delta\phi_{CA}$ is divided by 5 and sent forward to the carrier-loop RM/IPM at a 4-ms interval.

At the time this study was being conducted, the computation of $C_1 T_{CA} \hat{e}_{CA}$ was assumed to take place in the foreground, whereas the computation of v_n was in the background (4-12 ms delay). Under these conditions the delay in the v_n computation was constrained to be a full computation cycle (T_{CA} seconds), which is why v_{n-2} is used in Eq. (3-12) rather than v_{n-1}.

In concluding this section, it should be noted that the computations of Eqs. (3-12) to (3-14) are performed in the simulation in the order shown.

3.1.2.4 Carrier-Loop RM/IPM

The study model assumes that the phase change $\Delta\phi_{CA}$ will be corrected at a uniform rate over the 20-ms computation interval T_{CA}.

The RM/IPM samples the tracking-loop error signal at a 4-ms interval, i.e. a phase change $\Delta\phi_{CA}/5$ is made in this period.

The quantization level for the carrier-loop RM/IPM, i.e. the minimum increment of phase change is 1/64th of a cycle. The simulation model computes the number of quanta m_{CA}, corresponding to the phase change $\Delta\phi_{CA}$, using the relation:

$$m_{CA} = \text{TRUNC}\left[\frac{64}{2\pi}\ \Delta\phi_{CA}/5\right] \tag{3-15}$$

where the units of $\Delta\phi_{CA}$ are radians. The operation TRUNC(·) computes only that part of (·) to the left of the decimal point.

The actual RM/IPM phase change for the 4-msec interval $\Delta\phi^*_{CA}$ is thus:

$$\Delta\phi^*_{CA} = 2\pi\ m_{CA}/64 \tag{3-16}$$

where the units of $\Delta\phi^*_{CA}$ are radians. The remainder $\Delta\phi_{REM}$ (in radians) is

$$\Delta\phi_{REM} = \frac{\Delta\phi_{CA}}{5} - \frac{2\pi\ m_{CA}}{64} \tag{3-17}$$

The quantity $\Delta\phi_{REM}$ is saved and added to the desired phase change $\Delta\phi_{CA}/5$ to be applied at the next RM/IPM sampling time.

At the present time it is anticipated that a transport delay of as much as 4 ms may take place in the process of transmitting tracking-loop data to the RM/IPM. The simulation models this effect by holding $\Delta\phi^*_{CA}$ for 4 ms before sending it forward to the RM/IPM.

3.1.2.5 Frequency-Standard Disturbances

The frequence standard associated with the RM/IPM is a temperature-controlled quartz oscillator. It is subject to both random and deterministic disturbance inputs which degrade its performance. Three error sources have been considered in this study:

(1) white frequency noise
(2) flicker frequency noise
(3) acceleration-sensitive drift

Detailed discussions of these frequency-standard error sources can be found in Refs. 3-2 to 3-4.

The phase error introduced by the white frequency noise $\delta\phi_W$ was modeled by the difference equation

$$\delta\phi_{W_m} = \delta\phi_{W_{m-1}} + u_{W_m} \tag{3-18}$$

The Gaussian random sequence u_W, which increments $\delta\phi_W$ after each simulation computation cycle, has a zero mean value and a variance σ^2_{uW} of

$$\sigma^2_{uW} = h_0\left(\frac{2\pi c}{\lambda}\right)^2 \Delta t \tag{3-19}$$

where h_0 is the spectral level of the white frequency noise (sec), c is the velocity of light (ft/s), and λ is the carrier wavelength. The simulation integration step Δt was 1 ms. The assumed value for h_0, based on information from Refs. 3-2 and 3-5 was 10^{-22} seconds.

The flicker-noise model was based on passing white noise through two cascaded lag-lead networks (Ref. 3-5). This type of model can be made to approximate the 1/f spectral-density characteristic of flicker noise over a selected frequency band. The frequency-response function for the simulation-model shaping network, $G(\omega)$, was

$$G(\omega) = \left(\frac{j\omega + 1}{j10\omega + 1}\right)\left(\frac{j100\omega + 1}{j1000\omega + 1}\right) \tag{3-20}$$

where the angular frequency ω is in rad/s. These parameters give a good 1/f approximation over the time interval between 2 and 2×10^4 seconds, which is appropriate for a quartz clock, (Ref. 3-5). A flicker floor of 1×10^{-11} was assumed (Refs. 3-2 to 3-5), which gives a flicker-noise spectral level (h_{-1}) of 3.6×10^{-23}.

The phase error $\delta\phi_f$ introduced by the flicker-frequency noise is obtained from the difference equation set

$$\delta\phi_{f_n} = \delta\phi_{f_{n-1}} + f_0 x_{1_{n-1}} + g_0 w \tag{3-21}$$

$$x_{1_n} = (1 + f_1 \Delta t) x_{1_{n-1}} + f_2 \Delta t\, x_{2_{n-1}} + g_1 w \tag{3-22}$$

and $$x_{2_n} = x_{2_{n-1}} + f_3 \Delta t\, x_{1_{n-1}} + g_2 w \qquad (3\text{-}23)$$

where x_1 and x_2 are dummy variables, Δt is the simulation integration step, and w is a random sequence. The numerical relations for the quantities f_0- f_3, g_0- g_2, and the covariance of w, can be found in Ref. 3-5.

The phase change ($\delta\phi_{ac}$) caused by acceleration-sensitive drift was modeled as:

$$\delta\phi_{ac_m} = \delta\phi_{ac_{m-1}} + k_{ac}\left(\frac{2\pi c}{\lambda}\right) a\, \Delta t \qquad (3\text{-}24)$$

where a is the acceleration of the receiver caused by non-gravitational forces (in g's), and k_{ac} is the acceleration sensitive drift coefficient (in 1/g's).

3.1.3 Code-Tracking Loop

3.1.3.1 Code-Loop Correlator

The incoming signal for a given receiver channel is alternately correlated every 20 ms with early and late code signals from the RM/IPM for two consecutive 20 ms intervals, i.e. for a period of 40 ms. The early and late code signals used here are displaced w.r.t. the on-time code signal by one-half a chip ($\Delta/2$) or about 50 feet. The beginning and end of the correlation intervals are synchronized to the data-bit transitions (50 b.p.s.). The order in which these 20-ms correlations are made in the 40 ms block is random. Because of the time-sharing in the code loop, there is an interval of 160 ms between successive correlation periods for a given channel (data from the same satellite).

Quadrature and inphase signals are computed from the correlator output in a manner similar to that for the carrier loop [Eqs.(3-1) and (3-2)]. The simulation equations are

$$e_{q_{CO}} = D(t-\tau)C(t-\tau)C(t-\hat{\tau} \pm \Delta/2)\sin(e_{CA}) \qquad (3\text{-}25)$$

and $$e_{i_{CO}} = D(t-\tau)C(t-\tau)C(t-\hat{\tau} \pm \Delta/2)\cos(e_{CA}) \quad (3\text{-}26)$$

where $e_{q_{CO}}$ and $e_{i_{CO}}$ are the quadrature and inphase correlator output signals, $D(t-\tau)$ is the binary data (+1 or -1), and e_{CA} is the tracking error of the carrier loop.

The correlation term $C(t-\tau)C(t-\hat{\tau} \pm \Delta/2)$, which is the basis for the tracking-loop error signal, is triangular in shape as shown in Figure 3-4. The algebraic sign preceding $\Delta/2$ is + or -, depending on whether the correlation is with respect to the early or late code.

It is important to note that the carrier-loop tracking error directly influences the code-loop correlator outputs as shown in Eqs.(3-25) and (3-26).

3.1.3.3 Signal Converter

The signal-converter first averages the correlator outputs over the time-interval T, using integrate-and-dump circuits as in the carrier loop to generate quadrature and in-phase samples $Q'_{k_{CO}}$ and $I'_{k_{CO}}$. The simulation relations are

$$Q'_{k_{CO}} = \frac{1}{T}\int_{t_k-T}^{t_k} e_{q_{CO}}\, dt \quad (3\text{-}27)$$

$$I'_{k_{CO}} = \frac{1}{T}\int_{t_k-T}^{t_k} e_{i_{CO}}\, dt \quad (3\text{-}28)$$

where the integrate-and-dump interval (T) is 4 ms.

The code-channel input noise is incorporated into the simulation at the output of the integrate-and-dump circuits. Independent random sequences $n_{q_{CO}}$ and $n_{i_{CO}}$ of variance σ^2_{CO} are added to $Q'_{k_{CO}}$ and $I'_{k_{CO}}$ to obtain:

$$Q_{k_{CO}} = Q'_{k_{CO}} + n_{q_{CO}} \quad (3\text{-}29)$$

$$I_{k_{CO}} = I'_{k_{CO}} + n_{i_{CO}} \quad (3\text{-}30)$$

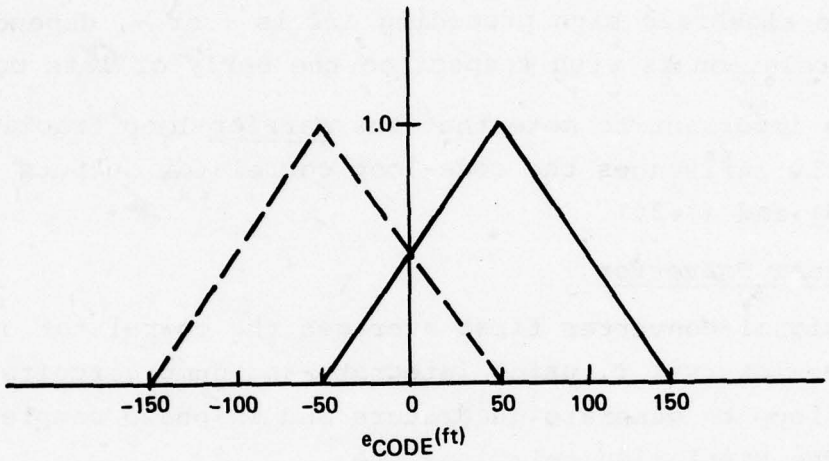

Figure 3-4. Early and late code correlator characteristics.

The variance σ^2_{CO} is given by

$$\sigma^2_{CO} = \frac{1}{2(C/N_0)T} \tag{3-31}$$

where C/N_0 is the ratio of signal power to noise p.s.d. (single-sided). The dimensions of σ^2_{CO} here are power.

An analog-to-digital (A/D) conversion is next performed on the Q_k and I_k signals, assuming 8-bit words. The study model assumes maximum values of unity for Q_k and I_k, and then uses the relations

$$Q_{k_{CO}} = (1/256)\ \text{TRUNC}\ (256\, Q_{k_{CO}}) \tag{3-32}$$

$$I_{k_{CO}} = (1/256)\ \text{TRUNC}\ (256\, I_{k_{CO}}) \tag{3-33}$$

where the operation TRUNC($\cdot$) saves only that part of ($\cdot$) to the left of the decimal point.

The non-coherent delay-locked loop generates its basic error signal (e_{CO}), from the relation (Ref. 3-1)

$$e_{CO} \approx \frac{P_e - P_\ell}{P_e + P_\ell} \tag{3-34}$$

where the quantities P_e and P_ℓ represent the average power in the early-code and late-code correlation signals. The simulation model approximates the average early and late power by the relations:

$$P_{e,\ell} = \left| \sum_{k=1}^{5} I_{k_{CO}} \right| + \left| \sum_{k=1}^{5} Q_{k_{CO}} \right|$$

where the notation $|\cdot|$ indicates the magnitude of the enclosed quantity. The early power P_e is, of course, based on I's and Q's from early-code correlations. Likewise, P_ℓ is based on late-code correlations. It should be noted that the starting points of the early and late correlations, as mentioned earlier, are at the data-bit transitions. The code-loop error signal in feet is then computed from

$$\hat{e}_{CO} = \frac{\Delta}{2}\left(\frac{P_e - P_\ell}{P_e + P_\ell}\right) \tag{3-35}$$

where the chip width (Δ) is 100 feet.

3.1.3.4 Tracking-Loop Network

The tracking-loop network here is simply a gain (k_{CO}) followed by a limiter, as shown in Fig. 3-2. The nominal value for this gain was chosen to give an open-loop gain of 0.1 for the 1st-order tracking loop, and a time constant of about 2 seconds. The limiter, as noted in Ref. 3-1, limits the magnitude of the error signal after the gain multiplication to 25 feet.

Because of the fact that a single code channel is time shared between the different received signals, the code tracking error for a particular satellite is computed only at 200-ms intervals (Ref. 3-1). The desired position change (Δx_{CO}) over the next RM/IPM interval, which is sent to the code-loop RM/IPM, is

$$\Delta x_{CO} = \begin{cases} 25 & \text{if } k_{CO}\, e_{CO} > 25 \\ k_{CO}\, \hat{e}_{CO} & \text{if } |k_{CO}\, e_{CO}| \leq 25 \\ -25 & \text{if } k_{CO}\, e_{CO} \leq 25 \end{cases} \tag{3-36}$$

where the units of Δx_{CO} and e_{CO} are feet.

3.1.3.5 Code-Loop RM/IPM

The code-loop RM/IPM advances (or retards) the receiver code by Δx_{CO} in a 4-ms interval. This is done uniformly at the rate $\Delta x_{CO}/.004$ f/s.

The quantization level for the code-loop RM/IPM is 1/64th of a chip. The simulation model computes the number of quanta m_{CO} corresponding to the position change Δx_{CO}, using the relation

$$m_{CO} = \text{TRUNC}\left(\frac{64}{100}\, \Delta x_{CO}\right) \tag{3-37}$$

where the units of Δx_{CO} are feet. The actual RM/IPM position change for the 4-ms interval is

$$\Delta x^{*}_{CO} = \frac{100}{64}\, m_{CO} \tag{3-38}$$

The remainder Δx_{REM} is

$$\Delta x_{REM} = \Delta x_{CO} - \frac{100}{64}\, m_{CO} \tag{3-39}$$

This quantity Δx_{REM} is saved and added to the desired position change Δx_{CO} to be applied at the next RM/IPM sampling time.

The same frequency-reference standard is used for both the code and carrier tracking loops. Accordingly, the same random and determinsitic disturbance inputs discussed in Sec. 3.1.2.4 for the carrier loop RM/IPM will be present here. The code-loop position disturbances (δx_{CO}) are related to the carrier-loop phase disturbances ($\delta\phi_{CA}$) by the expression

$$\delta x_{CO} = \lambda_{CA}(\delta\phi_{CA}/2\pi) \tag{3-40}$$

where λ_{CA} is the carrier transmission wavelength.

3.2 INERTIAL MEASUREMENT UNIT

3.2.1 Computation of Antenna Position and Velocity

The study-model Inertial Measurement Unit (IMU) contains an inertially-fixed instrument package with 3 single-degree-of-freedom gyros and accelerometers. From the viewpoint of receiver-aiding, it would be desirable to locate the IMU as close to the receiver antennas as possible. In this subsection it is assumed that the IMU and antenna are at essentially the same location. The case where the IMU and receiver antenna are not located close together is considered in a later section.

Integrating accelerometers are assumed whose outputs are the velocity change of the vehicle during the read interval, as a result of the non-gravitational forces on the vehicle. To obtain true position and velocity of the vehicle, it is necessary to compute the gravitational-force velocity change, and combine it with the accelerometer measured velocity change $\Delta\tilde{\underline{V}}$.†

The simulation model computes the vehicle velocity (w.r.t. the inertially-fixed frame) at time t_n, i.e. $\underline{V}_n$, from the relation

$$\underline{V}_n = \underline{V}_{n-1} + \Delta\tilde{\underline{V}} + \underline{g}\,\Delta t_I \tag{3-41}$$

where $\underline{V}_{n-1}$ is the velocity estimate at t_{n-1}, the accelerometer measurement $\Delta\tilde{\underline{V}}$ is for the read interval Δt_I which equals $t_n - t_{n-1}$. The

†The notation of a bar under a quantity, e.g. $\underline{V}$ is used to indicate a vector.

computed gravitational specific force $\underline{g}$ is based on the previous estimate of vehicle position with respect to the center of the earth ($\underline{r}_{n-1}$). Estimated vehicle position ($\underline{r}_n$) with respect to the center of the earth at t_n is computed from the relation

$$\underline{r}_n = \underline{r}_{n-1} + \left(\underline{V}_{n-1} + \frac{1}{2}(\Delta\underline{V} + \underline{g}\,\Delta t_I)\right)\Delta t_I \qquad (3\text{-}42)$$

Higher-order iterative integration routines could be used to obtain more accurate values for $\underline{r}_n$ and $\underline{V}_n$ if necessary, e.g. $\underline{g}$ could be recomputed using both $\underline{r}_n$ and $\underline{r}_{n-1}$ to give better estimates of $\underline{V}_n$ and subsequently $\underline{r}_n$.

IMU-derived aiding information can be provided to the RM/IPMs at a maximum 250 Hz rate ($\tau = 4$ ms). If, however, IMU data from the accelerometers are processed at a lower rate, e.g. 10 Hz, then it is necessary to extrapolate the position and velocity estimates between IMU-read times to get best receiver performance. The simulation performs the extrapolation as follows:

The vehicle (antenna) position ($\underline{r}$) at time t_j is given by:

$$\underline{r}_j = \underline{r}_n + \underline{v}_n(t_j - t_n) + \frac{\underline{a}_n}{2}(t_j - t_n)^2 + \frac{\underline{j}_n}{6}(t_j - t_n)^3 \qquad (3\text{-}43)$$

where $\underline{r}_n$ and $\underline{v}_n$ are IMU-derived estimates of vehicle position and velocity at the last IMU-processing time t_n. The estimated acceleration and jerk components at this time are $\underline{a}_n$ and $\underline{j}_n$.

The IMU-derived estimate of vehicle position change between times t and t + T (both between t_n and t_{n+1}) are obtained by using t and t + T in Eq. (3-43), and taking the difference between the resultant position estimates. The resultant expression for the position change $\delta\underline{r}$ for the computation interval T is:

$$\frac{\delta\underline{r}}{T} = \underline{v}_n + \underline{a}_n(t - t_n + \frac{T}{2}) + \underline{j}_n\left[\frac{(t - t_n)(t - t_n + T)}{2} + \frac{T^2}{6}\right]^* \qquad (3\text{-}44)$$

where $\underline{v}_n$, $\underline{a}_n$, and $\underline{j}_n$ represent IMU-derived estimates of vehicle velocity, acceleration, and jerk at the most recent IMU-data processing time t_n. The constant-rate signal applied to the RM/IPM over the interval T to implement the $\delta\underline{r}$ is simply $\delta\underline{r}/T$.*

* Near the end of the study, an algorithm that accounts for the transport lag in the RM/IPM was developed. Results using this algorithm are presented in Appendix A.

To compute $\underline{a}_n$ from the integrating-accelerometer data, the last two measurements are used in the relation:

$$\underline{a}_n = \frac{(1.5\Delta\underline{v}_n - 0.5\Delta\underline{v}_{n-1})}{t_n - t_{n-1}} - \underline{g}_n \qquad (3\text{-}45)$$

where $\Delta\underline{v}_n$ represents the accelerometer-measured velocity change over the time interval from t_{n-1} to t_n, and $\underline{g}_n$ is the average gravitational specific force acting on the vehicle during this period. The jerk $\underline{j}_n$ is obtained simply from the back difference $\underline{a}_n - a_{n-1}$ divided by $t_n - t_{n-1}$.

3.2.2 Velocity-Measurement Error Sources

Several sources of error in the measurement of $\Delta\underline{V}$ were incorporated into the simulation model. Among the errors included were IMU alignment, gyro drift-rate bias, acceleration sensitive drift, accelerometer bias, accelerometer scale-factor, and accelerometer quantization errors.

An important source of error in the IMU-derived velocity information is the uncertainty in the knowledge of the orientation of the instrument package (i.e. accelerometers). It is convenient here to assume that the alignment error is small, e.g. of the order of 1-2 degrees or less, so that it can be represented by a vector angle $\underline{\gamma}_{AL}(t)$. Under these conditions the alignment error can be modeled as

$$\underline{\gamma}_{AL}(t) = \underline{\gamma}_{AL_0} + \int_0^t \underline{\gamma}_{DR}(t)\, dt \qquad (3\text{-}46)$$

where $\underline{\gamma}_{AL_0}$ is the initial alignment error of the inertial package, and $\underline{\gamma}_{DR}(t)$ is the drift-rate of the gyro-stabilized instrument package.

If the coordinate system used for $\underline{\gamma}_{AL}$ and $\underline{\gamma}_{DR}$ in Eq.(3-47) is chosen with its axes parallel to those of the three gyro input

axes, then the components of inertial-package drift rates γ_{DR_i} correspond to the individual-gyro drift rates W_{GY_i}. The individual-gyro drift rate is approximated in the simulation by the relation (Ref. 3-6):

$$W_{GY_i} = k_0 + k_1 f_I + k_2 f_s + k_3 f_s f_I \tag{3-47}$$

where k_0 represents the drift-rate bias, and f_I and f_s are the components of specific force acting along the gyro input and spin axes respectively. The coefficients k_1, k_2, and k_3 correspond to mass-unbalance and anisoelasticity drift-rate terms. Drift-rate errors relating to output-axis specific force f_0, which are normally small, have been omitted from the model along with small terms relating to f_I^2 and f_s^2. The correlation times for all IMU drift-rate error sources modeled have been assumed to be sufficiently large so that bias models can be employed.

The resultant error in the measured velocity change $\underline{e}'_{\Delta V}$ is approximated by the relation

$$\underline{e}'_{\Delta V} = \Delta \underline{V} \times \underline{\gamma}_{AL} \tag{3-48}$$

where $\Delta \underline{V}$ is the measured velocity change over the interval t_{n-1} to t_n, and $\underline{\gamma}_{AL}$ is the average value of $\underline{\gamma}_{AL}(t)$ over this interval computed from Eqs. (3-46) and (3-47). The notation of (×) is used to indicate the vector cross-product operation.

Accelerometer bias and scale-factor errors in the velocity-change measurement $\Delta \underline{V}$ at the IMU read-time t_n are modeled by

$$e''_{\Delta V_i} = \gamma_{ABI_i} \Delta t_I + \gamma_{ASF_i} \Delta V_i \tag{3-49}$$

where the velocity-change measurement error and the sensed velocity change for the i-th accelerometer are denoted by $e''_{\Delta V_i}$ and ΔV_i, respectively. The individual accelerometer bias and scale-factor errors are γ_{ABI_i} and γ_{ASF_i}, and the IMU read-interval is Δt_I. The correlation times for γ_{ABI_i} and γ_{ASF_i} are assumed here to be sufficiently long so that these errors can be treated as time-invariant bias errors.

Accelerometer quantization error is modeled in the following manner. The number of quanta (m_V) in a $\Delta\underline{V}$-component reading (from a given accelerometer) is computed from

$$m_{V_i} = \text{TRUNC}\left(\frac{\Delta V_i}{\ell_q}\right) \tag{3-50}$$

where the operation TRUNC (•) retains only that part of (•) to the left of the decimal point, and the subscript i refers to the i-th accelerometer. The quantization level is denoted by ℓ_q. The actual measured output is thus

$$\tilde{V}_i^* = m_{v_i}\, \ell_q\, \text{SGN}\ (\Delta\tilde{V}_i) \tag{3-51}$$

where the operation SGN(•) means the algebraic sign of (•), i.e. +1 or -1. The remainder, i.e. the difference between $\Delta\tilde{V}_i$ and $\Delta\tilde{V}_i^*$, is saved to accumulate in the next accelerometer reading at time t_{n+1}. It should be noted that this model, which implies a non-destruct-count accelerometer, will provide a random error in the estimate of vehicle velocity of maximum magnitude one quantum.

3.2.3 IMU and Antenna at Different Locations

In the preceding subsections it was assumed that the IMU and receiver antenna were at essentially the same location in the vehicle. If the receiver antenna is displaced from the IMU, then IMU attitude (or attitude rate) measurements may be required for receiver aiding if significant vehicle orientation changes (rotations or vibrations) occur. These measurements make it possible to keep track of antenna position in the presence of vehicle rotations, under the assumed conditions of a rigid structure between IMU and receiver antenna.

The rotational velocity of the receiver antenna with respect to the IMU is given by the relation:

$$\underline{V}_R = \underline{\omega} \times \underline{r}_{IR} \tag{3-52}$$

where $\underline{\omega}$ is the angular velocity of the (rigid) vehicle structure about its center of mass, and the vector $\underline{r}_{IR}$ is the position of the antenna with respect to the IMU. In the absence of rotations and

flexure the IMU-accelerometer measurements would, of course, be sufficient to keep track of antenna motion.

A floated or gimballed IMU is assumed, which provides measurements of the orientation of the vehicle w.r.t. an inertial reference frame at discrete time intervals. To most effectively aid the receiver tracking loops, it is necessary to derive angular-rate information from the IMU angle measurements and use the computed rate $\underline{\omega}$ to obtain RM/IPM input signals as indicated in Eq.(3-52).

A fairly simple model has been assumed for the errors in the IMU angle measurements. It consists of an uncorrelated (random) angle measurement in combination with an orientation-dependent bias error.

A minimum-variance Kalman filter could be used to derive angular-rate estimates $\underline{\omega}$ from the discrete angle measurements $\underline{\Theta}$. For the problem of interest here, for reasons of computation simplicity, a least-squares 5-point fit to either a second-order or third-order polynomial has been used instead. Only the 5 latest angle measurements are used here (taken at τ second intervals).

The angular velocity corresponding to a time at the center of the 5-sample interval is computed from Ref. 3-7 as

$$\omega_c = \frac{1}{2\tau} \sum_{i=1}^{5} W_i' \Theta_i \qquad (3\text{-}53)$$

where ω_c is the angular-rate estimate at the interval center (scalar component), Θ_i is a scalar angle measurement, and τ is the interval between successive angle measurements $(t_i - t_{i-1})$. The relevant weighting factors for the 5-point second-order polynomial fit W_i' are given by Ref. 3.7 as

$$\underline{W}' = (-1,-0.5,0,+0.5,+1)/2.5 \qquad (3\text{-}54)$$

where the -1 is associated with the oldest sample (5th back), and the +1 with the current sample. The current estimate of an angular-rate component ω_n is computed from

$$\omega_n = \omega_c + \frac{2}{\tau} \sum_{i=1}^{5} W_i'' \Theta_i \qquad (3\text{-}55)$$

where ω_c is the center-of-interval estimate from Eq.(3-53). The relevant weighting factors W_i'' from Ref. 3-7 are

$$\underline{W}'' = (+1, -0.5, -1.0, -0.5, +1)/3.5 \qquad (3\text{-}56)$$

To obtain best tracking-loop performance, the angular-rate estimate used for aiding at time t_n is obtained by extrapolating the estimate ω_n (from Eq. 3-55) forward by 2 ms (one-half the RM/IPM processing interval). The center value ω_c is differenced with ω_n to implement the extrapolation.

In concluding this section, a few points should be noted. Insofar as possible the IMU and antenna should be located as close together as possible to minimize the rotational velocity of Eq.(3-52). If there is significant unmonitored bending or flexure in the structure between the IMU and antenna, then the utility of the aiding technique described in this subsection will be diminished. If the angle data are provided at erratically spaced intervals (e.g. not every τ seconds), then the Kalman filter might be better than the polynomial-fit scheme described here.

3.2.4 IMU-Derived Aiding Signals

In the preceding subsections relations have been presented for computing receiver antenna velocity from IMU measurements. The simulation computations to generate appropriate receiver velocity-aiding signals were also presented.

The actual aiding signal required for a given receiver channel, however, is the component of vehicle (or antenna) velocity along the Line-Of-Sight (LOS) from the satellite of interest to the receiver antenna. The mathematical relation for this aiding signal (V_A) is

$$V_A = \underline{V} \cdot \underline{i}_\rho \qquad (3\text{-}57)$$

where the IMU-derived antenna velocity $\underline{V}$ includes both the translational term of Eq.(3-41) and the rotational velocity of Eq.(3-52).

The unit vector $\underline{i}_\rho$ is from the satellite position vector ($\underline{r}_s$) to the receiver-antenna position vector ($\underline{r}$), i.e.

$$\underline{i}_\rho = \frac{\underline{r} - \underline{r}_s}{|\underline{r} - \underline{r}_s|} \tag{3-58}$$

where the changes in $\underline{r}$ are computed by numerical integration of Eqs.(3-41) and (3-52).

3.3 Sampling Rates in IMU-Aided X-Set

3.3.1 General Information

An extremely important characteristic of the X-Set Receiver is that it is basically a sampled-data system, with information being processed at different rates at different parts of the system. To meaningfully simulate the receiver, it is necessary to take this into account, i.e. a continuous-system model will not give correct results except at very low bandwidths. The present section reviews briefly the different sampling operations in the aided-receiver simulation, as indicated in Fig. 3-5.

3.3.2 Carrier Loop

The carrier loop will be discussed first. The tracking-loop correlation signal is processed continuously by the integrate-and-dump circuits. At 4-ms intervals, these networks send out average values of inphase and quadrature signal components for the preceding interval. The integrate-and-dump networks operate synchronously with respect to the data-bit interval (20 ms), so that essentially 5 output-signal samples are computed per data bit. The signal converter, as indicated in Fig. 3-5 uses 5 samples of the averaged inphase and quadrature signals to generate a tracking error at 20-ms intervals.

The tracking-error signal is passed through the proportional path of the tracking network with no delay. There is a delay of 20 ms, however, before the integral-path outputs are sent out. As a result, the tracking-network output (which changes only at 20-ms intervals) will contain integral-path signals delayed 20 ms behind the straight-through signal.

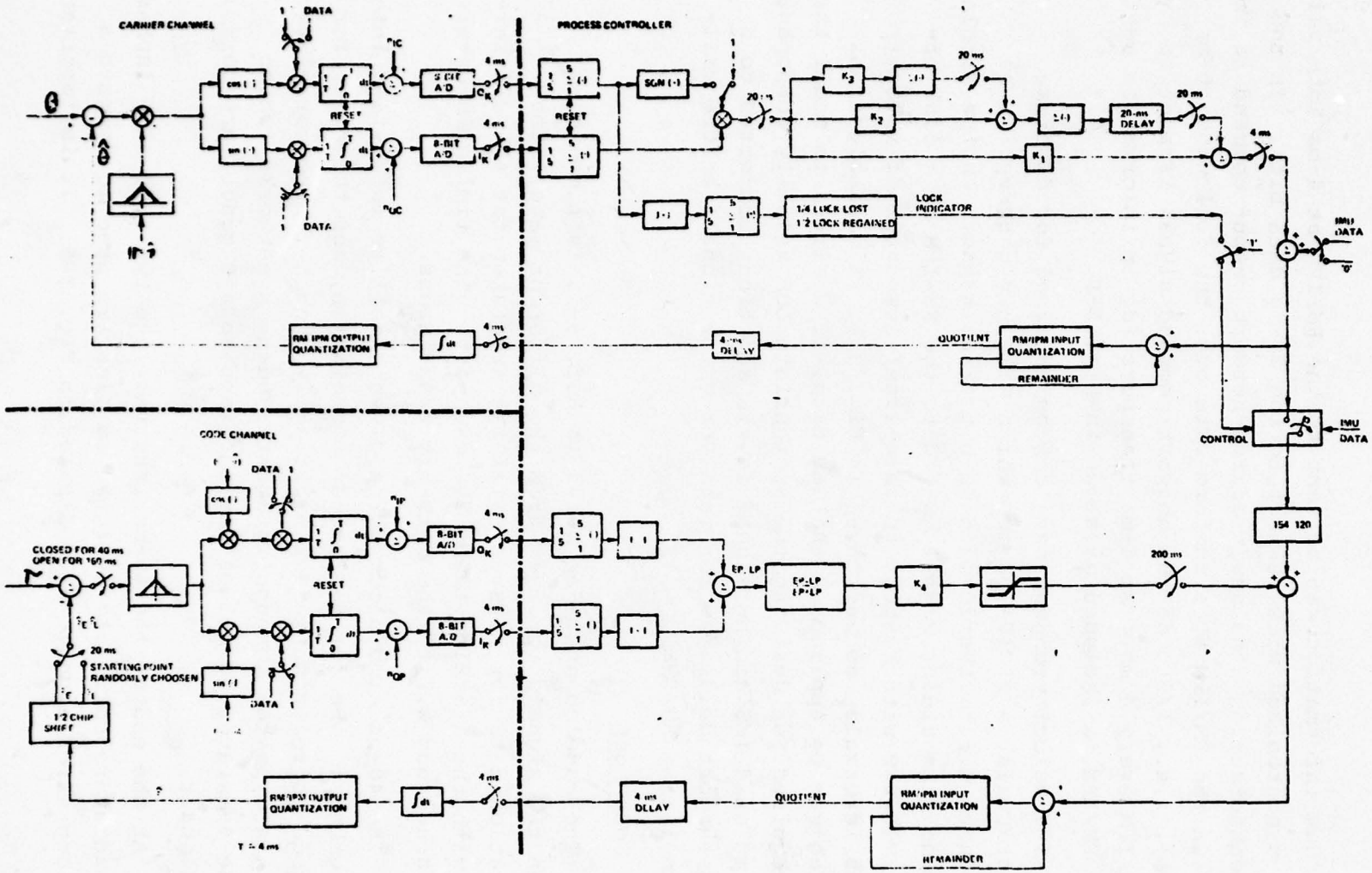

Figure 3-5: Simulation model of Magnavox GPS X-receiver.

New information can be sent to the RM/IPM at 4-ms intervals (again synchronized with respect to the 20-ms data bit). In the current mechanization, the new tracking-network output command is implemented in the RM/IPM at a uniform rate over the following 20-ms interval, i.e., 1/5th of the network command signal is sent to the RM/IPM every 4 ms. At 4-ms transport lag in information sent to the RM/IPM is included as shown in Fig. 3-5.

IMU velocity-change data can be obtained for discrete time intervals, e.g. 10-100 ms, which will not necessarily be synchronous w.r.t. the 20-ms data-bit transitions. In the simulation model the aiding signal is fed to the RM/IPM as a line-of-sight (vehicle with respect to satellite) component of velocity at 4-ms intervals, as indicated in Fig. 3.5. A variable transport lag can be applied to the IMU data, if desired, to model the time required for deriving the appropriate LOS velocity component. The simulated IMU aiding signal is, in addition, subjected to a 4-ms transport delay (as for receiver error signal) before utilization in the RM/IPM.

3.3.3 Code Loop

The code channel, as noted in Ref. 3-1, is time-shared between the signals received from the different satellites. Correlation data for a given satellite are taken for 40-ms intervals, with the starting times 200 ms apart. The timing intervals are synchronous w.r.t. the data-bit transitions.

The 40-ms time block for a given satellite is divided into two segments: one for early-code correlation, and the other for late-code correlation (order arbitrarily chosen). The correlation signals are passed through integrate-and-dump networks, which provide 4-ms average values for the inphase and quadrature correlation signals.

At the end of the 40-ms interval, the two sets of 5 inphase and quadrature correlation-signal samples are used to compute a code-loop error signal, as indicated in Fig. 3-5. It is important

to note here that a new code-loop tracking error signal for a given receiver channel (satellite) is computed only at 200-ms intervals. The error signal is passed through the tracking network without delay and sent ahead to the RM/IPM.

In the current model, a rate signal is then computed for the RM/IPM such that the tracking-network command is implemented in a 4-ms interval. A 4-ms transport lag is included on the command signal to the RM/IPM.

Velocity-aiding information from the receiver tracking loop or the IMU can be provided to the code-loop channel at a much higher rate, as indicated in Fig. 3-5. This type of information provided at 4-ms intervals helps the tracking loop operate properly over the 200-ms intervals between successive code-loop error signal outputs.

SECTION 4

SIMULATION RESULTS

4.1 PROBLEM DEFINITION

Accurate tracking of a high-dynamics input signal requires wide receiver tracking-loop bandwidths. Minimizing the errors introduced by input noise, on the other hand, requires small tracking-loop bandwidths. The conflicting requirements are the root of the tracking-loop design problem.

An IMU is capable of measuring the velocity changes of a vehicle due to non-gravitational forces acting on the vehicle. In addition, the IMU can provide information on the orientation of the vehicle w.r.t. an inertial reference frame. By using an IMU to keep track of receiver-antenna motion (i.e. locating it close by the antenna), it should be possible for the receiver to track the input dynamics with a reduced tracking-loop bandwidth. This in turn will result in a reduced tracking-loop sensitivity to input noise.

The basic problem of interest is the definition of the interface between the receiver and the IMU. The particular receiver is the Magnavox X-Set, and the inertial measurement unit chosen is the AIRS IMU. The key questions are:

(1) The type of information to be passed between the IMU and the receiver, e.g. the IMU-derived aiding commands.

(2) The manner in which data is transmitted between IMU and receiver, e.g. from IMU to code loop directly, or to the carrier loop, or should dedicated microprocessors be used.

(3) Required rates at which data must be transferred between IMU and receiver.

(4) Algorithms necessary for effective utilization of the IMU data, i.e. operations to be performed on the raw measurements and the required smoothing or prediction.

(5) Performance benefits derived from aiding, e.g. smaller noise bandwidths to track given input dynamics.

4.2 SYSTEM DESIGN CONSIDERATIONS

4.2.1 Design-Reference Input Trajectory

The design-reference input dynamics trajectory assumed here is extremely severe. It consists of a jerk pulse of 10 g/s for 0.6 seconds followed by a period of constant acceleration thereafter. It is felt that if the X-set receiver can successfully operate against these dynamics, it will probably be able to handle the typical missile launch-phase dynamics.

4.2.2 Receiver Carrier-Tracking Loop

The tracking accuracy requirement stems from the fact that the baseband output signal from the error detector (correlator plus signal conditioner) is proportional to the sine of the phase-tracking error rather than to the tracking error itself. In order to maintain reasonably constant loop gains under these conditions, it is necessary to limit the tracking errors to about 0.5 radians or less. At the carrier-frequency of 1.6 GHz (wavelength about 0.6 ft.) this corresponds to an error of about 0.05 ft.

The presence of binary-data modulated on the carrier (at 50 b.p.s.) requires that a Costas loop, which is capable of tracking suppressed-carrier signals, be utilized in the carrier tracking system, to remove (demodulate) the data. In the current tracking-loop mechanization, which is described in Ref. 4-1, the end result is an error-detector output proportional to the product of the sine of the phase-tracking error and the sign of the cosine of the tracking error. The tracking error under these conditions must be kept smaller than 90 degrees to avoid abrupt changes in the sign of the error-detector output, which lead to cycle slips and possibly loss of lock. At the carrier frequency of 1.6 GHz this corresponds to an error of about 0.15 feet.

In order to track the high-jerk reference input with a constant steady-state error, the unaided X-set receiver utilizes a

digital tracking network with both single and double integration paths in the carrier tracking loop. The overall tracking loop under these conditions is essentially a third-order system (ignoring sampling and other lags for the moment), which is conditionally stable, i.e. can go unstable for both high and low loop gains. To hold the peak transient error following the 10 g/s input below the desired limit of 0.15 ft, the required single-sided noise bandwidths (B_L) are of the order of 25 Hz or more under ideal conditions. Tracking loop stabilization at these high noise bandwidths (or high natural frequencies) is extremely difficult.

A major factor contributing to the carrier tracking-loop stabilization problem is the computer-throughput problem in the current X-set. The end result is that error-detector data are sent to the tracking network at only a 50-Hz rate, i.e. every 20 ms. This information in effect represents the average tracking error signal for the preceding 20-ms period. The straight-through path output from the network is sent forward to the RM/IPM with no additional significant delay. The integral-path data, however, is delayed by as much as an additional 20 ms, before being sent forward to the RM/IPM. Under these conditions, tracking-loop stability with the existing tracking-loop network is extremely difficult at the high noise bandwidths required for unaided tracking of the high-jerk reference input, e.g. greater than 25 Hz.

Other factors that affect the design and performance of the X-set receiver carrier channel are:

(1) Cross coupling between the code and carrier channels in the signal correlator.

(2) Quantization errors in the RM/IPM.

(3) An additional transport lag of 4 ms in the transmission of data between the tracking network and RM/IPM.

(4) User frequency-reference errors.

(5) Satellite-clock drift, ephemeris errors, and ionosphere-induced propagation velocity changes.

(6) Antenna motion caused by orientation changes of the vehicle (rotations or oscillations about mass center).

A brief discussion of these factors follows next.

The cross coupling between code and carrier channels in effect reduces the carrier tracking-loop gain as the code-loop error is increased. For large code-loop tracking errors this could lead ultimately to loss-of-lock in the carrier loop . In most cases studied here this was not a major problem.

RM/IPM quantization errors are of the order of 1/64 cycle or about 0.01 feet in the carrier loop. Small-amplitude limit-cycle oscillations can be induced in the tracking-loop by this error source but, in general, it has not been found to be a major problem.

The 4-msec transport lag on the data from tracking network to RM/IPM is small in comparison to the 20-ms sampling interval of the error-detector data, and the 20-ms transport delay on the integration-path data. Accordingly, its net effect is small.

User frequency-reference drift errors are a more serious problem. The acceleration-sensitive component in particular is significant for user accelerations of several g's, as would be encountered in typical missile launch maneuvers. The receiver carrier channel must have sufficient bandwidth to track this uncompensated frequency drift (which is typically 1 part in 10^9 per g).

Satellite-clock drift, ephemeris errors, and ionosphere-induced propagation velocity changes also pose lower limits on carrier-loop tracking bandwidth. It is felt, however, that the more stringent requirements, i.e. the larger minimum bandwidth, will be dictated by the user-clock acceleration disturbance rather than by these other error sources.

Rotational maneuvers of the vehicle (missile) also place lower bounds on the permissible receiver tracking-loop bandwidth.

By utilizing an IMU as an aiding device, the effective lever arm of the rotational disturbance is reduced to the distance between the IMU (not the vehicle center of gravity) and antenna.

4.2.3 IMU Aiding System

The IMU is capable of providing accurate information on non-gravitational-force induced velocity changes of the vehicle in which it is mounted. It can also provide accurate orientation reference data.

The basic IMU measurement is velocity change over a finite read interval or, in effect, average vehicle acceleration (from non-gravitational forces, of course). To utilize this information for aiding the receiver, the velocity-change data (with estimated measurement errors removed) must be combined with an estimate of the gravitational force on the vehicle, and then used to derive the component of vehicle (or receiver-antenna) velocity along the line-of sight from the receiver antenna to the satellite of interest. Since, at best, the IMU provides vehicle or antenna velocity-change information, the receiver's tracking loop must always have sufficient bandwidth to track out user frequency-reference and other disturbance inputs to the overall system.

The fact that IMU-derived velocity data are available only at discrete times and with possible processing delays also present, makes the aiding process more difficult. To derive the maximum benefit from the aiding data under these conditions, it is desirable to extrapolate the aiding-velocity estimates between successive update times unless new data can be provided directly at very high rates (e.g. 100-200 Hz). The extrapolation process can be based on previous IMU velocity-change measurement data.

If the IMU is displaced a significant distance from the receiver antenna, e.g. on the order of a few feet or more, then velocity estimates derived from IMU-accelerometer data alone will not properly describe the receiver-antenna motion if vehicle rotations occur. Under these conditions the rotational-velocity of the antenna with respect to the point at which the IMU is located can be deter-

mined from IMU-derived attitude data (assuming a rigid structure between the IMU and antenna), and a better aiding-velocity estimate can be obtained.

Accelerometer scale-factor, IMU alignment, gyro drift-rate bias, and accelerometer bias errors will all introduce errors into the IMU-derived aiding signals. The receiver tracking loop must have sufficient bandwidth to track these errors to acceptable accuracy in order to obtain maximum benefit from the IMU aiding. Velocity-readout noise from the IMU will introduce jitter on the RM/IPM output, but this should not be a major problem with the high-accruacy IMU considered here.

IMU-angle readout noise will limit the accuracy to which rotational-velocity estimates can be made. Velocity-estimate extrapolation may be desirable for best accuracy, depending on the angle-measurement data rate and the frequency content of the angular rotations. The extrapolation process here will likely be more sensitive to noise than with the accelerometer data, since the raw measurement is angle (i.e. position) rather than velocity change (i.e. average acceleration). In the application of interest here, on the other hand, it is expected that the IMU will be close to the receiver antenna, which will minimize the rotational-velocity effect.

4.3 PERFORMANCE-EVALUATION DATA

The presented data will consist primarily of:

1) Carrier-loop tracking-error time histories for various input signals, e.g. the design-reference high-jerk trajectory, a step change of input phase (antenna position), user frequency-reference drift caused by the effects of acceleration experienced during high-jerk trajectory.

2) Curves of maximum or r.m.s. tracking error as a function of single-sided tracking-loop noise bandwidth for a variety of different assumed conditions.

3) Tracking performance, i.e. successful track or loss of lock, v.s input C/N_0 levels for a limited number of Monte-Carlo runs using the high-jerk reference trajectory as an input signal.

4.4 NOISE-BANDWIDTH CALCULATION

It is appropriate here to discuss briefly the "noise bandwidth" as utilized in the study results. The input noise to the tracking system can reasonably be assumed to be white over the tracking-loop frequency band of interest, e.g. see Refs. 4-2 to 4-4. If the tracking-loop can be modeled as a linear continuous system with a closed-loop frequency-response function $H(\omega)$, then the response of the tracking-loop to the input noise is given by:

$$\sigma_0^2 = \frac{1}{2\pi}\int_0^\infty S(\omega)\,|H(\omega)|^2\,d\omega \qquad (4\text{-}1)$$

where the variance of the output σ_0^2 is in units of power (e.g. ft^2 or rad^2), and the input spectral density $S(\omega)$ is in units of power/Hz. The angular frequency ω is in rad/sec, and the notation $|(\ )|$ indicates the magnitude of $(\ )$ is used.

It is convenient to rewrite Eq.(4-1) as

$$\sigma_0^2 = S_i\,B_n^* \qquad (4\text{-}2)$$

where S_i is the constant input-noise spectral density (single-sided). The single-sided noise bandwidth B_n^* is then given by:

$$B_n^* = \frac{1}{2\pi}\int_0^\infty |H(\omega)|^2\,d\omega \qquad (4\text{-}3)$$

where the integral is w.r.t. angular frequency in rad/sec, but the units of B_n^* are Hz.

Assume for the moment that the carrier tracking loop can be modeled as a continuous, linear, 3rd-order system with an open-loop frequency-response function from error detector to tracking-loop output of the form

$$\frac{\theta_0}{e} = \frac{\omega_0^3}{s^3} + \frac{a\omega_0^2}{s^2} + \frac{b\omega_0}{s} \qquad (4\text{-}4)$$

where θ_0 is the tracking-loop output, e is the error-detector output, and s is the Laplace-transform variable d/dt. The constants a, b, and ω_0 are tracking-loop parameters, with ω_0 referred to as the closed-loop natural frequency. For a system as described by Eq.(4-4), the closed-loop single-sided noise bandwidth is given by Ref. 4-5.

$$B_n^* = \left[\frac{a\,b^2 + a^2 - b}{4\,a\,b - 4}\right]\omega_0 \qquad (4\text{-}5)$$

where ω_0 is in rad/sec, and B_n^* is in Hz.

If the parameters a and b are both set at 2, then a Wiener-design tracking loop is obtained, which minimizes integrated-square tracking error and also peak-transient tracking error for a specified noise bandwidth with a step acceleration input (i.e. ramp in frequency). If, on the other hand, a is set at 3.8 and b at 3.6, then a Mallinckrodt-design tracking loop is obtained (Refs. 4-6 and 4-7), whose closed-loop poles and zeros are all equal. This latter design gives small, integrated-square tracking errors and smaller peak-transient tracking errors for a specified noise bandwidth than the Wiener design with a step velocity input (i.e. step in frequency).

Under actual conditions, the simple model of Eq.(4-4) is reasonable for the carrier loop only at low noise bandwidths, e.g. $B_n < 3$ Hz, because of the sampling process (50 Hz) and the transport lag on integral-path data (20 ms). Under these conditions a closed-loop calculation of noise bandwidth analagous to Eq.(4-5) is possible (see Ref. 4-8) but the resultant equations are extremely complicated and not illuminating.

The approach adopted here was to determine "noise bandwidth" as given in Eq.(4-2) by direct simulation, linearizing the error detector but otherwise including all sampling processes and transport delays. Quantization errors, A/D conversion errors, and frequency-reference noise must, of course, be excluded here to obtain meaningful results. The simulation-determined noise bandwidths are given in Table 4-1 for several different tracking-loop gain sets corresponding to Mallinckrodt and Wiener designs. Also included for comparison are the idealized noise bandwidths from Eq.(4-5). For convenience here, the tracking-loop frequency-response function of Eq.(4-4) is rewritten as

$$\frac{\theta_0}{e} = \frac{c_1}{s} + \frac{c_2}{s^2} + \frac{c_3}{s^3} \qquad (4\text{-}6)$$

where the relationship between the constants c_1, c_2, and c_3, and the parameters a, b, and w_0 of Eq.(4-4) can be determined by comparison of Eqs.(4-4) and (4-6).

4.5 UNAIDED-SYSTEM SIMULATION RESULTS

4.5.1 General Information

As a starting point, it is useful to examine carrier-tracking loop performance under the highly idealized conditions where:

(1) No input noise is present

(2) No quantization or A/D conversion errors are included

(3) No drift or other noise present in either the receiver or a satellite frequency references

Table 4-1: Noise bandwidths.

Network Type	B_n^* - Theoretical (Hz)	B_n - from sim. (Hz)	Gain Values		
			Prop.	Integ.	2-Integ.
Wiener	1	0.9	2.4	2.9	1.7
	2	1.9	4.8	5.8	14
	5	4.8	12.1	72	274
	6	7.3	14.4	104	376
	8	11.2	19.2	184	885
Mallinckrodt	1	0.9	3.0	2.7	0.6
	3	3.1	9.1	24.3	16.2
	4	4.6	12	43	38
	6	6.8	18	97	130
	8	10.7	24	173	307
	10	13.8	30	270	601
	12	20.0	36	390	1040
	14	25.0	42	530	1650
	18	43.2	55	877	3507

NOTE: (1) Theoretical values assume no transport or sampling delays present

(2) Simulation-determined values include all receiver transport and sampling delays

(4) The tracking-error detector is linearized, i.e. the output signal is proportional to the tracking error.

The 50-Hz sampling-rate of error-detector output signal, and the 20-ms transport lag on tracking-network integration-path data, on the other hand, are both included here.

4.5.2 Tracking Errors for High-Jerk Input

The peak-transient tracking errors for the high-jerk input trajectory under these conditions are presented in Fig. 4-1 as a function of single-sided noise bandwidth B_n (in Hz)*. For convenience a logarithmic scale is used on both the horizontal and vertical axes. The units of tracking error here are in feet (λ = 0.6 feet). To approximately convert the tracking errors to radians (at the frequency of 1.6 GHz) the vertical-axis numbers on Fig. 4-1 are simply multiplied by a factor of 10.

Two different curves are shown in Fig. 4-1, corresponding to two different tracking-network gain-selection procedures. In one case the parameters a and b of Eq. (4-5) are both set at 2, corresponding to an idealized Wiener design. In the other case, a and b were set at 3.8 and 3.6, corresponding to an idealized Mallinckrodt design.

The horizontal line in Fig. 4-1 at an error of 0.15 feet (about 90 degrees) represents the point at which the Costas tracking-loop will start to slip cycles or lose lock, because of the non-linear error-detector characteristic. In non-idealized situations with input noise and other disturbances present, it is desirable to limit the peak transient error to a value substantially smaller than 0.15 ft., e.g. 0.05 ft., about 30 degrees.

The noise bandwidth (B_n) used in Fig. 4-1 is single-sided, and determined by simulation (as described in Sec. 4.4) for the

*The notation B_n refers to the simulation-determined noise bandwidth, whereas B_n^* is the theoretical idealized-condition value (linearity and continuous system assumed with no transport lags).

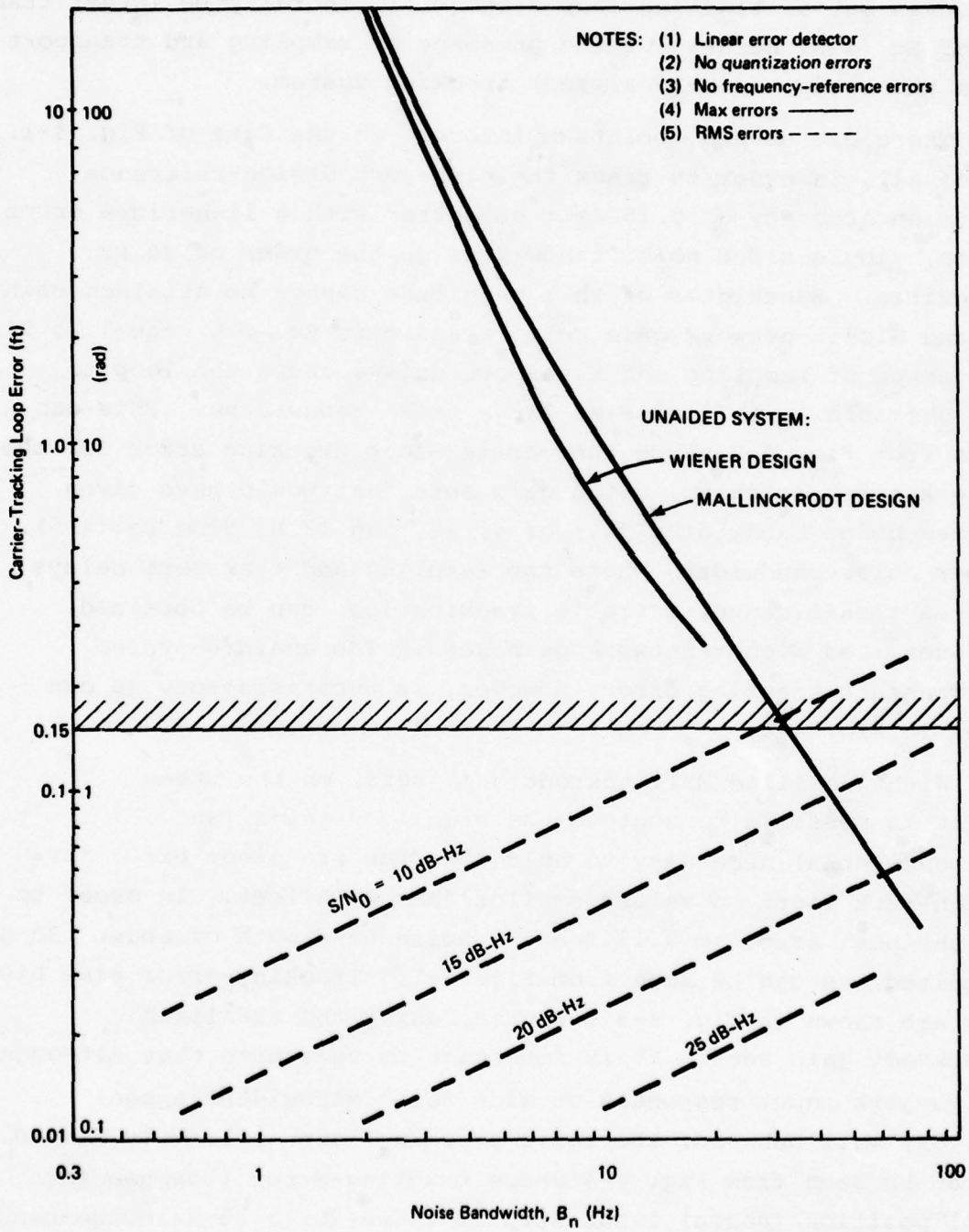

Figure 4-1. Carrier tracking errors for high-jerk trajectory.

chosen tracking-loop parameter sets (a, b, ω_0 or c_1, c_2 and c_3). It should be noted that the simulation-determined noise bandwidths for a given set of tracking-loop gains will generally be larger than those of Eq.(4-5) because of the presence of sampling and transport lags in the actual (non-idealized) tracking system.

There are several points of interest in the data of Fig. 4-1. First of all, in order to track the high-jerk design-reference input to an accuracy of 0.15 feet or better with a linearized error detector, single-sided noise bandwidths on the order of 30 Hz. are required. Bandwidths of this magnitude cannot be attained using idealized Wiener-network gain sets (a and b in Eq. 4-5 equal to 2). The presence of sampling and transport delays cause the loop to become unstable in this case at large noise bandwidths. This can be seen from Fig. 4-2 where the carrier-loop tracking error for the high-jerk input is shown, using gain sets that would have given idealized noise bandwidths (B_n^*) of 4, 10, and 12 Hz from Eq.(4-5). At lower noise bandwidths where the sampling and transport delays have less significance, a stable tracking loop can be obtained using idealized Wiener-network gain sets. The unaided-system peak-transient tracking error, however, is unsatisfactory as can be seen in Fig. 4-2.

With idealized Mallinckrodt gain sets, on the other hand, it is possible to achieve the high loop gains (and noise bandwidths) necessary to hold the peak transient error for the high-jerk input to values smaller than 0.15 feet. In order to limit the peak error to 0.15 feet, a noise bandwidth of about 30 Hz is required, as can be seen from Fig. 4-1. Tracking-error time histories are shown in Fig. 4-3 for cases using the idealized Mallinckrodt gain sets. It is important to recognize that although the high-jerk input responses at wide noise bandwidths appear relatively well behaved, the basic tracking loop is lightly damped. This can be seen from Fig. 4-4 where tracking-error response for a small position (phase) input step is shown for a 32 Hz noise-bandwidth. The initial peak overshoot is extremely large, but the error damps out in a relatively short time.

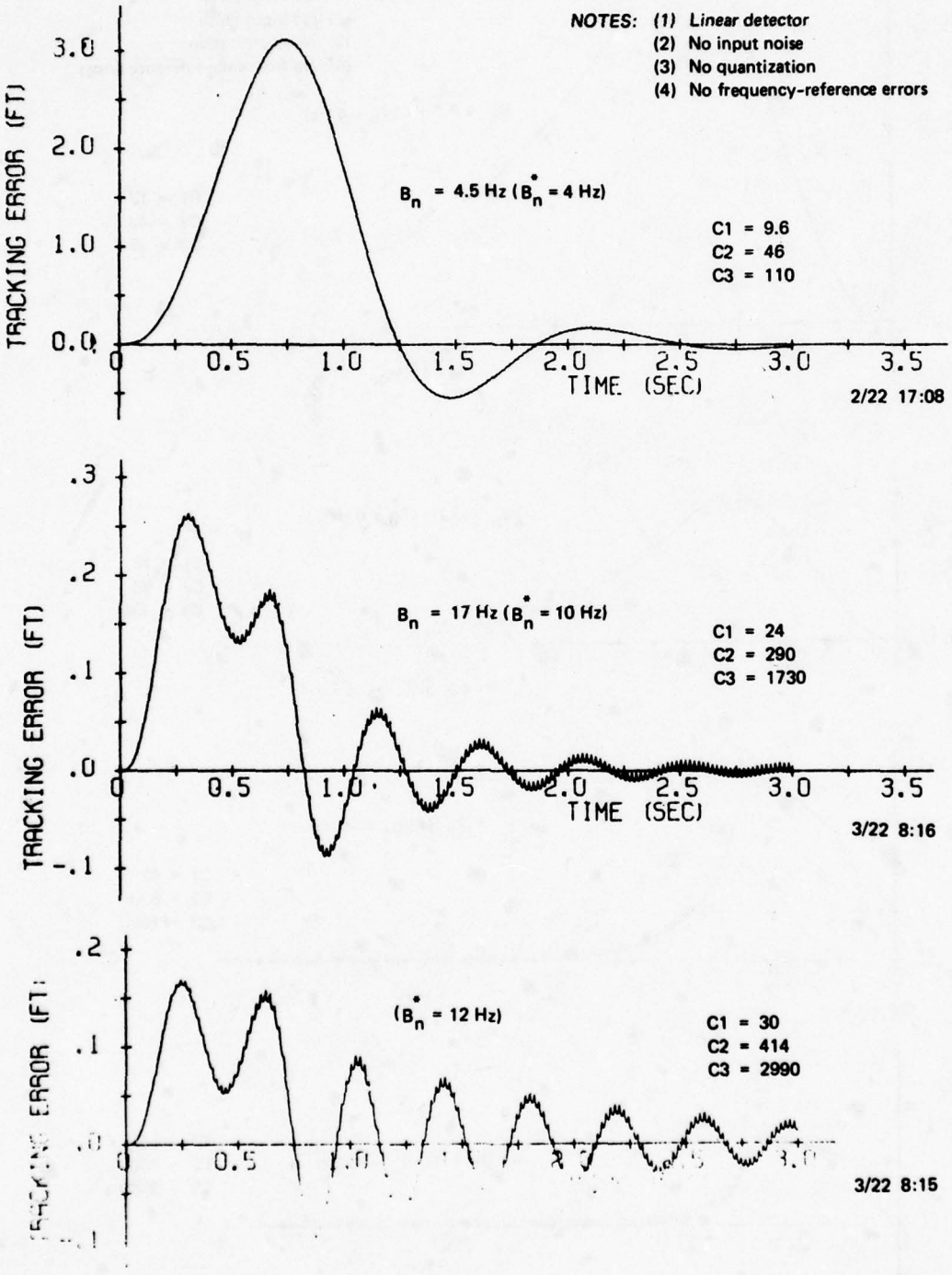

Figure 4-2. Carrier-loop errors for high-jerk trajectory unaided system - Wiener design.

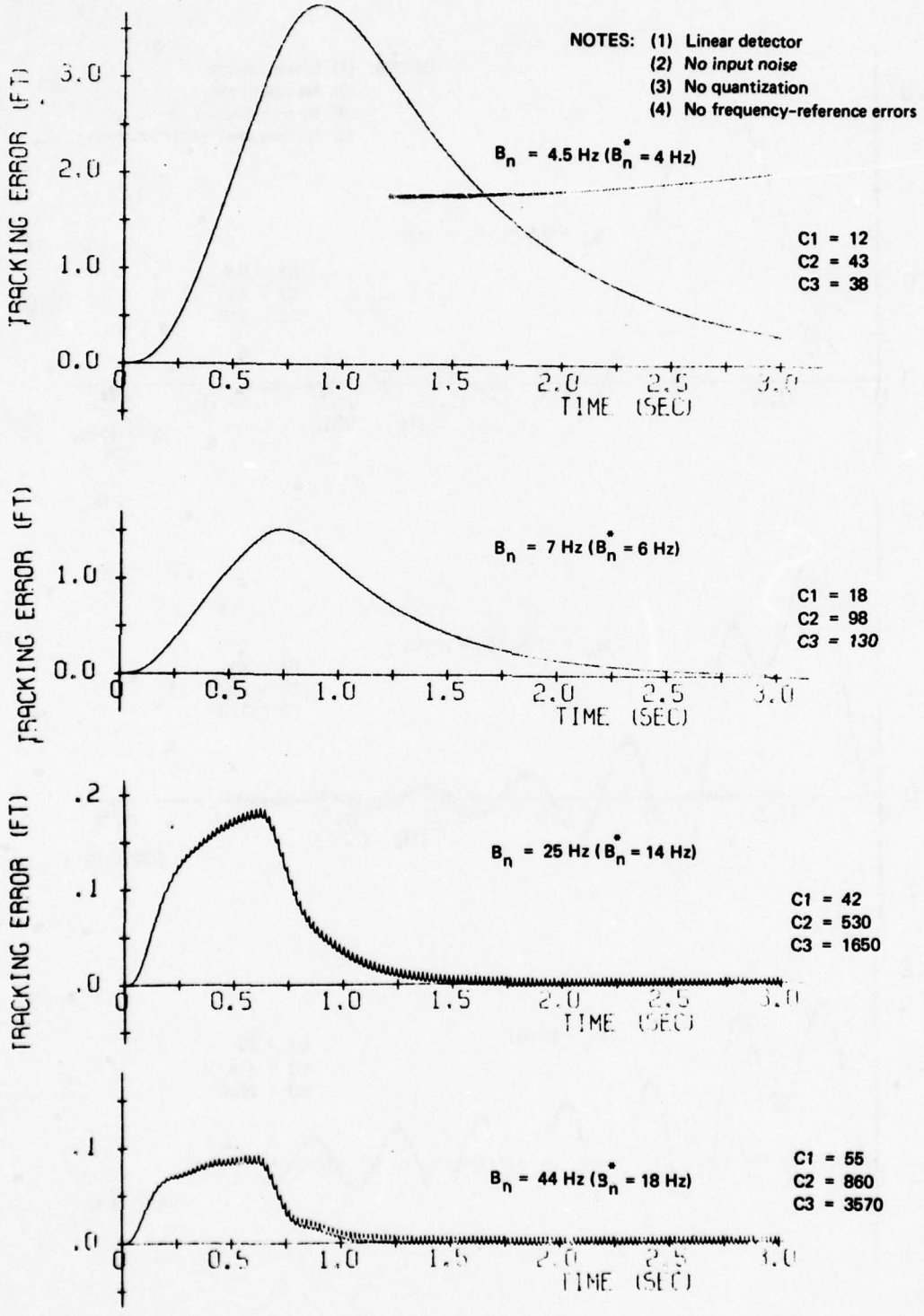

Figure 4-3. Carrier-loop errors for high-jerk trajectory unaided system - Mallinckrodt design.

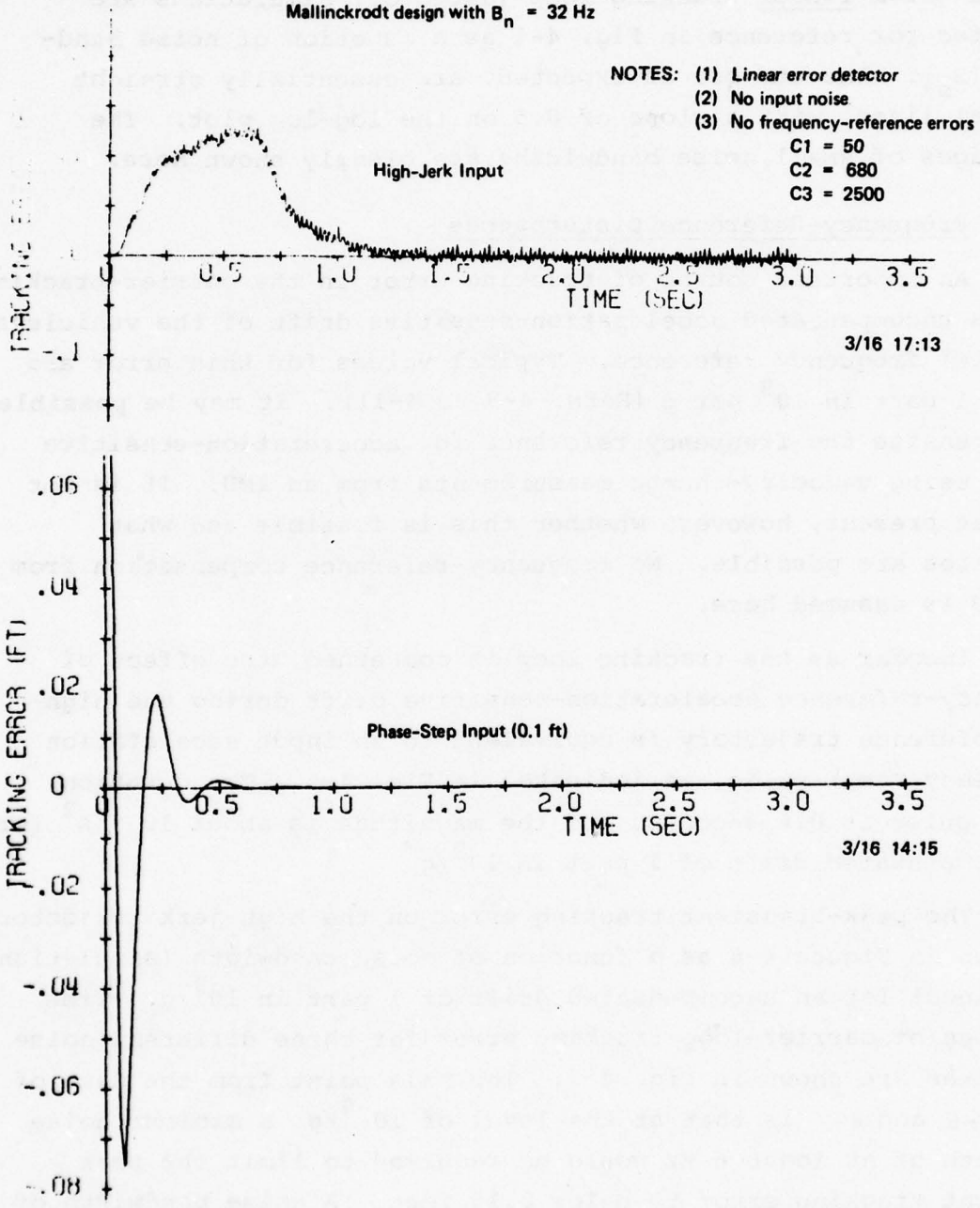

Figure 4-4. Carrier-loop errors for phase-step and high-jerk input.

4.5.3 Input-Noise Response

The r.m.s. tracking errors for various values of C/N_0, as obtained from linear tracking-loop (detector) simulations are presented for reference in Fig. 4-1 as a function of noise bandwidth (B_n). The curves, as expected, are essentially straight parallel lines, with a slope of 0.5 on the log-log plot. The advantages of small noise bandwidths are clearly shown here.

4.5.4 Frequency-Reference Disturbances

An important source of tracking error in the carrier-tracking loop is uncompensated acceleration-sensitive drift of the vehicle's (missile) frequency reference. Typical values for this error are about 1 part in 10^9 per g (Refs. 4-9 to 4-11). It may be possible to compensate the frequency reference for acceleration-sensitive drift, using velocity-change measurements from an IMU. It is not known at present, however, whether this is feasible and what accuracies are possible. No frequency-reference compensation from the IMU is assumed here.

Insofar as the tracking loop is concerned, the effect of frequency-reference acceleration-sensitive drift during the high-jerk reference trajectory is equivalent to an input acceleration (frequency ramp) pulse, as indicated in Fig. 4-5. The duration of the pulse is 0.6 seconds, and the magnitude is about 10 f/s^2 for an uncompensated drift of 1 part in $10^9/g$.*

The peak-transient tracking error on the high-jerk trajectory is shown in Figure 4-6 as a function of noise bandwidth (simulation determined) for an uncompensated drift of 1 part in $10^9/g$. Time histories of carrier-loop tracking error for three different noise bandwidths are shown in Fig. 4-7. The main point from the data of Figs. 4-6 and 4-7 is that at the level of $10^{-9}/g$, a minimum noise bandwidth of at least 6 Hz would be required to limit the peak transient tracking error to below 0.15 feet. A noise bandwidth of

---

* As in all the simulation runs evaluating the effects of translational motion on the tracking loops, the high-jerk trajectory is line-of-sight to the satellite.

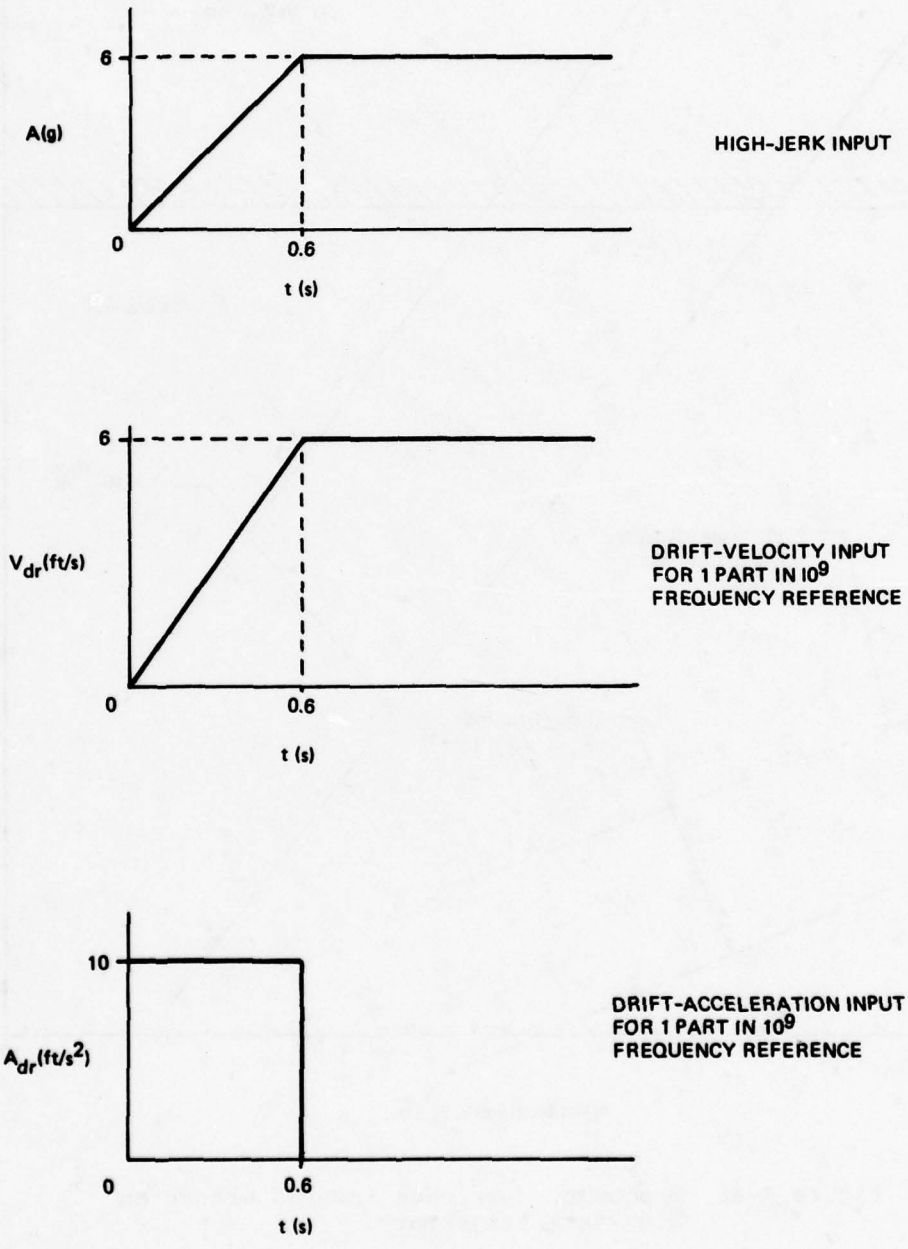

Figure 4-5. Acceleration-sensitive frequency-reference drift during high-jerk trajectory.

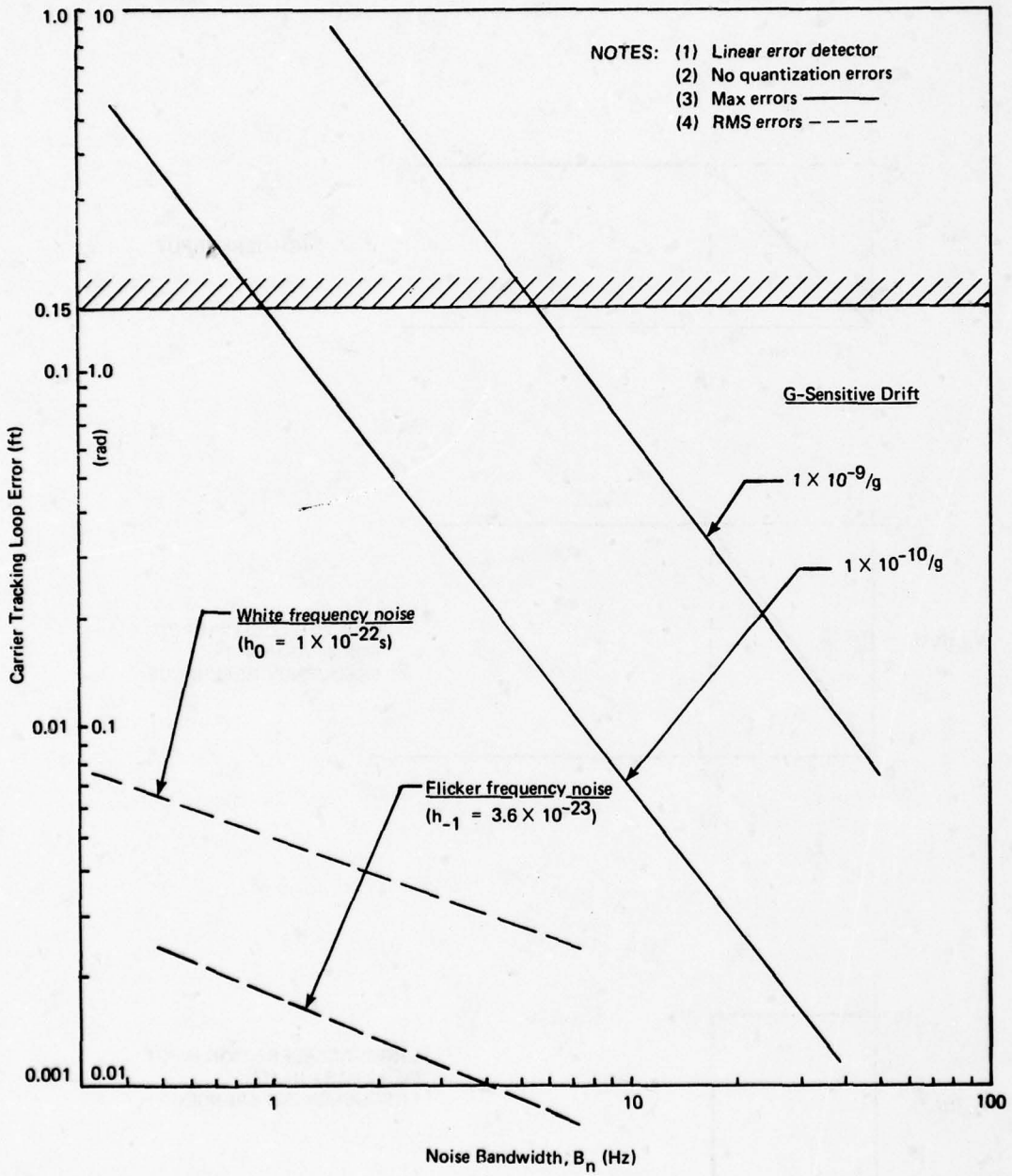

Figure 4-6. Frequency-reference induced errors on high-jerk trajectory.

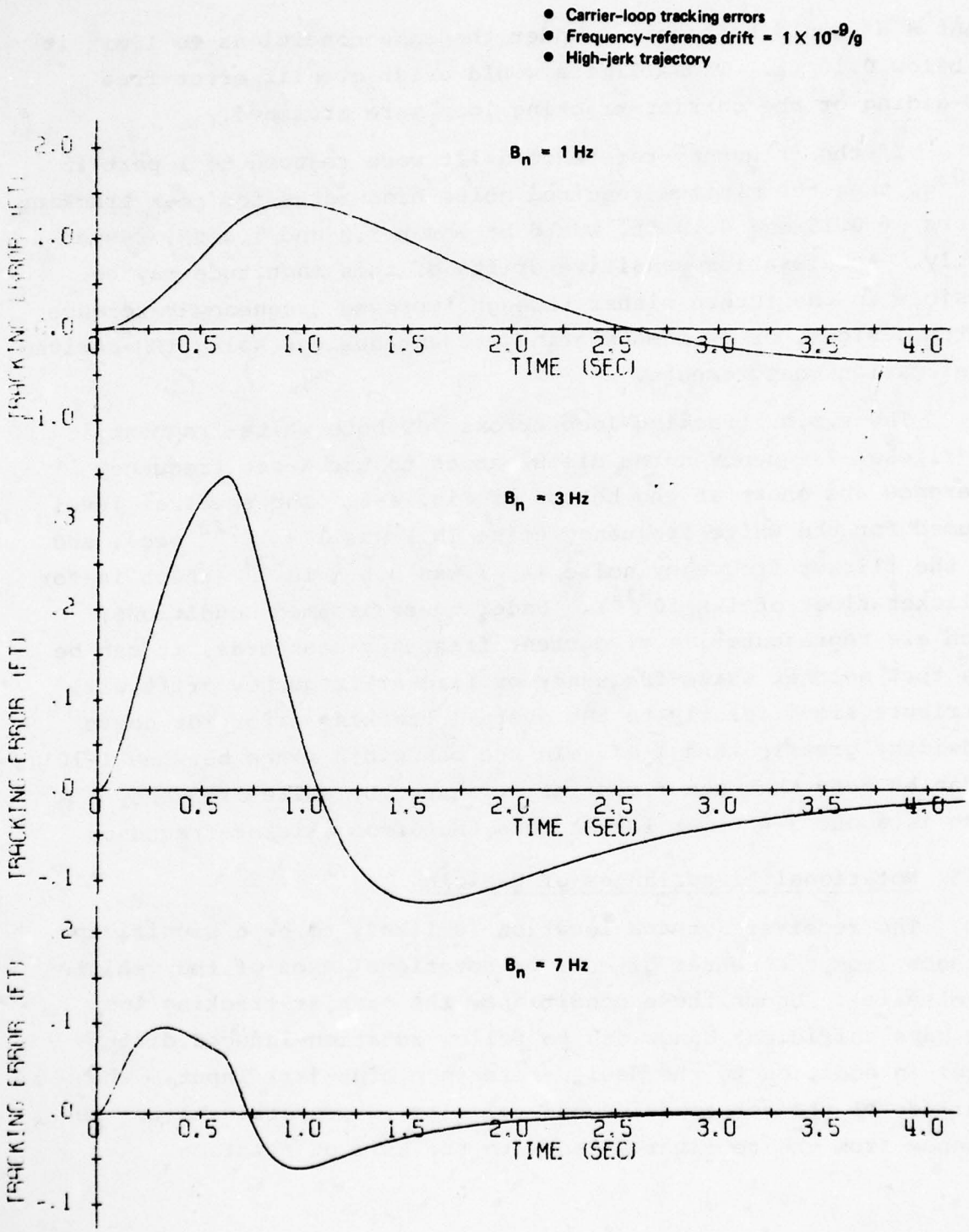

Figure 4-7. Acceleration-sensitive frequency-reference drift.

about 8 Hz would be required under the same conditions to limit it to below 0.10 ft. These limits would exist even if error-free IMU-aiding of the carrier-tracking loop were attained.

If the frequency-reference drift were reduced to 1 part in 10^{10}/g, then the minimum required noise bandwidths for peak tracking errors of 0.15 and 0.10 ft. would be about 1.0 and 1.4 Hz, respectively. Acceleration-sensitive drifts of this magnitude may be possible in the future either through improved frequency-reference system designs, or by compensating present designs using IMU-derived acceleration measurements.

The r.m.s. tracking-loop errors for both white-frequency and flicker-frequency noise disturbances to the X-set frequency reference are shown at the bottom of Fig. 4-6. The spectral level assumed for the white frequency noise (h_0) was 1×10^{-22} sec., and for the flicker frequency noise (h_{-1}) was 3.6×10^{-23} (which is for a flicker floor of 1×10^{-11}). Under these assumed conditions, which are representative of current frequency standards, it can be seen that neither white-frequency or flicker-frequency drift will contribute significantly to the overall tracking error for noise bandwidths greater than 1 Hz. In the bandwidth range between 1-10 Hz it can be seen that the r.m.s. error caused by white-frequency noise is about 3-4 times larger than that from flicker-frequency.

4.5.5 Rotational Disturbances of Vehicle

The receiver antenna location is likely to be a significant distance from the center of mass or rotational axes of the vehicle (or missile). Under these conditions, the carrier-tracking loop must have sufficient bandwidth to follow rotation-induced disturbances in addition to the design-reference high-jerk input. The magnitude of the rotation-induced velocity is proportional to the distance from the receiver antenna to the axis of rotation.

The importance of vehicle rotations on tracking-loop performance is, of course, a function of the magnitude and rates of change of the angular motions. For the purposes here, a sinusoidally varying rotation has been assumed, with a peak-to-peak amplitude of 1.4 degrees at a frequency of about 1.1 Hz. This particular trajectory provides maximum angular velocities of about 5 deg/sec and maximum angular accelerations of about 0.5 rad/s^2.

The r.m.s. tracking error for the unaided carrier loop is shown in Fig. 4-8 as a function of tracking-loop noise bandwidth. Receiver-antenna locations of 2 and 5 feet from the axis of rotation are assumed here. A linear error detector is used, as mentioned earlier, so that the results for other displacements can be obtained by a simple scaling of the data, i.e. the errors for a 1-ft. displacement would be 1/5 of those for a 5-ft. displacement. The peak transient errors for these cases are about 1.4 times as large as the rms errors.

At very low noise bandwidths, e.g. less than 2-3 Hz, the unaided tracking loop is not able to accurately follow the assumed input motion. As the noise bandwidth is increased to several Hz, the loop begins to track the input signal, as indicated by the reduced tracking errors. Large noise bandwidths, on the other hand, are not desirable since the variance of the errors induced by input noise are proportionately increased.

4.6 AIDED-SYSTEM SIMULATION RESULTS

4.6.1 General Information

IMU aiding of the carrier loop will, as mentioned earlier, permit high-dynamics inputs to be tracked with lower noise bandwidths than possible in an unaided system. The IMU, of course, only measures the components of the input signal resulting from vehicle motion. Error sources such as receiver frequency-reference drift and uncompensated satellite ephemeris or frequency-reference drift will, of course, have to be tracked out by the carrier loop without IMU assistance. Likewise, errors or delays in the IMU-derived data must be tracked out by the carrier loop.

NOTES: (1) θ_m = 1.4° (peak-to-peak)
(2) f = 1.1 Hz
(3) Linear error detector
(4) No quantization or frequency-reference errors

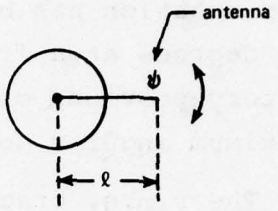

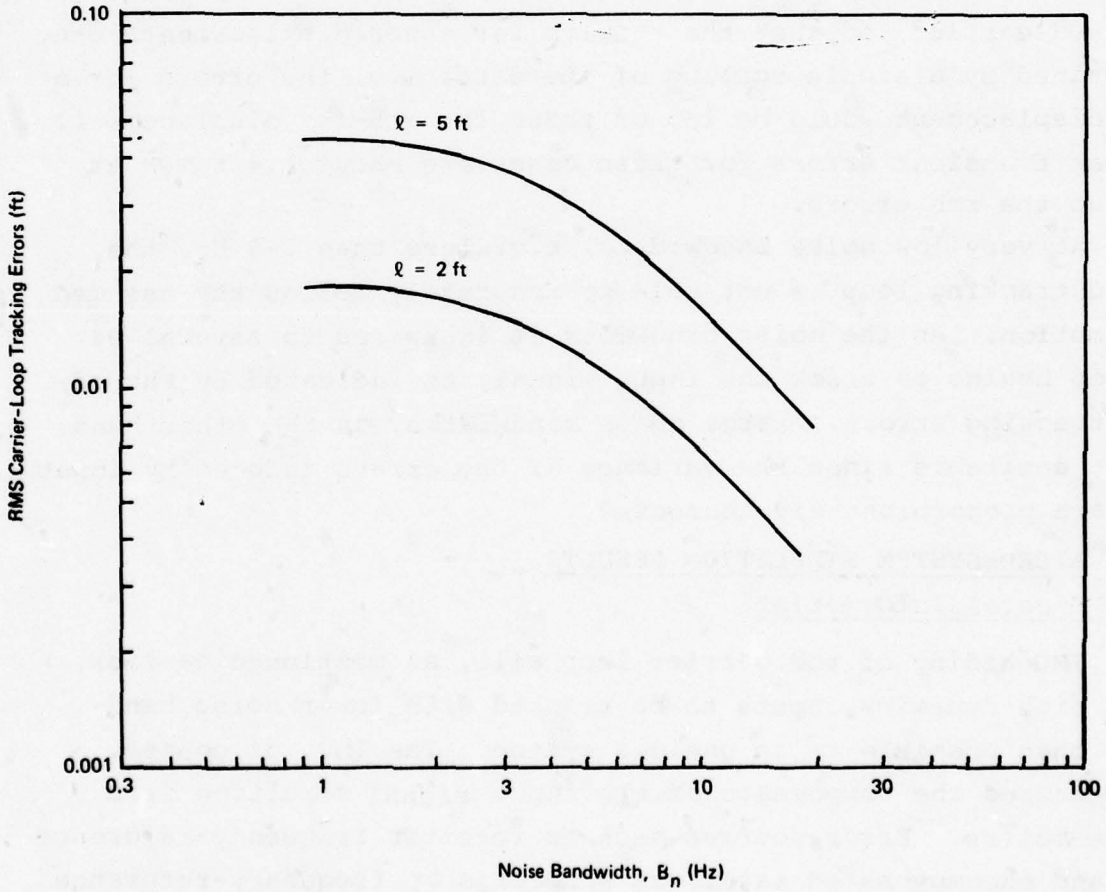

Figure 4-8. Carrier tracking errors for rotational inputs Unaided system.

The tracking-loop RM/IPM, as noted earlier in this report, can accept input commands, i.e. desired changes in phase, at 4-msec intervals. Accordingly, to make best use of the IMU-derived aiding data, position-change predictions are made over the intervals when no data are provided, possibly using a dedicated microprocessor. These predictions, as mentioned previously, are computed from the preceding values of the velocity-change measurements. The end result is that aiding information is provided to the RM/IPM at 4-ms intervals, even though the new IMU measurements may be processed at a lower rate.

4.6.2 High-Dynamics Inputs

The peak-transient tracking errors for the IMU-aided carrier loop are presented in Fig. 4-9 for the design-reference high-jerk input signal as a function of tracking-loop noise bandwidth. Two specific cases are considered here: one with IMU-derived aiding data provided at 100-ms intervals, and the other with IMU data provided more frequently at 10-ms intervals.* For convenience and to facilitate extrapolation of results, a linear error detector has been assumed. Also, for clarity, IMU errors, input noise, and frequency-reference drift are not included in these particular data.

There are several points of interest to be seen from the data of Fig. 4-9. First of all, with IMU data provided at 100-ms intervals, a 1-sided noise bandwidth of about 1.7 Hz is required to limit the peak transient tracking error to a value of about 0.15 ft. (the desired maximum value to avoid loss of lock). If IMU-aiding data is provided more frequently at 10-ms intervals, then the required minimum noise bandwidth is about 1.2 Hz for the same desired peak tracking error.* With error-detector nonlinearities and frequency-reference error included, somewhat larger tracking-loop bandwidths will, of course, be required.

*Near the end of the study, an algorithm that accounts for the transport lag in the RM/IPM was developed. Using this algorithm a significant reduction in peak-tracking error was obtained by increasing the IMU-aiding data rate from 10 Hz to 100 Hz. Results using this algorithm are presented in Appendix A.

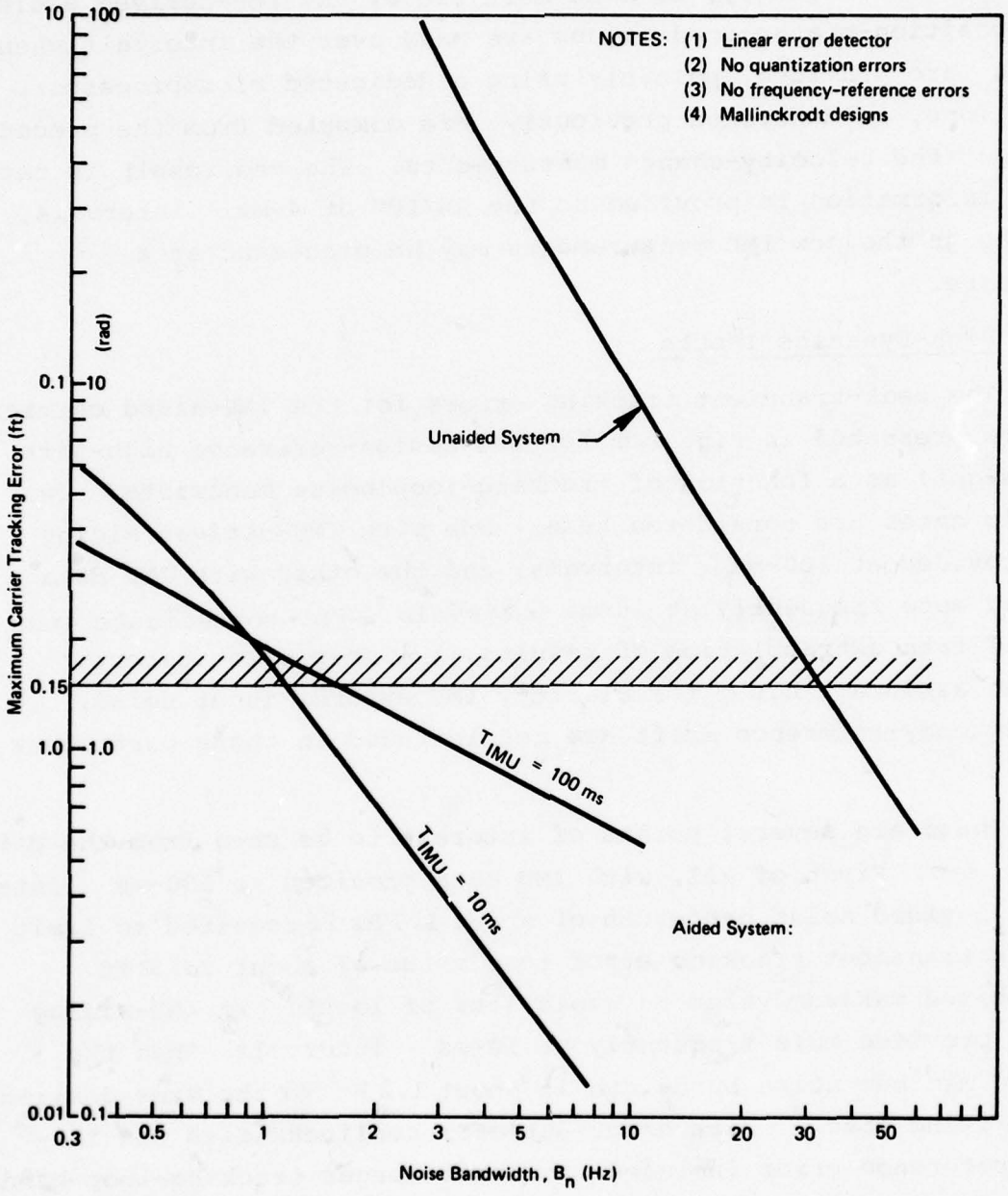

Figure 4-9. Maximum carrier tracking errors, IMU-aiding for high-jerk trajectory.

In order to properly interpret the results of Fig. 4-9 two important points should be noted. First of all, for most effective aiding, the IMU-derived information must get to the VCO input point (where it can reduce the effective input dynamics) with a minimum delay. In this regard, computation delays in the IMU-data processing and transmission to the RM/IPM can limit the ability of the IMU to aid the receiver. Secondly, the algorithm used to extrapolate (i.e. predict) aiding signals in between IMU-data processing times is extremely important, particularly at low IMU-data rates such as 10 Hz (100-ms intervals). In the problem of interest here, for example, a 3rd-order extrapolation algorithm including all terms up to jerk, provides better performance than a 2nd-order algorithm including only terms up to acceleration.

As a result of the above-mentioned computation lags and extrapolation-algorithm imperfections, errors were introduced into the IMU-aiding process (in addition to those caused by the basic instrument errors and finite sampling rate). These errors must ultimately be tracked out by the receiver and, hence, place lower limits on the permissible tracking-loop noise bandwidths. With large noise bandwidths, as can be seen in Fig. 4-9 the peak-transient tracking errors for the aided systems are reduced, because of the greater tracking capability of the receiver.

It is interesting to note that in the cases shown in Fig. 4-9 the aiding-algorithm extrapolation errors tended to cancel in part the errors caused by delays in the IMU-aiding data. Under these conditions, the data indicate slightly smaller peak-transient errors with a 10-Hz update-rate than with a 100-Hz rate at very low noise bandwidths (e.g. 0.3 Hz). With a more sophisticated extrapolation algorithm, however, or with all IMU-data processing delays (and other errors) eliminated, the 100-Hz update-rate will provide better performance than the 10-Hz update-rate at all noise bandwidths.

Time histories of carrier-loop tracking errors are presented in Figs. 4-10 and 4-11 for the same assumed conditions as in Fig. 4-9 i.e. linear error detector and no noise or other disturbance inputs.

NOTES: (1) *Linear error detector*
(2) No quantization errors
(3) No frequency-reference errors
(4) No IMU errors
(5) No input noise

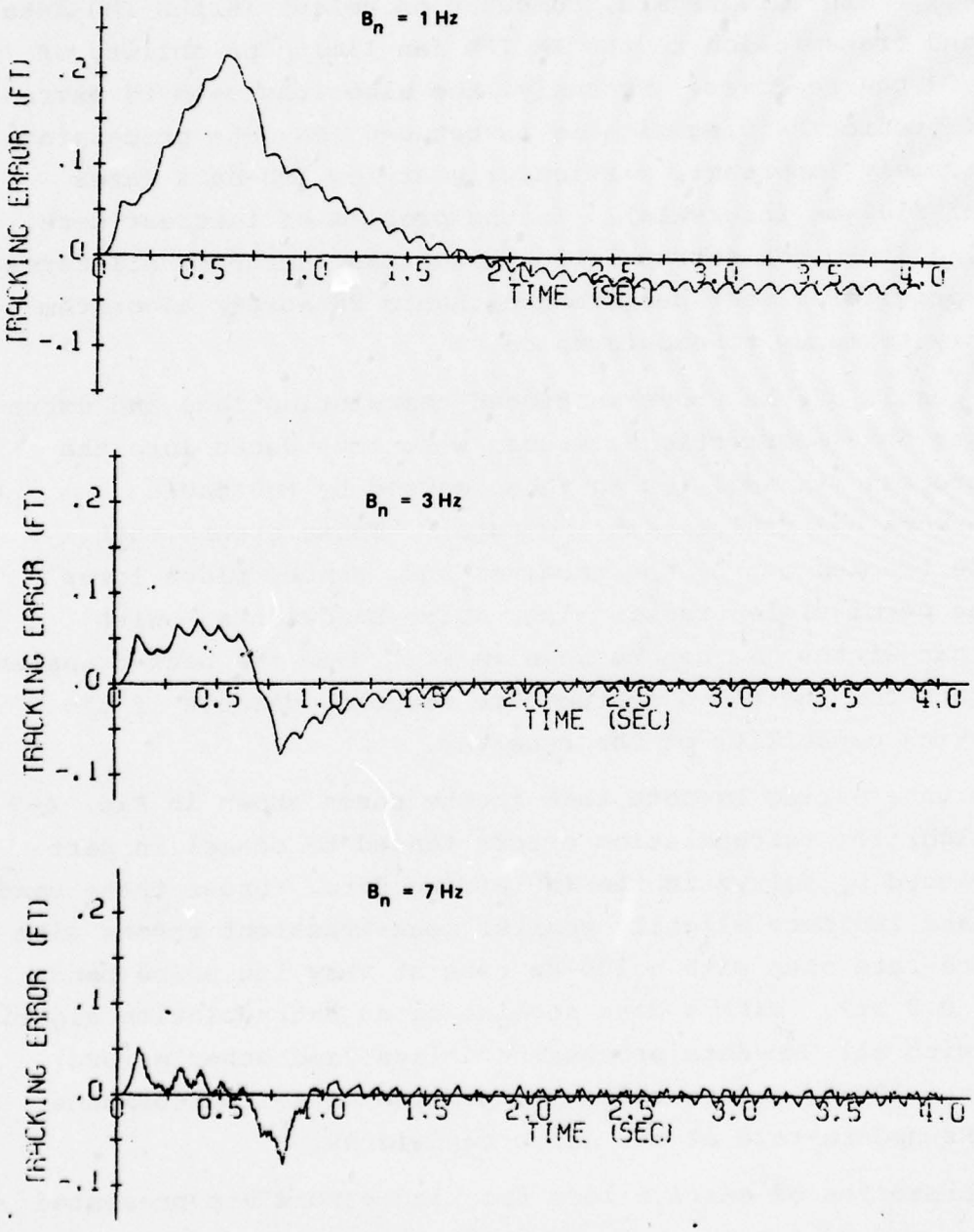

Figure 4-10. Carrier tracking errors, IMU-aiding (T = 100 ms) for high-jerk trajectory.

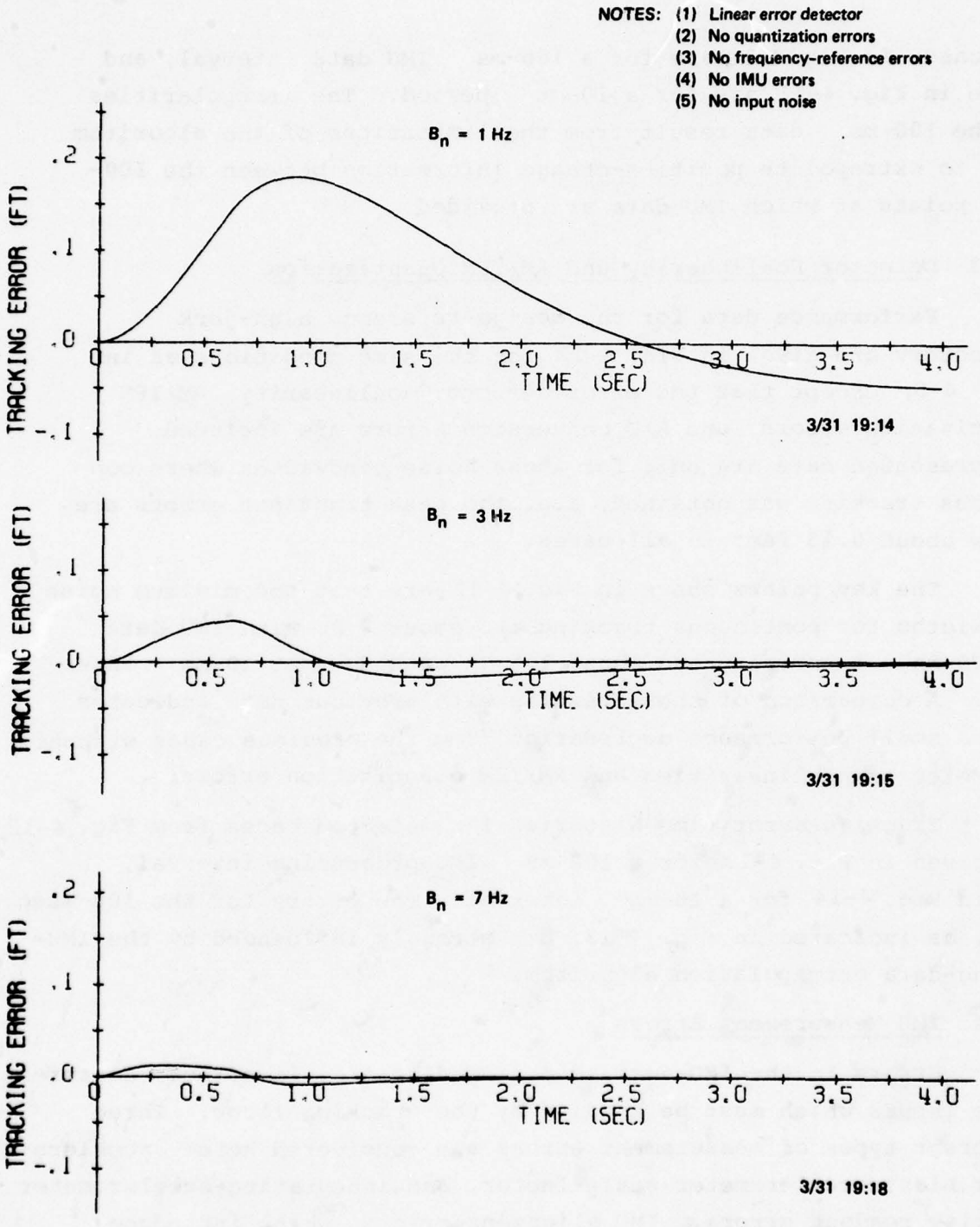

Figure 4-11. Carrier tracking errors, IMU-aiding (T = 10 ms) for high-jerk trajectory.

The cases in Fig. 4-10 are for a 100-ms IMU data interval, and those in Fig. 4-11 are for a 10-ms period. The irregularities in the 100-ms data result from the limitations of the algorithm used to extrapolate position-change information between the 100-ms points at which IMU data are provided.

4.6.3 Detector Nonlinearity and RM/IPM Quantization

Performance data for the design-reference high-jerk trajectory are given in Fig. 4-12 for the same conditions as in Fig. 4-9, except that the error-detector nonlinearity, RM/IPM quantization errors, and A/D conversion errors are included. The presented data are only for those noise bandwidths where continuous tracking was obtained, i.e. the peak transient errors are below about 0.15 feet in all cases.

The key points shown in Fig. 4-12 are that the minimum noise bandwidths for continuous tracking are about 2 Hz with IMU data at 100-ms intervals, and about 1.5 Hz with data at 10-ms intervals. A comparison of these results with previous data indicates only a small performance degredation from the previous cases without the detector nonlinearities and RM/IPM quantization errors.

Tracking-error time histories for selected cases from Fig. 4-12 are given in Fig. 4-13 for a 100-ms IMU-processing interval, and in Fig. 4-14 for a 10-ms interval. The errors for the 100-msec case, as indicated in Fig. 4-13, are strongly influenced by the IMU-aiding-data extrapolation algorithm.

4.6.4 IMU Measurement Errors

Errors in the IMU-derived aiding data are, in effect, disturbance inputs which must be handled by the tracking loops. Three different types of measurement errors are considered here: accelerometer bias, accelerometer scale-factor, and integrating-accelerometer velocity readout errors. IMU alignment errors, which introduce tracking errors similar in form to those from accelerometer scale-factor errors, are not explicitly considered here.

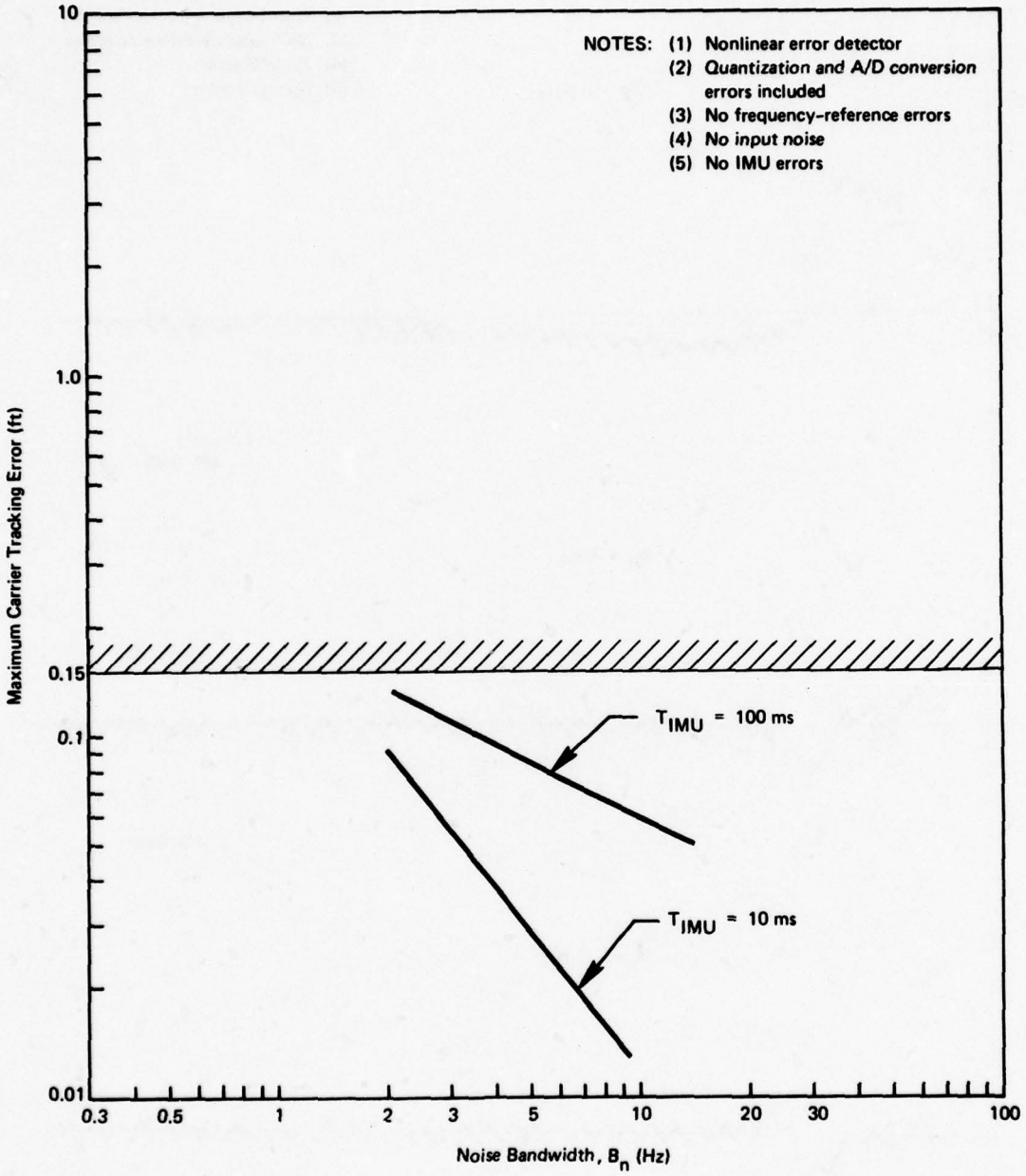

Figure 4-12. Maximum carrier tracking errors, IMU-aiding for high-jerk trajectory.

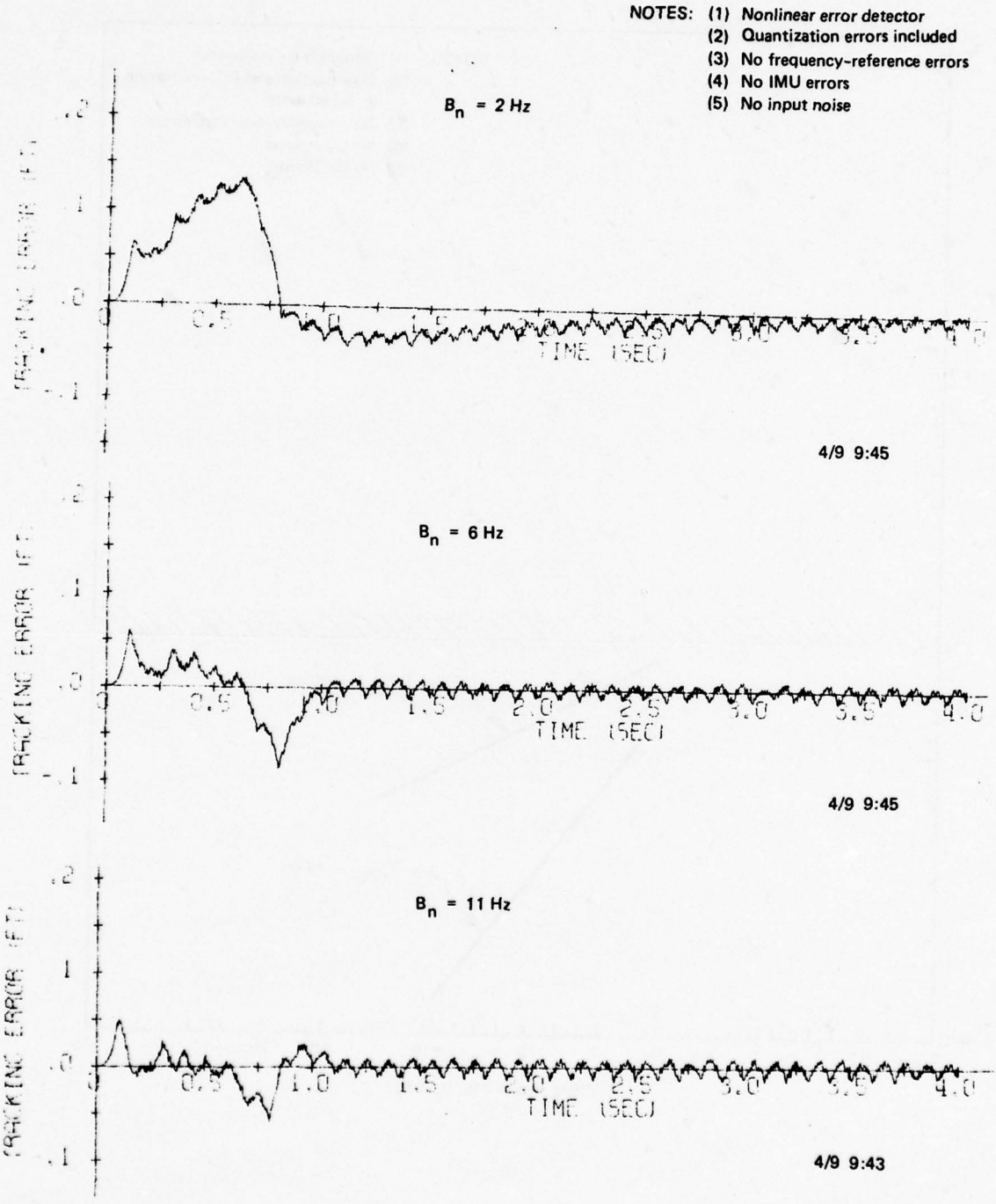

Figure 4-13. Carrier tracking errors, IMU-aiding (T = 100 ms) for high-jerk trajectory.

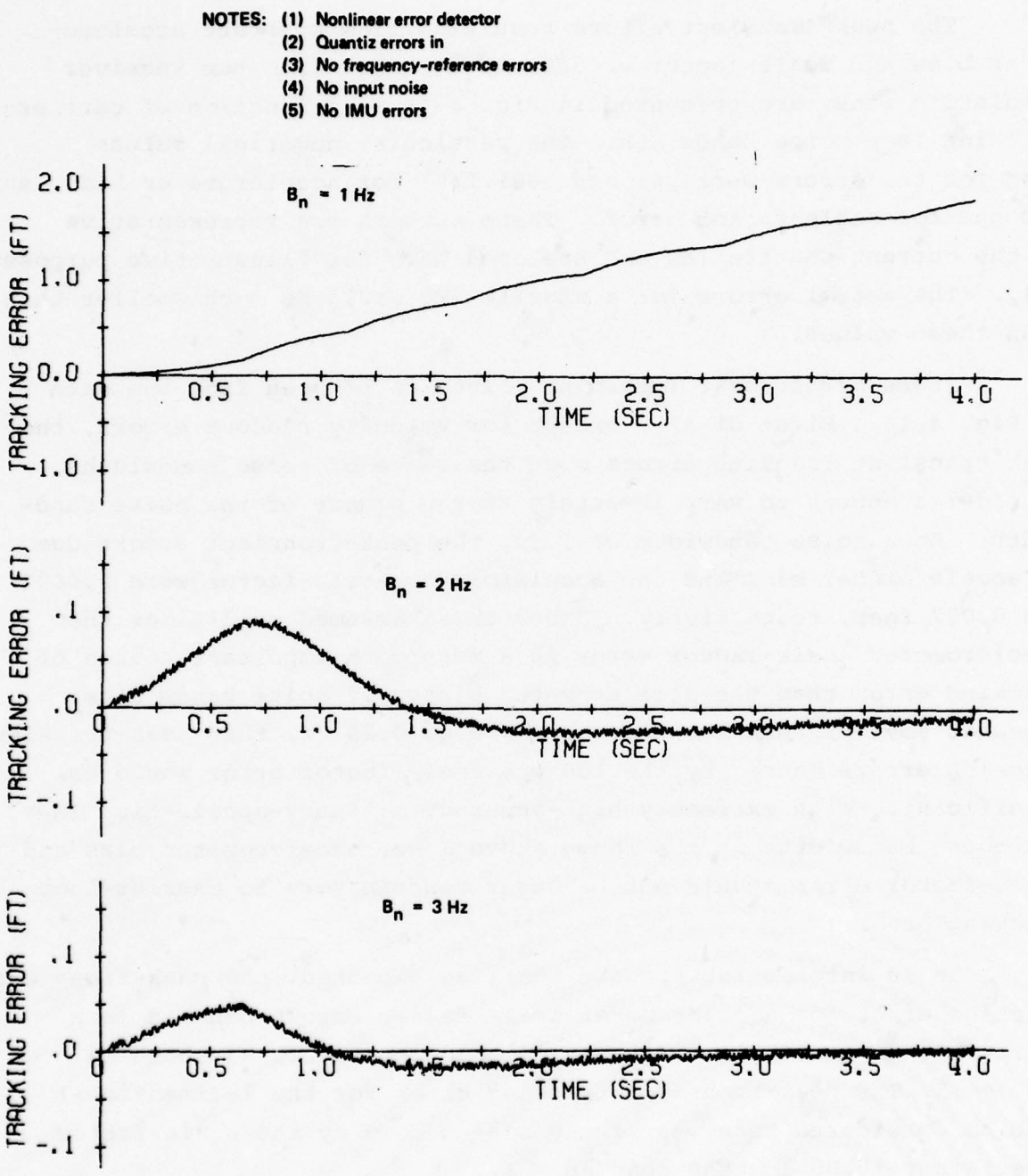

Figure 4-14. Carrier tracking errors, IMU-aiding (T = 10 ms) for high-jerk trajectory.

The peak transient errors resulting from constant accelerometer bias and scale-factor errors, as obtained from the receiver simulation runs, are presented in Fig. 4-15 as a function of carrier-tracking loop noise bandwidth. The particular numerical values used for the errors were .01 and .001 f/s^2 for accelerometer bias, and 100 ppm for scale-factor error. These numbers are representative of the current shuttle IMU and are used here for illustrative purposes only. The actual errors for a missile IMU would be much smaller than than these values.

There are several important points to be seen from the data of Fig. 4-15 First of all, except for velocity readout errors, the peak-transient tracking errors over the range of noise bandwidths considered appear to vary inversely as the square of the noise bandwidth. At a noise bandwidth of 1 Hz, the peak-transient errors due to accelerometer bias and the accelerometer scale-factor were 0.0003 and 0.007 feet, respectively. Under these assumed conditions the accelerometer scale-factor error is a much more important source of tracking error than the accelerometer bias. If noise bandwidths somewhat smaller than 1 Hz were used, e.g. 0.25 Hz, then peak-transient tracking errors caused by the 100 ppm scale-factor error would be significant. With extremely high-accuracy military-application IMUs and noise bandwidths in the range above 1 Hz, accelerometer bias and scale-factor error should not be major contributors to carrier-loop tracking error.

It is interesting to note that, as expected, the peak-transient tracking error for accelerometer scale-factor errors behaved in a similar manner to the unaided-system tracking error, as shown in Fig. 4-15. The peak-transient tracking error for the 1-dimensional problem considered here was simply scaled down by the scale-factor uncertainty (0.0001 in the case shown).

The effect of integrating-accelerometer velocity readout noise on carrier-loop tracking error is also shown in Fig. 4-15 as a function of tracking-loop noise bandwidth. The readout noise model used here assumes that the error in the IMU-derived measurement of velocity is uncorrelated between IMU read times and has a

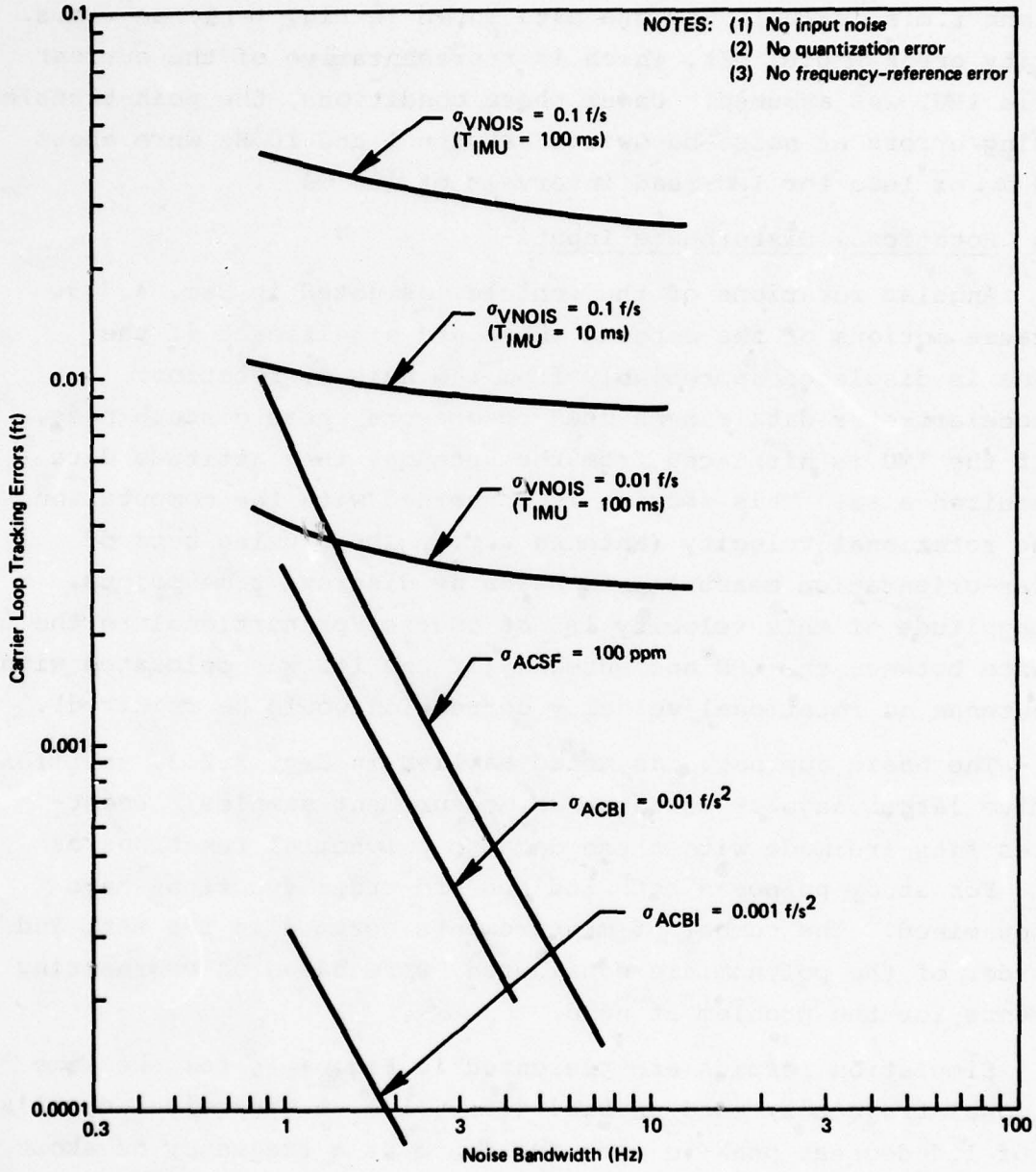

Figure 4-15. IMU measurement errors for high-jerk trajectory maximum carrier tracking errors.

constant r.m.s. value. For the data shown in Fig. 4-15, an r.m.s. velocity error of 0.01 f/s, which is representative of the current shuttle IMU, was assumed. Under these conditions, the peak-transient tracking errors at noise bandwidth between 1 and 10 Hz were about 0.004 ft, or less for IMU-read intervals of 100 ms .

4.6.5 Rotational Disturbance Inputs

Angular rotations of the vehicle, as noted in Sec. 4.5.5. can cause motions of the antenna which are significant if the antenna is displaced appreciably from the axis of rotation. IMU accelerometer data can be used to measure these disturbances, but if the IMU is displaced from the antenna, then attitude data is required also. This section is concerned with the computation of the rotational velocity (antenna w.r.t. IMU), using sets of angular-orientation measurements taken at discrete time points. The magnitude of this velocity is, of course, proportional to the distance between the IMU and antenna (if the IMU was colocated with the antenna no rotational-velocity correction would be required).

The basic approach, as noted earlier in Sec. 3.2.3, utilizes the five latest angular orientation measurement samples. Least-squares fits are made with these data to polynomial functions of time. For study purposes both 2nd and 3rd order functions have been examined. The number of measurements assumed in the set, and the order of the polynomials considered, were based on engineering judgments for the problem at hand.

Simulation results are presented in Fig. 4-16 for the same rotational trajectory used in Sec. 4.5.5, i.e. a sinusoidal oscillation of 1.4 degrees peak-to-peak amplitude at a frequency of about 1 Hz. The presented data are in the form of r.m.s. tracking errors as a function of single-sided noise bandwidth. A displacement of 2 feet between IMU and receiver antenna phase center is assumed in all cases.

To evaluate data-rate requirements, two different spacings between successive angle measurements were considered: 100 ms

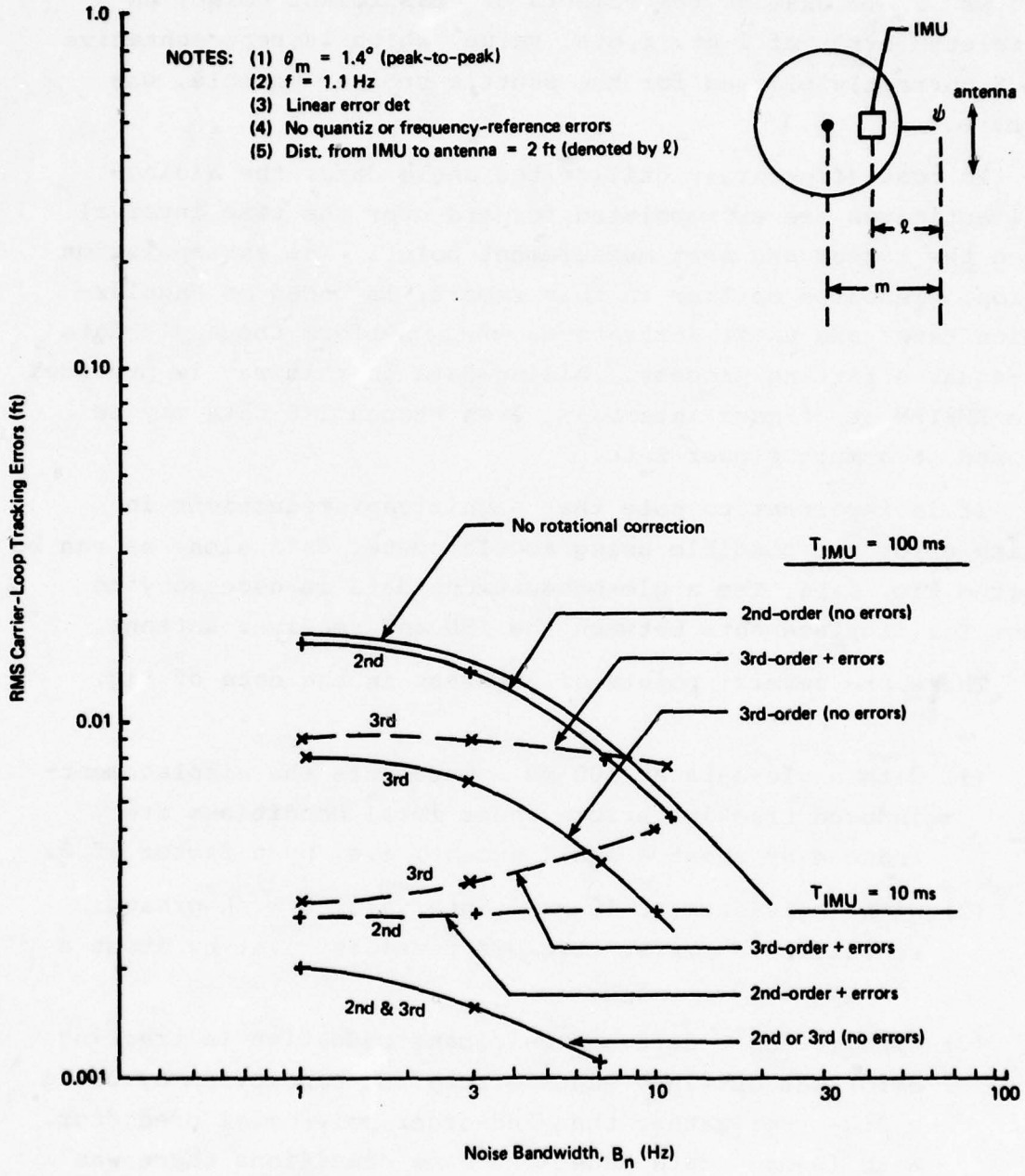

Figure 4-16. Carrier tracking errors for rotational inputs. Aided system.

and 10 ms . To examine the effects of measurement noise, an uncorrelated error of 1-mr. r.m.s. value, which is representative of IMUS currently planned for the shuttle orbiter vehicle, was used here.

To most effectively utilize the angle data, the aiding-signal estimates are extrapolated forward over the time interval between the latest and next measurement point. The extrapolation relation, presented earlier in this report, is based on angular-rotation rates and their derivatives, obtained form the angle-data least-squares fitting process. Aiding-data in this way is provided to the RM/IPM at 4-msec intervals, even though IMU data may be processed at a much slower rate.

It is important to note that significant reductions in tracking error are possible using accelerometer data alone as can be seen from Fig. 4-16. The angle-measurement data is necessary to account for displacements between the IMU and receiver antenna.

There are several points of interest in the data of Fig. 4-16.

(1) With angle-data at 100-ms intervals the displacement-induced tracking errors under ideal conditions are reduced by about a small amount, i.e. by a factor of 2.

(2) With angle-data at 10-ms intervals, a much greater reduction in r.m.s. error is possible, i.e. by about a factor of 10.

(3) With 100-ms data, a significant reduction in tracking error was obtained under error-free conditions by using a 3rd-order rather than 2nd-order polynomial predictor. With 10-ms data under the same conditions there was no significant difference between the two predictors.

(4) With measurement errors present on the IMU data, a significant degredation in aiding performance occurred, particularly at the larger noise bandwidths.

(5) The 3rd-order predictor, as expected, suffered more from angle-measurement errors than did the 2nd-order predictors.

To further demonstrate the usefulness of the angle-measurement data, carrier tracking-loop error time histories are presented in Fig. 4-17 with and without IMU angle-measurement aiding. For simplicity here, the IMU is located on the axis of rotation of the vehicle, and the receiver antenna is 2 feet to the side. The same sinusoidal rotation trajectory as in the preceding results is assumed here, i.e. peak-to-peak amplitude of about 1.4 degrees and oscillation frequency of about 1.1 Hz.

The same conclusions can be drawn from these data as in the previous results. The IMU angle data can significantly reduce carrier tracking-loop errors resulting from vehicle rotation, provided that the data are obtained at a sufficiently rapid rate. Noise on the angle-measurement data will, of course, limit the effectiveness of the aiding, particularly at the higher tracking-loop noise bandwidths.

4.6.6 Performance vs. Input Noise

Several sets of Monte-Carlo runs were made to evaluate tracking-loop performance as a function of input signal to noise p.s.d., i.e. C/N_0 (dB-Hz). All important aiding-system error sources were included in these test cases: e.g. error-detector nonlinearities, sampling and transport lags in receiver, RM/IPM quantization errors, code and carrier loop cross-coupling. IMU-data processing intervals and receiver frequency-reference drift were treated as separate quantities to be varied parametrically. A high quality IMU is assumed here with essentially no accelerometer bias or scale-factor errors.

The test input to the tracking system in these Monte-Carlo runs was the high-jerk design-reference trajectory, i.e. 10 g/s for 0.6 sec and constant acceleration thereafter. No rotational velocity inputs were included here. The typical test-run duration in these data was 5-10 seconds. To limit simulation costs, the size of the Monte-Carlo run sets was limited to 10 runs per test case. In all cases presented here, IMU data was provided directly to the

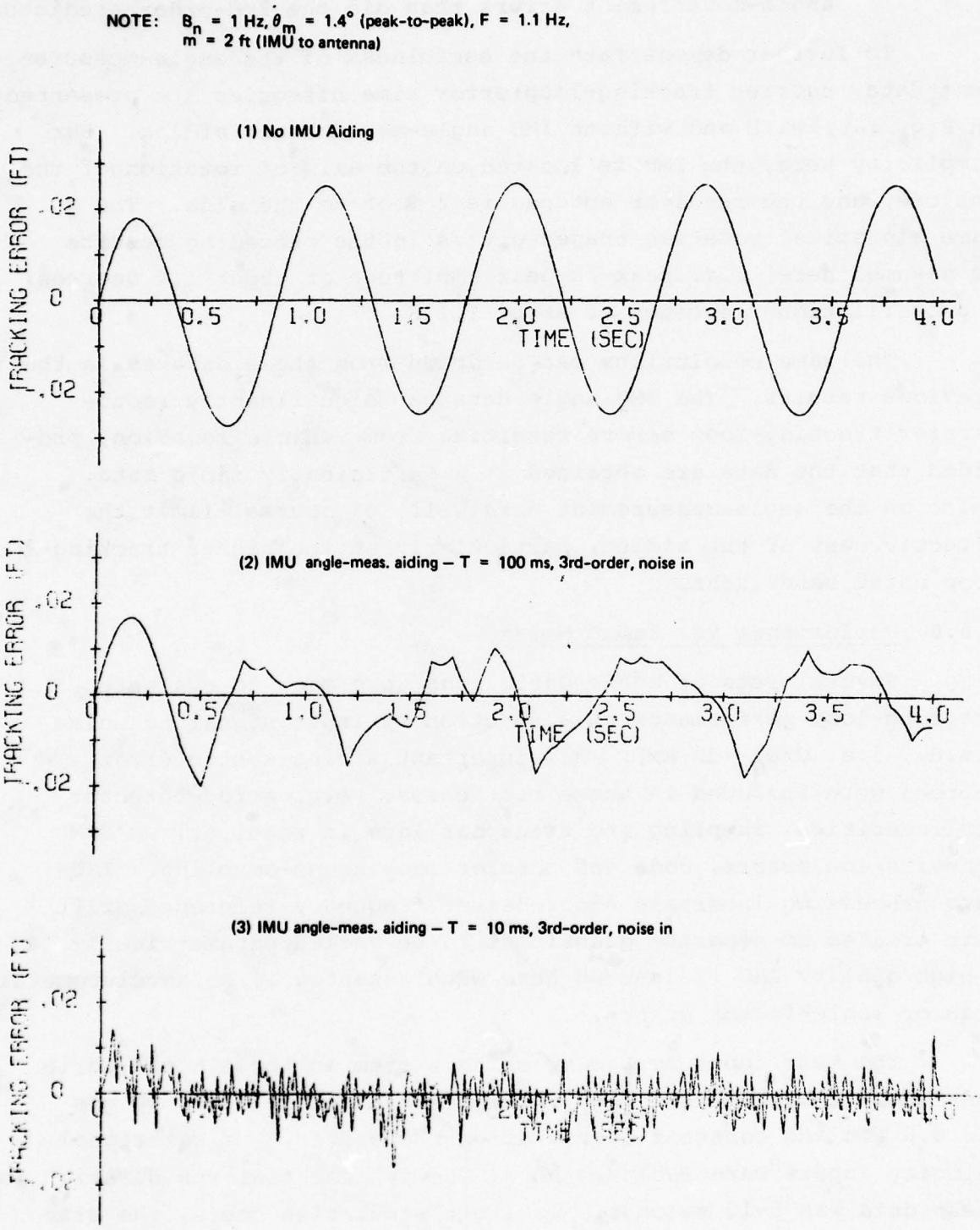

Figure 4-17. Carrier tracking errors with rotational input.

carrier loop at a point preceding the RM/IPM. The velocity-aiding signal to the carrier-loop RM/IPM (combination of IMU and carrier-loop derived signals) with appropriate scaling was then used to aid the code loop. The time constant of the first-order code loop in these studies was about 2 seconds.

The presented data show the number of test runs for a particular set of conditions for which the receiver was able to maintain lock. In addition a number of tracking-error time histories are presented to show the detailed error behavior for a variety of conditions.

Tracking performance data are presented in Table 4-2 for an unaided system, in Table 4-3 for an IMU data-processing interval of 100 ms , and in Table 4-4 for an interval of 10 ms . In the high noise-bandwidth case of Tables 4-2 and 4-3 acceleration-sensitive frequency-reference errors of as large as 1 part in 10^9/g are considered. In the low-bandwidth cases, the maximum frequency-referenced error considered was 1 part in 10^{10}/g.

Some definitions used in these tables need to be clarified at this point. A successful run is one in which the carrier loop does not lose lock, or temporarily slips cycles and recovers shortly thereafter. A failed situation is one in which the carrier loses lock and does not recover.

The unaided case will be considered first. From the simulation results it appears that a threshold, i.e. minimum C/N_0, of about 28 dB-Hz is obtained for reliable tracking without IMU aiding. The minimum required noise bandwidths to accomplish this are about 50 Hz. A typical set of tracking-error time histories for this situation are shown in Fig. 4-18.

The case where IMU data were processed at 100-ms intervals will be discussed next. With an acceleration-sensitive frequency-reference drift of 1 part in 10^9/g and a noise bandwidth of 11 Hz, the smallest permissible C/N_0 for reliable tracking was about 26 dB-Hz. Increasing the noise bandwidth to 22 Hz with the same frequency-reference drift, provided a slightly smaller minimum C/N_0 of about

Table 4-2. Monte Carlo runs - unaided receiver.

B_n (Hz)	Accel. Sens. Freq. Ref. Drift	C/No (dB-Hz)	Successful Runs	Slipped Cycles	Failed
60	$1 \times 10^{-10/g}$	28	11/12	0/12	1/12
		26	5/12	0/12	7/12
		24	0/12	0/12	12/12
	$1 \times 10^{-9/g}$	28	11/12	0/12	1/12
		26	4/12	3/12	8/12
50	$1 \times 10^{-10/g}$	30	12/12	0/12	0/12
		28	12/12	0/12	0/12
		26	3/12	0/12	9/12

NOTES: (1) High-jerk trajectory input

(2) Successful run - maintains lock or temporarily slips cycle

(3) Failed run loses lock and does not recover

(4) 10-run Monte Carlo sets

Table 4-3. Monte Carlo runs - IMU-aided receiver.

B_n (Hz)	Accel. Sens. Freq. Ref. Drift	C/No (dB-Hz)	Successful Tracking	Slipped Cycles	Failed
22	$1 \times 10^{-9/g}$	24	10/10	1/10	—
		22	9/10	2/10	1/10
11	$1 \times 10^{-9/g}$	28	10/10	—	—
		24	7/10	3/10	3/10
		20	4/10	2/10	6/10
	$1 \times 10^{-10/g}$	24	10/10	—	—
		20	10/10	—	—
		18	4/10	3/10	6/10
5	$1 \times 10^{-10/g}$	20	9/10	5/10	1/10
9	$1 \times 10^{-9/g}$	∞	YES		
7		∞	NO		
3	$1 \times 10^{-10/g}$	∞	YES		
2		∞	NO		

NOTES: (1) High-jerk trajectory input

(2) T_{IMU} = 100 ms

Table 4-4. Monte Carlo runs - IMU-aided receiver.

B_n (Hz)	Accel. Sens. Freq. Ref. Drift	C/No (dB-Hz)	Successful Tracking	Slipped Cycles	Failed
11	$1 \times 10^{-9/g}$	28	10/10	—	—
		24	9/10	—	1/10
		20	9/10	0/10	10/10
	$1 \times 10^{-10/g}$	18	7/10	3/10	3/10
		16	0/10	0/10	10/10
5	$1 \times 10^{-10/g}$	24	10/10	—	—
		20	10/10	1/10	—
		18	9/10	7/10	1/10
		16	6/10	4/10	4/10
9	$1 \times 10^{-9/g}$	∞	YES		
7		∞	NO		
3	$1 \times 10^{-1-/g}$	∞	YES		
2		∞	NO		

NOTE: (1) High-jerk trajectory input

(2) T_{IMU} = 10 ms

NOTE: (1) Monte-Carlo Run #650, 4/13, 19:41
(2) T_{IMU} = 100 ms
(3) B_n = 11 Hz (C1 = 24, C2 = 173, C3 = 308)
(4) No frequency-reference drift
(5) S/N_0 = 24 dB-Hz

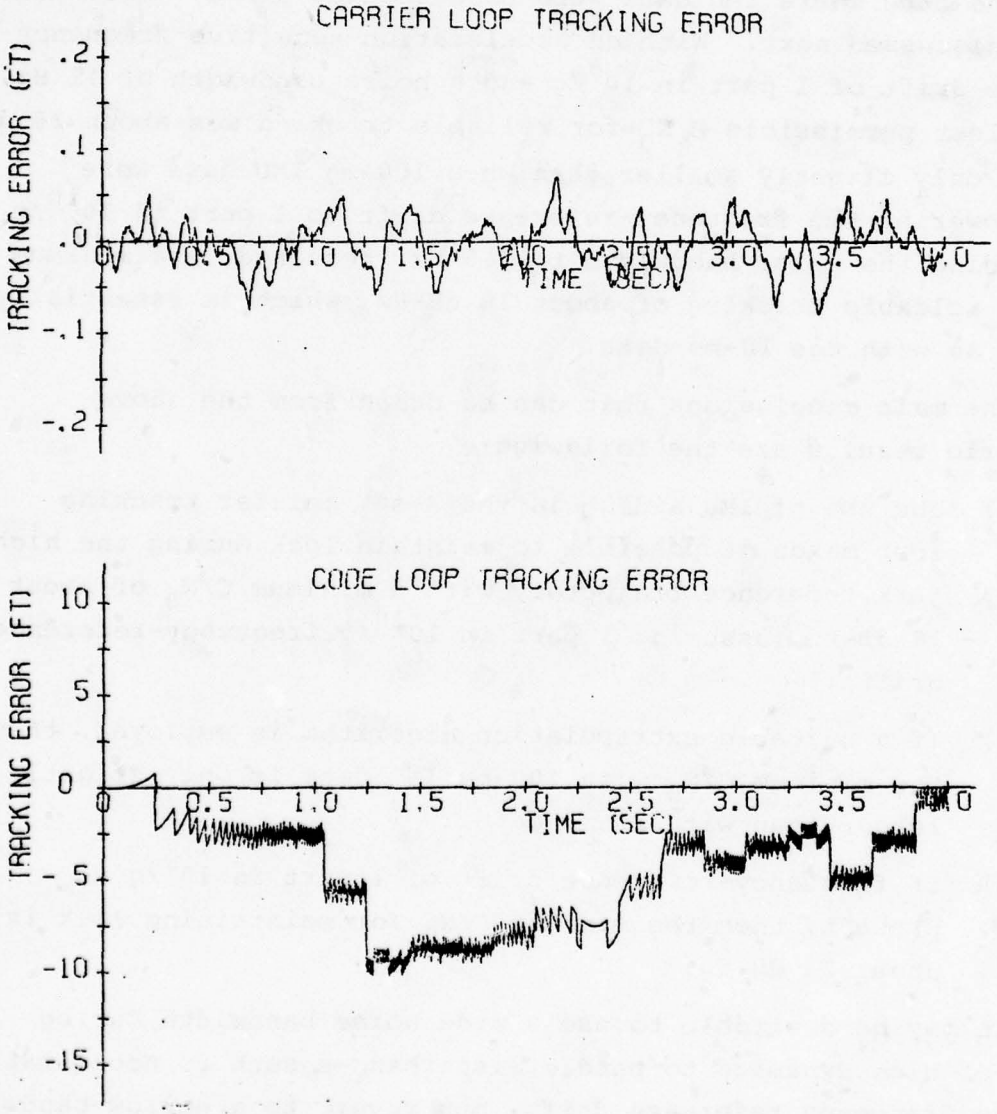

Figure 4-18. IMU-aided receiver with high-jerk input.

22 dB-Hz. The reason for this was that the error caused by acceleration-sensitive frequency-reference drift was reduced more than the increased additional noise passed through the loop. Lowering the frequency-reference drift to 1 part in 10^{10}/g with a noise bandwidth of 11 Hz, resulted in a slightly lower tracking threshold of about 20 dB-Hz.

The case where IMU data were processed at 10-ms intervals will be discussed next. With an acceleration-sensitive frequency-reference drift of 1 part in 10^{9}/g and a noise bandwidth of 11 Hz, the smallest permissible C/N_0 for reliable tracking was about 26 dB-Hz. This was only slightly smaller than when 100-ms IMU data were used. Lowering the frequency-reference drift to 1 part in 10^{10}/g and reducing the noise bandwidth to 4.5 Hz, resulted in a minimum C/N_0 for reliable tracking of about 18 dB-Hz, which is essentially the same as with the 10-ms data.

The main conclusions that can be drawn from the above Monte-Carlo results are the following:

1) The use of IMU aiding in the X-set carrier tracking loop makes it possible to maintain lock during the high-jerk reference trajectory with a minimum C/N_0 of about 18 dB-Hz (assuming 1 part in 10^{10}/g frequency-reference drift).

2) If a suitable extrapolation algorithm is employed, then the minimum C/N_0 with 100-ms IMU data is only slightly larger than with 10-ms data.

3) If frequency-reference drift of 1 part in 10^{9}/g is present, then the minimum C/N_0 for maintaining lock is about 24 dB-Hz.

It may be desirable to use a wide noise bandwidth during periods of high dynamics to handle disturbances such as acceleration-sensitive frequency reference drift, but revert to a narrow-bandwidth during periods of low dynamics to reduce the minimum C/N_0 at those times. The IMU-derived vehicle acceleration information could be the basis for changing tracking-loop gains and bandwidth.

Time histories of carrier and code loop tracking errors from several representative Monte-Carlo runs are shown in Figs. 4-19 to 4-26. The runs in Figs. 4-19 to 4-22 are for a 100-ms IMU-data processing interval, whereas those in Figs. 4-23 to 4-26 are for a 10-ms interval.

The first case in Fig. 4-19 shows the typical tracking errors with a 24 dB-Hz C/N_0, an IMU-processing interval of 100 ms, but with no frequency-reference drift present. The carrier-loop errors, as can be seen, are noisy but are generally smaller than 0.10 feet. Code-loop tracking errors, on the other hand, were as large as 10 feet in this particular case.

The effect of acceleration-sensitive frequency reference drift is shown in Fig. 4-20, which is essentially the same as the case of Fig. 4-19 except for the addition of 1 part in 10^9/g frequency-reference drift. The main point of interest here is that there is a significant increase in carrier-loop tracking error during the initial period of high-jerk input. Otherwise, the tracking-errors are not changed.

The carrier-tracking loop can sometimes slip cycles. This is shown in Fig. 4-21 where the input C/N_0 is 24 dB-Hz and the frequency-reference drift is 1 part in 10^9/g. In this particular case a slip of 1.5 carrier cycles takes place during the period of high-jerk input. Eventually the carrier loop reacquires lock and maintains accurate tracking thereafter. The code loop in this case was not significantly affected by the temporary loss-of-lock in the carrier loop.

A typical case with a C/N_0 of 20 dB-Hz is shown in Fig. 4-22. For the assumed noise bandwidth of 11 Hz, tracking errors of about 0.10 feet occur frequently. Further reduction of C/N_0 would lead to frequent cycle-slip situations and possible total loss of lock.

NOTES: (1) Monte-Carlo Run #650, 4/13, 19:41
(2) T_{IMU} = 100 ms
(3) B_n = 11 Hz (C1 = 24, C2 = 173, C3 = 308)
(4) No frequency-reference drift
(5) S/N_0 = 24 dB-Hz

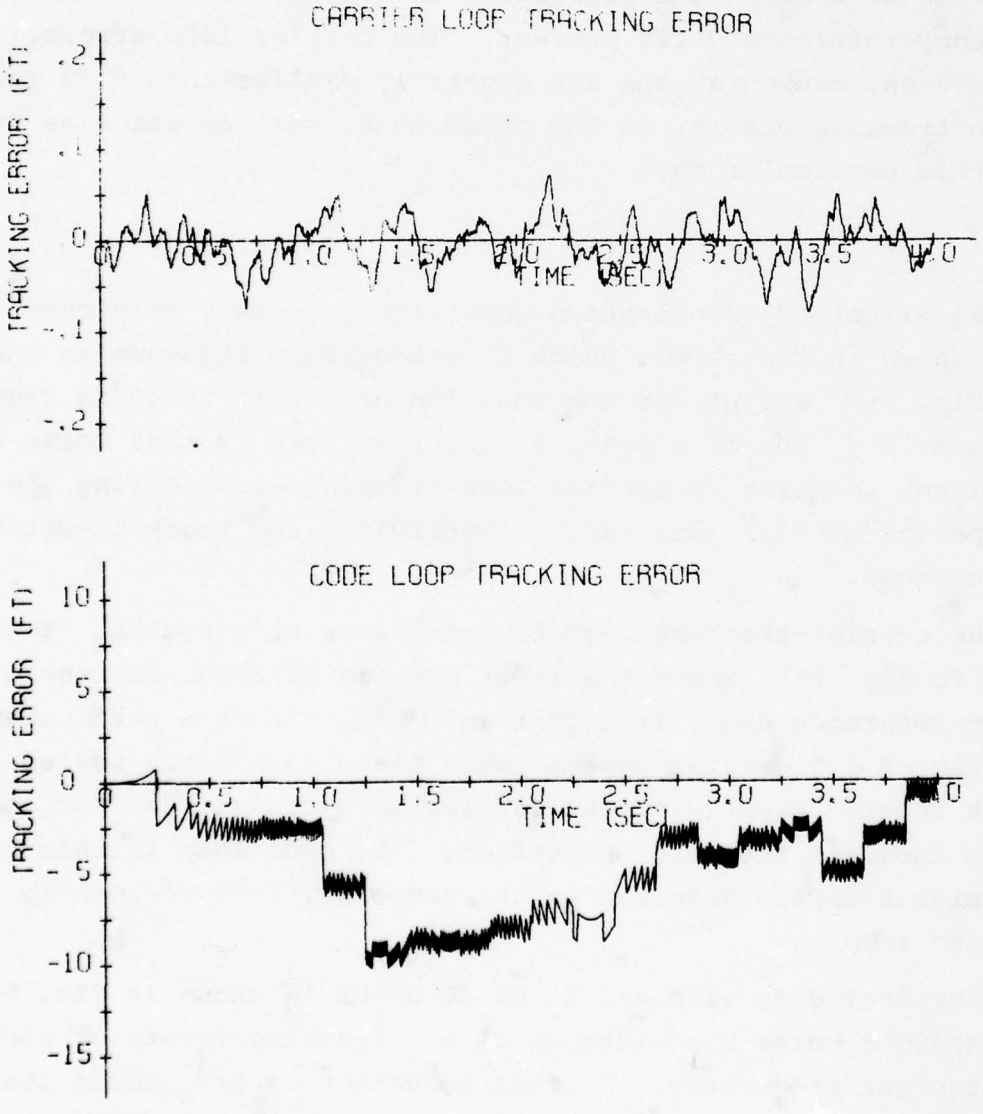

Figure 4-19. IMU-aided receiver with high-jerk input.

NOTES: (1) Monte-Carlo Run #650, 4/14, 1:30
(2) T_{IMU} = 100 ms
(3) B_n = 11 Hz
(4) Frequency-reference drift = 1 part in 10^9/g
(5) S/N_0 = 24 dB-Hz

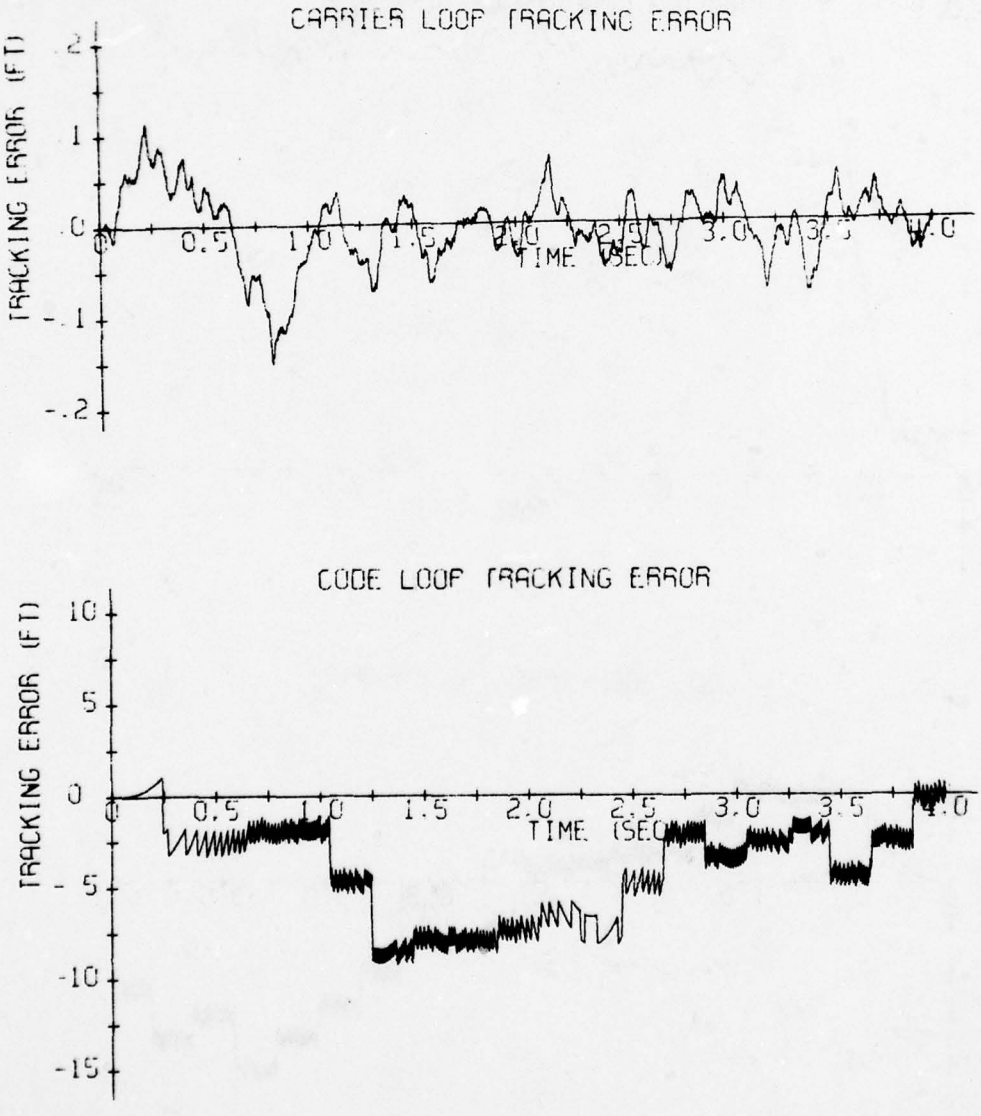

Figure 4-20. IMU-aided receiver with high-jerk input.

NOTES: (1) Monte-Carlo Run #1450, 4/14, 20:27
(2) T_{IMU} = 100 ms
(3) B_n = 11 Hz
* (4) Frequency-reference drift = 1 part in 10^9/g
(5) S/N_0 = 24 dB-Hz

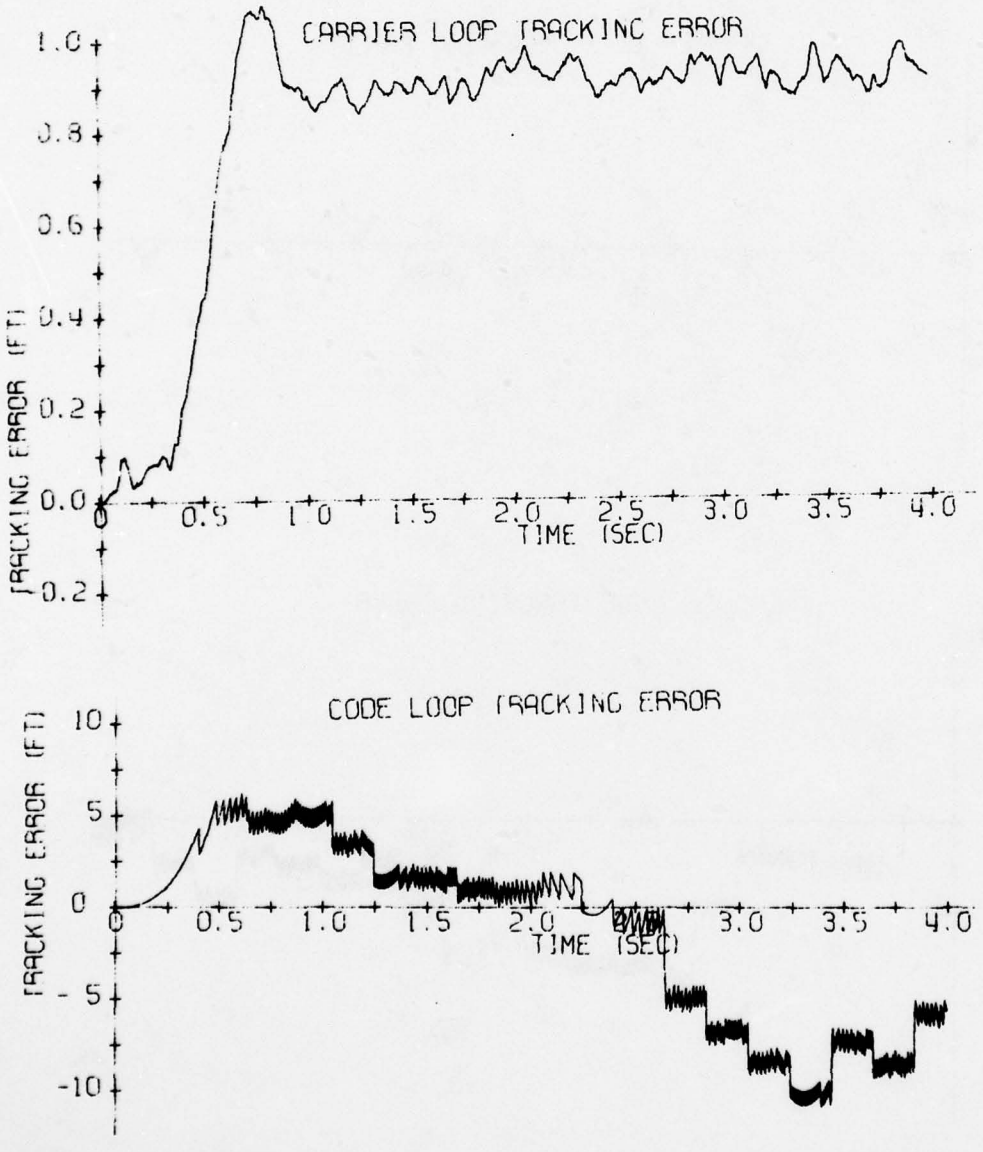

Figure 4-21. IMU-aided receiver with high-jerk input.

NOTES: (1) Monte-Carlo Run #1550, 4/14, 20:07
(2) T_{IMU} = 100 ms
(3) B_n = 11 Hz
(4) Frequency-reference drift = 1 part in 10^{10}/g
* (5) S/N_0 = 20 dB-Hz

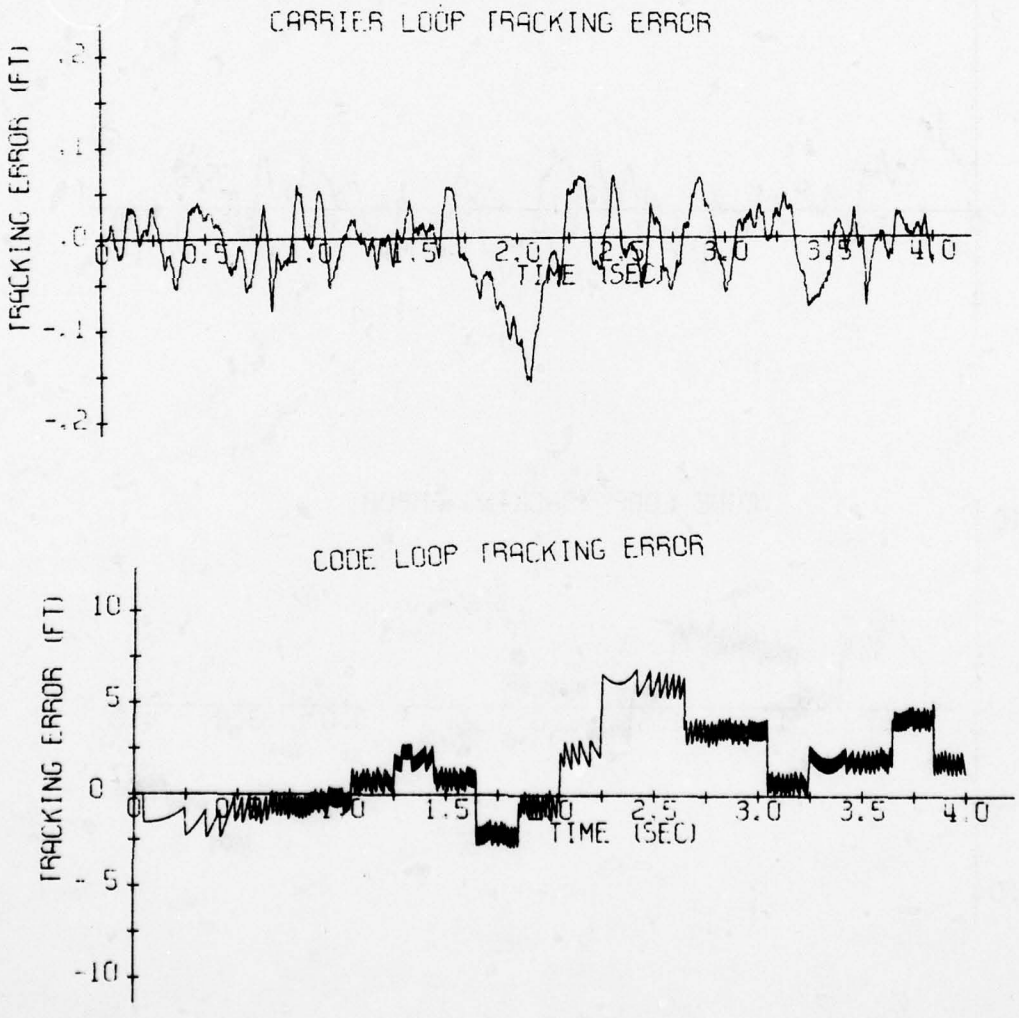

Figure 4-22. IMU-aided receiver with high-jerk input.

NOTES: (1) Monte-Carlo Run #1350, 4/26, 19:58
(2) T_{IMU} = 10 ms
(3) B_n = 4.5 Hz (C1 = 12, C2 = 45, C3 = 38)
(4) No frequency-reference drift
(5) S/N_0 = 18 dB-Hz

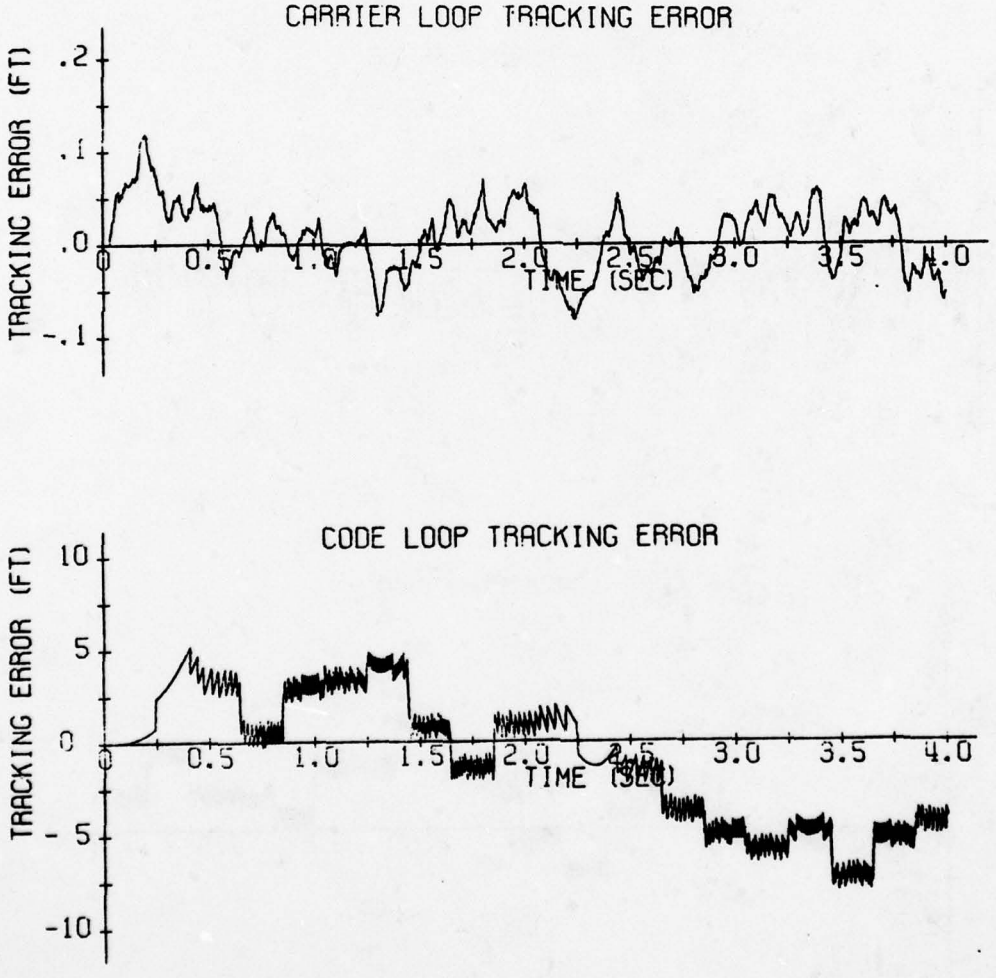

Figure 4-23. IMU-aided receiver with high-jerk input.

NOTES: (1) Monte-Carlo Run #1550, 4/14, 20:28
(2) T_{IMU} = 10 ms
(3) B_n = 4.5 Hz
* (4) Frequency-reference drift = 1 part in $10^{10}/g$
(5) S/N_0 = 18 dB-Hz

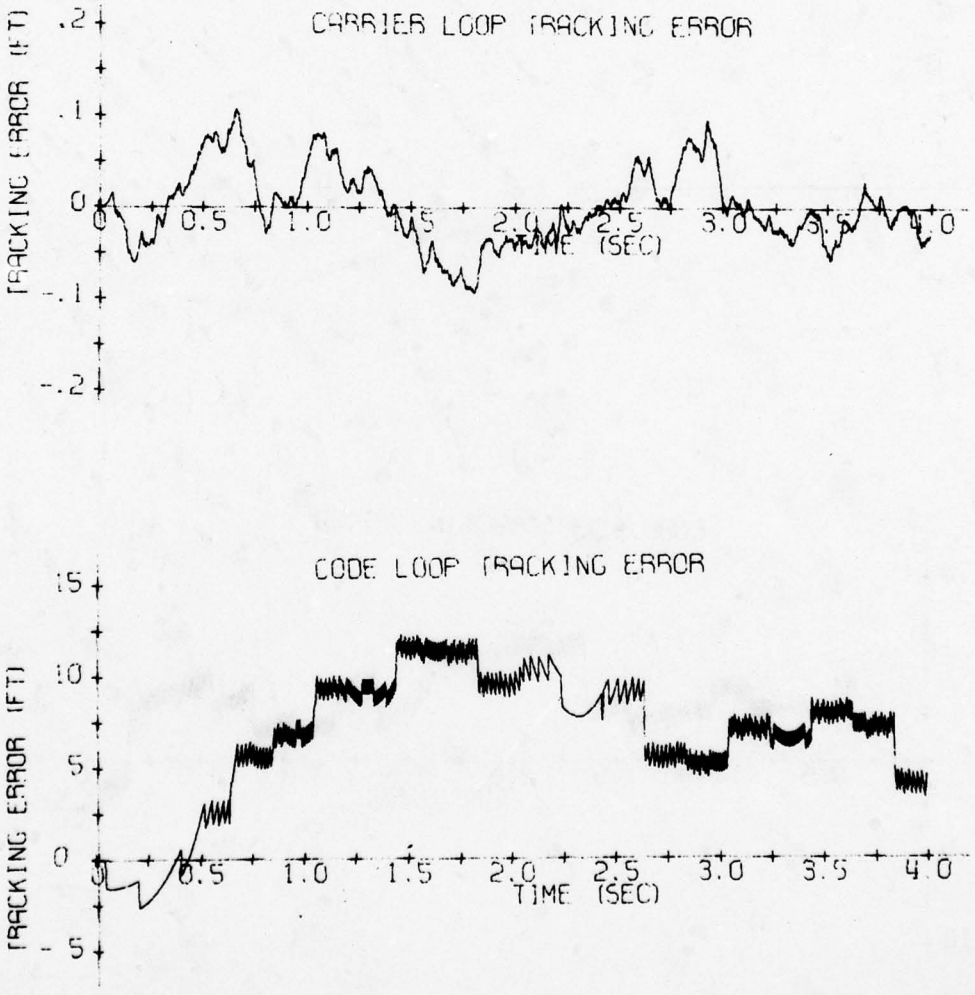

Figure 4-24. IMU-aided receiver with high-jerk input.

NOTES: (1) Monte-Carlo Run #1650, 4/14, 20:43
(2) T_{IMU} = 10 ms
(3) B_n = 4.5 Hz
(4) Frequency-reference drift = 1 part in 10^{10}/g
(5) S/N_0 = 16 dB-Hz

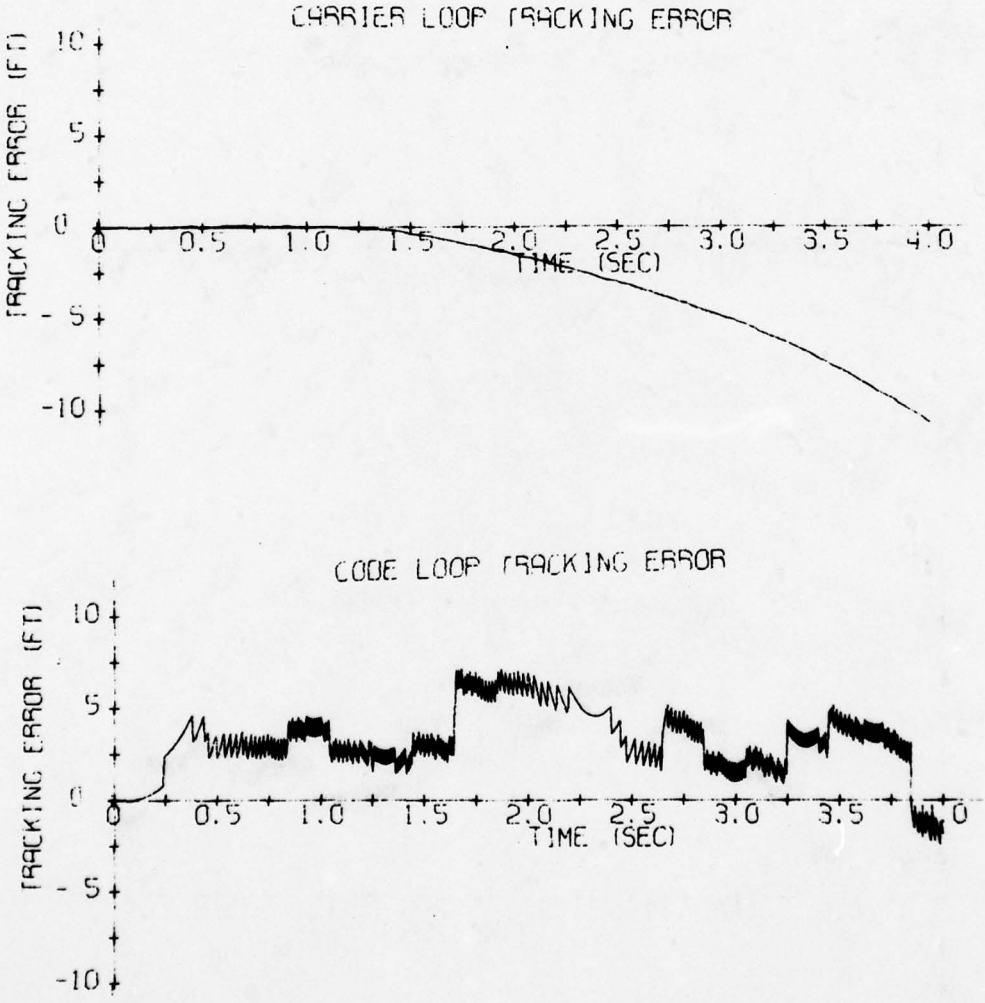

Figure 4-25. IMU-aided receiver with high-jerk input.

NOTES: (1) Monte-Carlo Run #1050, 4/15, 1:02
(2) T_{IMU} = 10 ms
(3) B_n = 11 Hz
(4) Frequency-reference drift = 1 part in 10^9/g
(5) S/N_0 = 24 dB-Hz

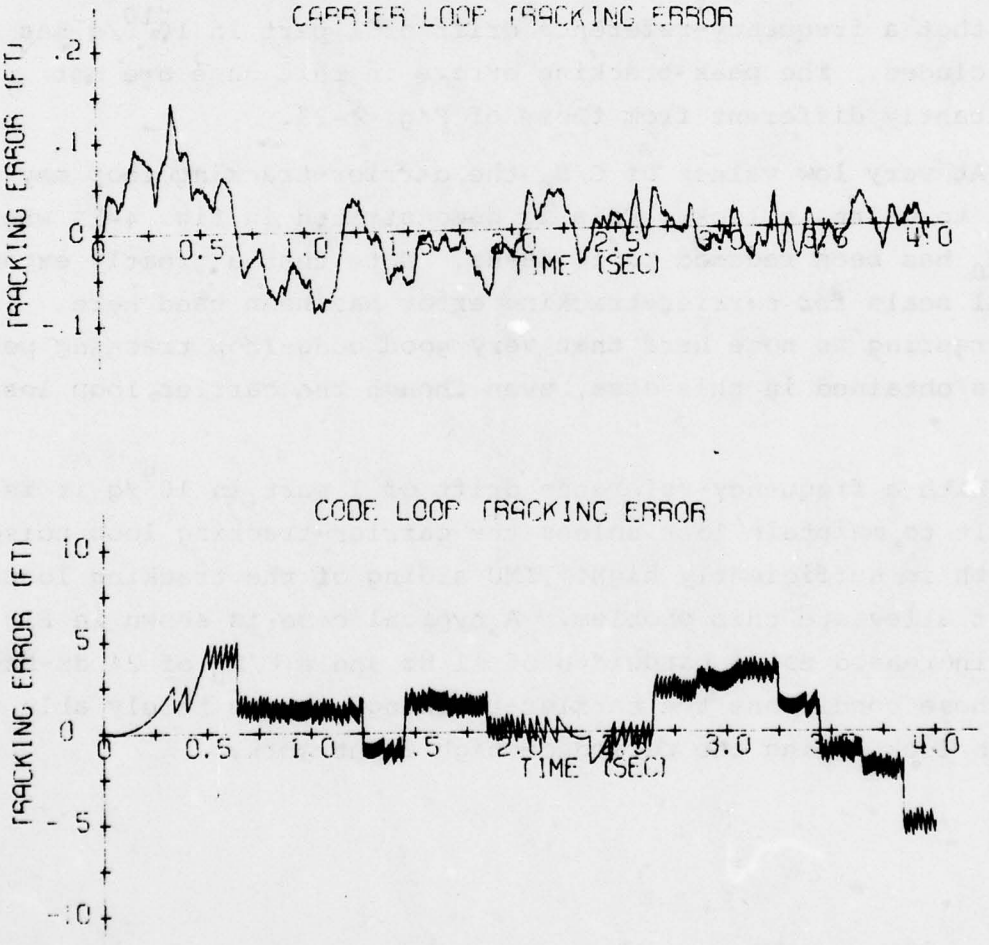

Figure 4-26. IMU-aided receiver with high-jerk input.

Tracking-error time histories for a typical case where IMU data are provided at 10-ms intervals are given in Fig. 4-23 for a C/N_0 of 18 dB-Hz. A noise bandwidth of 4.5 Hz was used here, which is smaller than the 11-Hz value used in the preceding 100-ms results. No frequency-reference acceleration-sensitive drift is included here. Tracking performance under these conditions is satisfactory, but peak carrier-tracking errors of about 0.10 feet occur.

A case similar to that of Fig. 4-23 is shown in Fig. 4-24, except that a frequency-reference drift of 1 part in 10^{10}/g has also been included. The peak tracking errors in this case are not significantly different from those of Fig. 4-23.

At very low values of C/N_0 the carrier-tracking loop may not be able to maintain lock. This is demonstrated in Fig. 4-25 where the C/N_0 has been reduced to 16 dB-Hz. Note that a greatly expanded vertical scale for carrier-tracking error has been used here. It is interesting to note here that very good code-loop tracking performance is obtained in this case, even though the carrier loop lost lock.

With a frequency-reference drift of 1 part in 10^9/g it is difficult to maintain lock unless the carrier-tracking loop noise bandwidth is sufficiently high. IMU aiding of the tracking loops does not alleviate this problem. A typical case is shown in Fig. 4-26 for an increased noise bandwidth of 11 Hz and a C/N_0 of 24 dB-Hz. Under these conditions the carrier-tracking loop is barely able to maintain lock during the period of high input jerk.

SECTION 5

SUMMARY

An investigation has been made of the use of IMU-derived information to aid the X-set carrier and code tracking loops in a high-jerk environment. Detailed simulations of the X-set receiver and an IMU such as AIRS have been developed and used to accomplish this study.

For an unaided carrier tracking loop with a linearized detector, no noise inputs, no quantization error, and no oscillator variations, a single-sided loop noise bandwidth B_n on the order of 30 Hz (measured) is required to track the incoming signal with an error of less than 0.15 feet. For the same conditions but with IMU aiding (with update periods of 100 ms and 10 ms), the loop noise bandwidth can be lowered to 1.2 Hz and <0.1 Hz, respectively.

Acceleration-sensitive frequency reference drift, which must be tracked out by the receiver, is an important factor in limiting the minimum noise bandwidths that can be used. In this study, two values were used for this parameter, 1×10^{-9}/g and 1×10^{-10}/g, the latter of which can be achieved using a g-compensated crystal oscillator. With all error sources included (acceleration sensitive drift of 1×10^{-9}/g), a nonlinear detector and no IMU aiding, a B_n of 60 Hz and a C/N_o of 28 dB-Hz is required to maintain lock. If the loop is IMU aided, B_n and C/N_o can be reduced to 11 Hz and 24 dB-Hz. If the acceleration sensitive drift were limited to 1×10^{-10}/g, B_n and C/N_o can be reduced to 50 Hz and 28 dB-Hz and 5 Hz and 20 dB-Hz for unaided and aided tracking loops, respectively.

Improvements in tracking-loop performance were obtained when the rate at which IMU-derived data were processed was increased from 10 Hz (100-ms intervals) to 100 Hz (10-ms invervals). In particular, rotational-velocity estimates were greatly improved by an increase in attitude data rates. However, in terms of translational dynamics, this data-rate change did not significantly affect the carrier-tracking threshold because of the dominant effect of acceleration-sensitive frequency-reference drift.

Finally, it should be noted that to most effectively IMU-aid the X-set receiver, all delays in the transmission of aiding signals to the RM/IPM must be minimized and accounted for in the aiding estimation algorithms. Errors introduced into the tracking loop by sources such as the IMU-data extrapolation algorithm or frequency-reference acceleration-sensitive drift, limit the extent to which tracking-loop noise bandwidth can be reduced.

SECTION 6

LIST OF REFERENCES

2-1 System Specification for the NAVSTAR Global Position System Phase 1, SS-GPS-101B, SAMSO/YE.

3-1 Stonestreet, W.M., A Functional Description of the NAVSTAR GPS Receiver Model X, Charles Stark Draper Laboratory Report R-981, May 17, 1976.

3-2 Time and Frequency: Theory and Fundamentals, NBS Monograph 140, May 1974.

3-3 Hellwig, H., A Review of Precision Oscillators, NBS Technical Note 662, February 1975.

3-4 Proceedings of IEEE, Vol. 54, February 1966.

3-5 Mealy, G., Time Standard Error Modeling with Applications to Satellite Navigation, 29th Annual Symposium of Frequency Control, May 1975.

3-6 Britting, K., Inertial Navigation Systems Analysis, McGraw-Hill, 1956.

3-7 Hildegrand, F.B., Introduction of Numerical Analysis, McGraw-Hill, 1956.

4-1 Stonestreet, W.M., A Functional Description of the NAVSTAR GPS Receiver Model X, Charles Stark Draper Laboratory Report R-981, May 17, 1976.

4-2 Papoulis, A., Probability, Random Variables, and Stochastic Processes, McGraw-Hill, Inc., 1965.

4-3 Viterbi, A., Principles of Coherent Communication, McGraw-Hill, Inc., 1966.

4-4 Lindsey, W., Synchronization Systems in Communication and Control, Prentice Hall, 1972.

4-5 Lewis, P.W., and Weingarten, W., "A Comparison of Second, Third, and Fourth Order Phase-Locked Loops," IEEE Transactions on Aerospace and Electronics Systems, Vol. AES-3, No. 4, July 1967.

4-6 Taylor, R.E., "Satellite Tracking Simultaneous-Lobing Monopulse Receiving System with Polarization Diversity Capability," IEEE Transactions on Aerospace and Electronics Systems, Vol. AES-3, No. 4, July 1967.

4-7 Filippi, E., CO^2 Laser Ranging Systems Study, Old Dominion Systems, Inc., May 1975, N75-29410.

4-8 Lindorff, D., Theory of Sampled Data Control Systems, John Wile & Sons, Inc., 1965.

4-9 Harton, P., Frequency Standard Stability for Doppler Measurements On-Board the Shuttle, Lockheed Electronics Co., Inc., Report LEC-3964, July 1974.

4-10 Hellwig, H., A Review of Precision Oscillators, NBS Technical Note 662, February 1975.

4-11 Time and Frequency: Theory and Fundamentals, NBS Monograph 140, May 1974.

The Charles Stark Draper Laboratory, Inc.
555 Technology Square, Cambridge, Massachusetts 02139 Telephone (617) 258- 1287

BAK-GPS-9

TO: Distribution
FROM: B.A. Kriegsman
DATE: 17 June 1977
SUBJECT: New IMU-Aiding Algorithm - Study Results

SUMMARY

In recent studies where IMU aiding was used in the carrier tracking loop, it was found that a 4-ms lag in the transmission of IMU data to the RM/IPM has created problems (Refs. 1 and 2). A new algorithm has been developed which accounts for the presence of this transport lag. Simulation results are presented to show the maximum carrier-loop tracking errors as a function of tracking-loop noise bandwidth. Also included are time histories of the carrier-loop tracking errors. No input noise or frequency-reference errors are included in any of the test runs, and a linear error detector is assumed.

The main point of interest is that with the transport lag accounted for in the extrapolation algorithm, a significant reduction in carrier tracking error (with respect to the data of Refs. 1 and 2) is obtained at the 100-Hz data-rate case. Under these conditions a significant reduction in peak tracking error is obtained by increasing the IMU data rate, as indicated in Figure 1.

REFERENCES

1) Kriegsman, B., "Transport Lags on IMU-Aiding Data", CSDL Memo BAK-GPS-8, May 25, 1977.

2) Kriegsman, B., Cox, D., Stonestreet, W., "IMU-Aided GPS Receiver" CSDL Report P-490, June 1977.

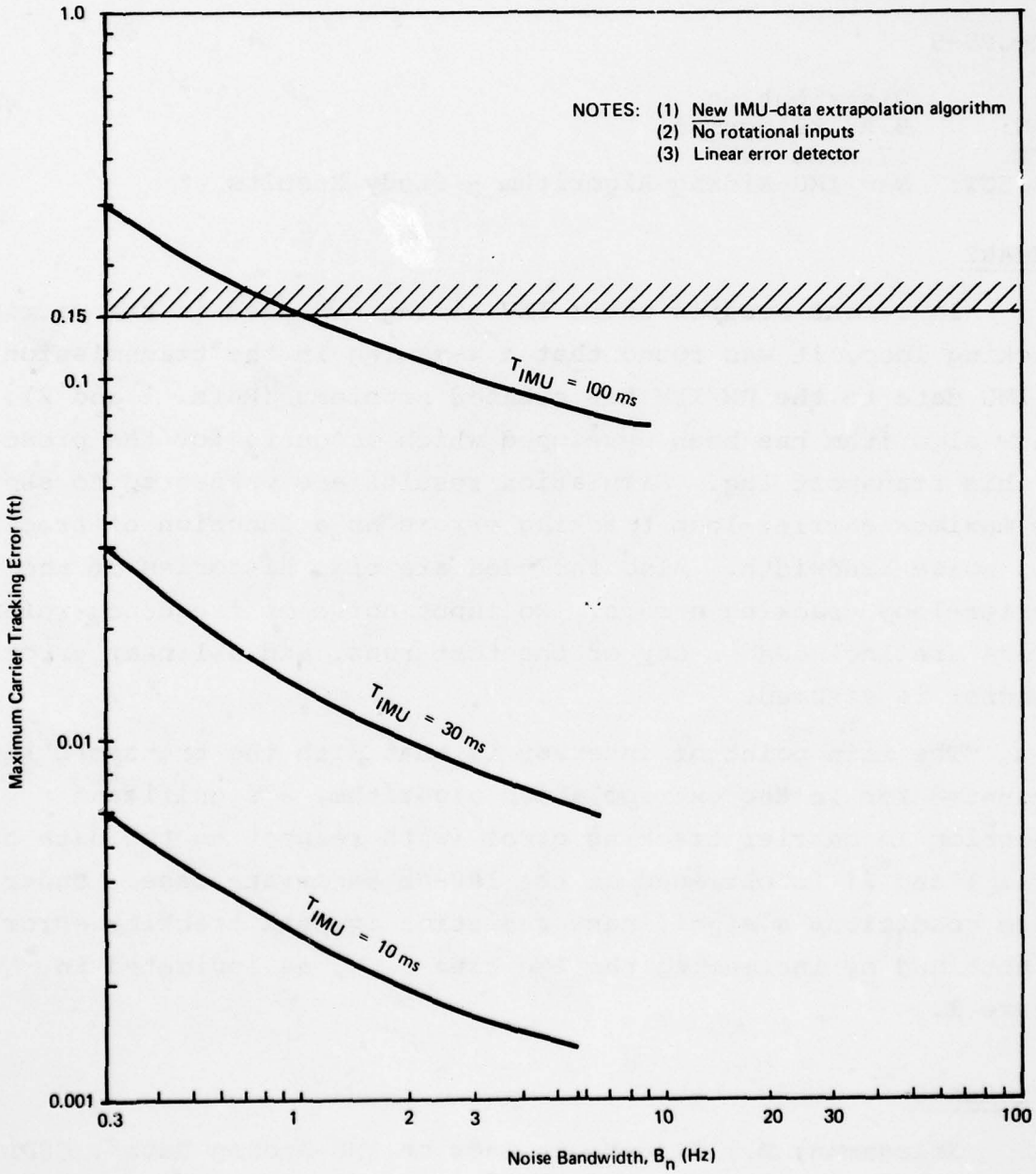

Figure 1. Carrier tracking errors for high-jerk trajectory.

AD-A057 656 CHARLES STARK DRAPER LAB INC CAMBRIDGE MA F/G 17/7
FUNCTIONAL REQUIREMENTS OF THE INTERFACE BETWEEN THE NAVSTAR GP--ETC(U)
DEC 77 B A KRIEGSMAN, W M STONESTREET F04701-75-C-0212
UNCLASSIFIED R-981-VOL-2 SAMSO-TR-77-120-VOL-2 NL

2 OF 2
AD
A057656

END
DATE
FILMED
9-78
DDC

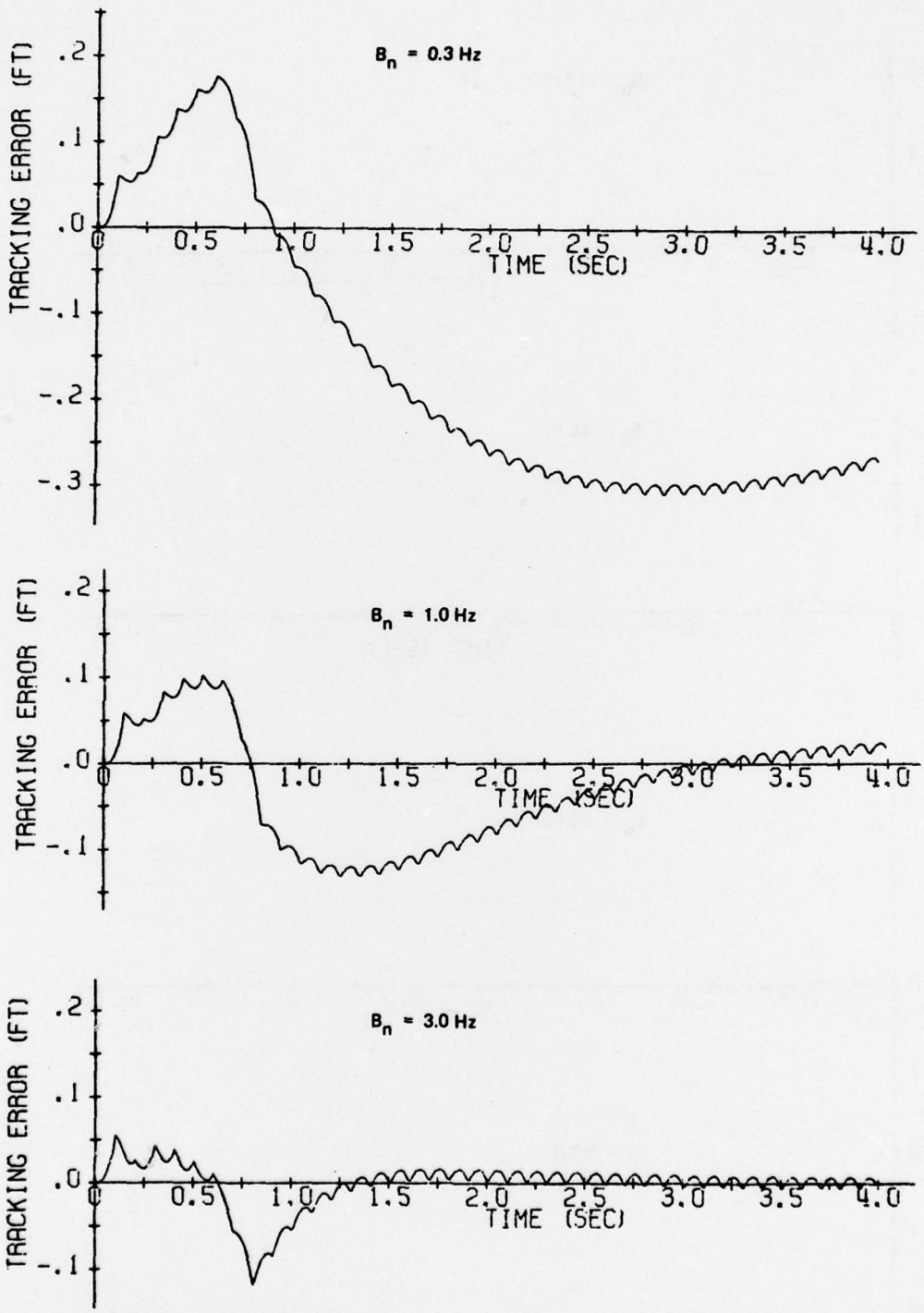

Figure 2. Carrier tracking errors, T_{IMU} = 100 ms.

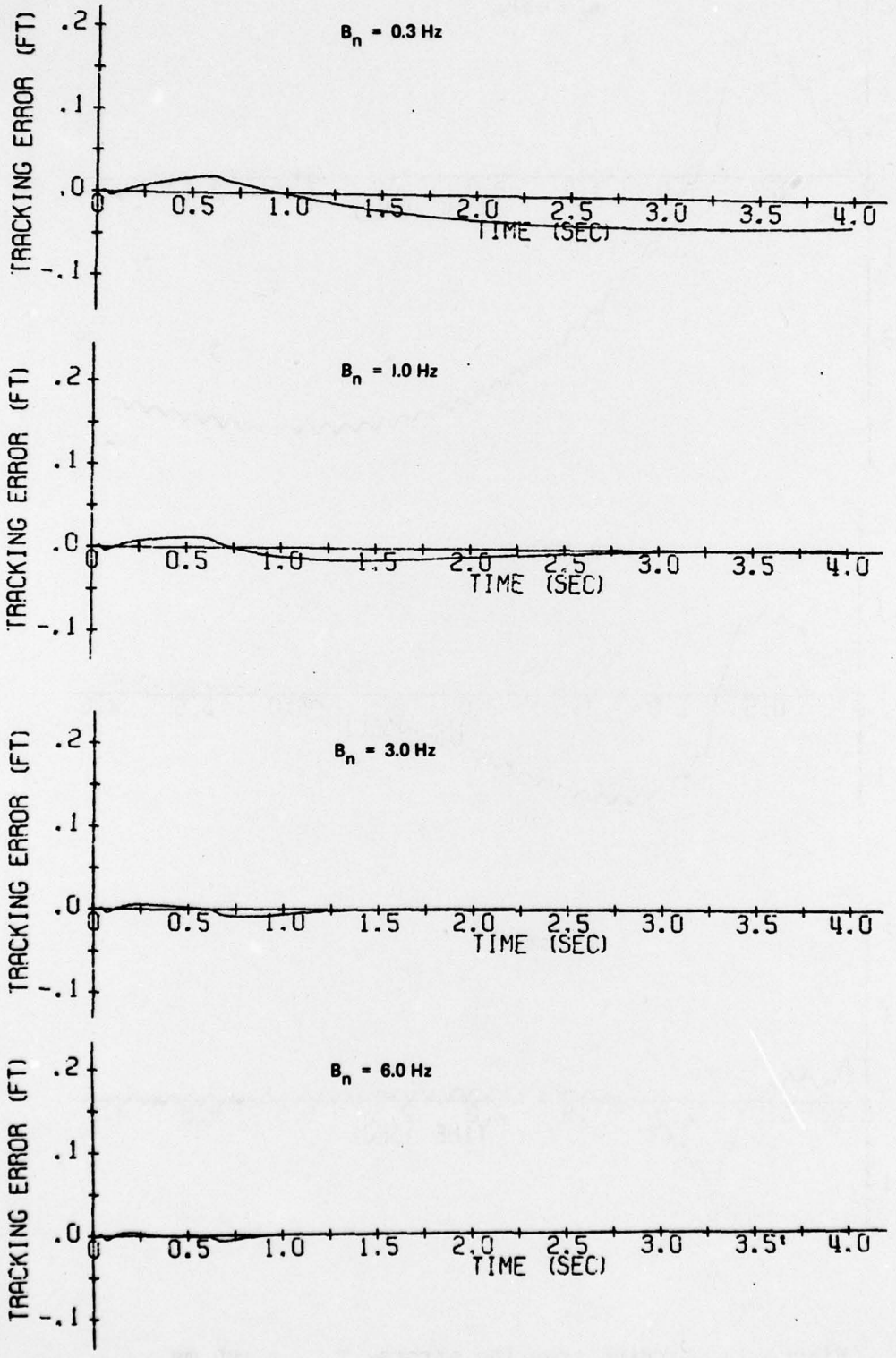

Figure 3. Carrier tracking errors, T_{IMU} = 30 ms.

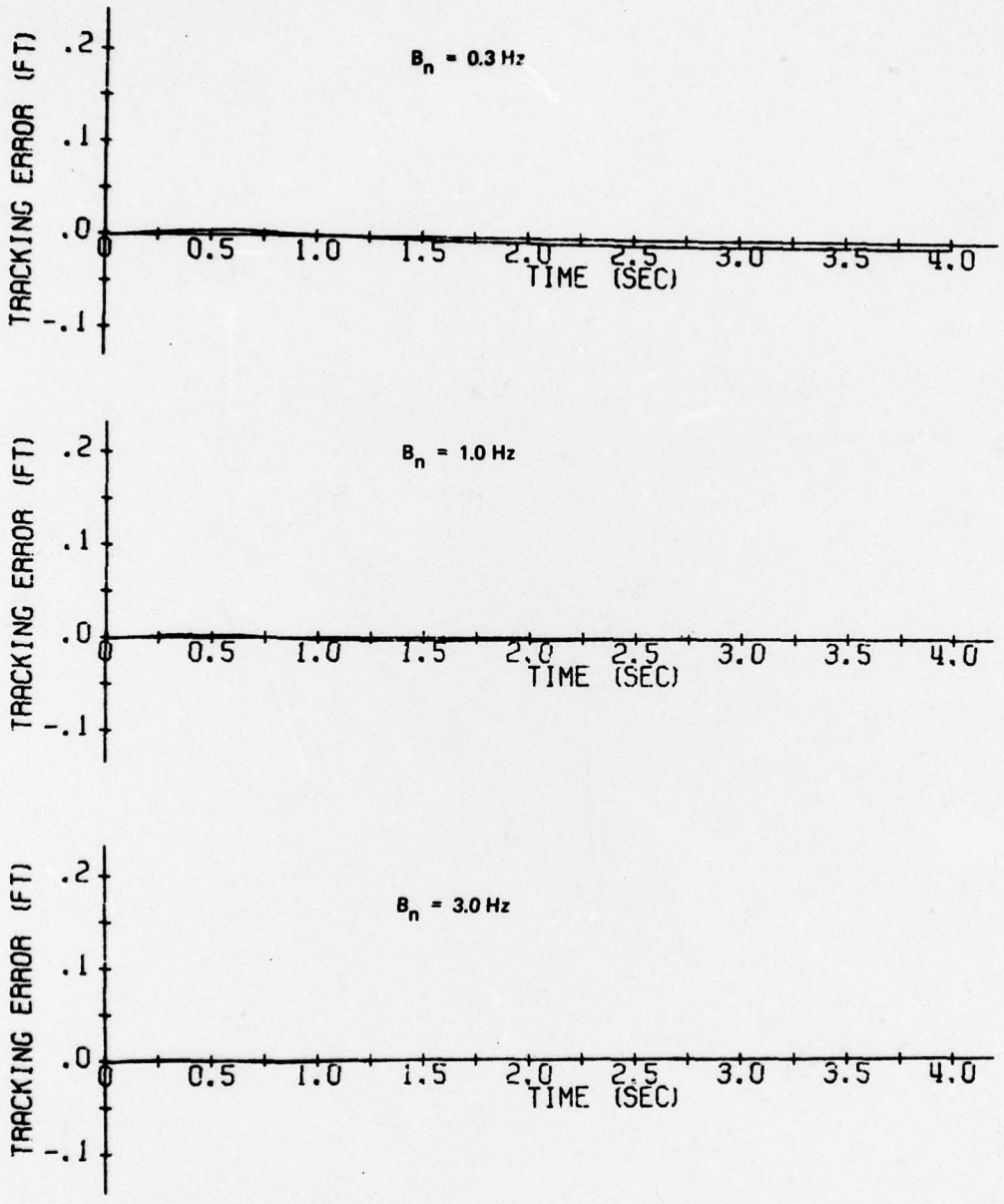

Figure 4. Carrier tracking errors, T_{IMU} = 10 ms.